

The Phenomenology of Extra Neutral Gauge Bosons

A. Leike

*Ludwigs-Maximilians-Universität, Sektion Physik, Theresienstr. 37,
D-80333 München, Germany*

E-mail: leike@graviton.hep.physik.uni-muenchen.de

Abstract

The phenomenological constraints on extra neutral gauge bosons at present and at future colliders are reviewed. Special attention is paid to the influence of radiative corrections, systematic errors, and kinematic cuts on the Z' constraints. Simple estimates of the Z' constraints from different reactions are derived. They make the physical origin of these constraints transparent. The results existing in the literature are summarized and compared with the estimates. The consequence of model assumptions on the Z' constraints is discussed. The paper starts with an overview of Z' parameters and the possible links between them by model assumptions. It continues with a discussion of Z' limits and Z' measurements in different reactions at e^+e^- and $\mu^+\mu^-$ colliders. It follows an overview of the corresponding limits at proton colliders. Possible Z' constraints from other reactions as ep collisions, atomic parity violation, neutrino scattering and cosmology are briefly mentioned.

Contents

| | | |
|----------|---|------------|
| 0 | Introduction | 3 |
| 1 | Preliminary considerations | 6 |
| 1.1 | Parameters describing extra neutral gauge bosons | 6 |
| 1.2 | Extra neutral gauge bosons in E_6 models | 14 |
| 1.3 | Extra neutral gauge bosons and contact interactions | 16 |
| 1.4 | Four fermion interactions and form factors | 17 |
| 1.5 | Model dependence of Z' constraints | 20 |
| 1.6 | Extracting Z' limits from data | 21 |
| 2 | Z' search at e^+e^-, e^-e^- and $\mu^+\mu^-$ colliders | 23 |
| 2.1 | Z' search in $e^+e^- \rightarrow f\bar{f}$ | 24 |
| 2.2 | Z' search in $e^+e^- \rightarrow e^+e^-$ and $e^-e^- \rightarrow e^-e^-$ | 61 |
| 2.3 | Z' search in $e^+e^- \rightarrow W^+W^-$ | 67 |
| 2.4 | Z' search in other reactions | 79 |
| 3 | Z' search at pp and $p\bar{p}$ colliders | 81 |
| 3.1 | Born cross section of $pp(p\bar{p}) \rightarrow Z' \rightarrow f\bar{f}$ | 81 |
| 3.2 | Higher order processes and background | 82 |
| 3.3 | Observables | 84 |
| 3.4 | Z' constraints | 85 |
| 4 | Z' search in other experiments | 93 |
| 4.1 | ep collisions | 93 |
| 4.2 | Atomic parity violation | 95 |
| 4.3 | Neutrino scattering | 97 |
| 4.4 | Cosmology | 98 |
| 5 | Summary and conclusions | 99 |
| A | Notation | 120 |
| B | Available FORTRAN programs for Z' fits | 123 |

Chapter 0

Introduction

A neutral gauge boson is a spin-one particle without charge. It transmits forces in gauge theories. One well known neutral gauge boson is the photon. In 1923, A. H. Compton found the direct experimental confirmation that the photon is an elementary particle. The photon is connected with the $U(1)_{em}$ gauge symmetry of electrodynamics. Noether's theorem states that this symmetry must correspond to a conserved quantity, the electric charge. The $U(1)_{em}$ gauge symmetry is exact. Therefore, the mass of the photon is zero. It can mediate interactions to infinite distances.

Matter interacts not only through electromagnetic forces. In particular, weak decays as the β -decay violate quantum numbers respected by electrodynamics. These processes indicate that there must be additional fundamental interactions. In 1961, S.L. Glashow, S. Weinberg and A. Salam proposed the unified description of electromagnetic and weak phenomena in a gauge theory based on the gauge group $SU(2)_L \times U(1)_Y$. At low energies, we can only observe the $U(1)_{em}$ symmetry. Therefore, the $SU(2)_L \times U(1)_Y$ gauge symmetry must be broken at some energy scale E_{weak} . Processes with energies $E \ll E_{weak}$ feel only the $U(1)_{em}$ symmetry of electrodynamics. At energies $E > E_{weak}$, the interaction has the full $SU(2)_L \times U(1)_Y$ gauge symmetry. In the language of particles, this means that the weak interaction must be mediated by gauge bosons, which have masses of the order of E_{weak} . We know experimentally that $E_{weak} = O(100) GeV$.

The theory of weak interactions explains β decay by the virtual exchange of a heavy positively or negatively charged gauge boson, the W^\pm . These charged gauge bosons are associated to the $SU(2)_L$ gauge group. The $SU(2)_L$ gauge symmetry has also one neutral (diagonal) generator. The particle associated with this neutral generator must be a neutral gauge boson with a mass of the order of E_{weak} . Because the electromagnetic symmetry $U(1)_{em}$ is different from the $U(1)_Y$ symmetry, the mass eigenstates γ and Z of the neutral gauge bosons are a linear combination of the two neutral gauge bosons associated to the $SU(2)_L$ and $U(1)_Y$ gauge groups. Their properties are predicted in the electroweak theory. The predictions for the Z boson are confirmed by the experiments at LEP and SLC with an incredible precision.

In addition to electroweak interactions, there exist at least two other fundamental interactions, the strong interaction and gravity.

Many physicists believe that all fundamental interactions must have one common root. They don't like the complicated gauge group of the SM. They suppose that strong and electroweak interactions can be described by one simple gauge group G at very high en-

energies $E > E_{GUT}$. Such theories are called grand unified theories (GUT's) [1]. For energies $E \ll E_{GUT}$ the gauge group G must be broken [2] to retain the SM gauge symmetry $SU(3)_c \times SU(2)_L \times U(1)_Y$. One can imagine this symmetry breaking similar to the breaking of the $SU(2)_L \times U(1)_Y$ symmetry to $U(1)_{em}$ in the SM.

As was shown by H. Georgi and S.L. Glashow in 1974, the smallest simple gauge group G , which can contain the SM, is $G = SU(5)$. The number n of neutral gauge bosons of a GUT is given by $n = rank[G]$. We have $rank[SU(5)] = 4$. Therefore, there is no room for additional neutral gauge bosons in the $SU(5)$ GUT.

GUT's make predictions which can be tested in experiments. In particular, they predict that the proton must decay. This decay is mediated by the exchange of gauge bosons with a mass $O(E_{GUT})$. It is the analogue of the β decay described in the electroweak theory. To be consistent with present experiments on proton decay, we get the condition $E_{GUT} > 10^{15} GeV$. This energy is much larger than E_{weak} . It is important that it is smaller than the Planck mass, $M_P = \sqrt{\hbar c/G_N} \approx 1.2 \cdot 10^{19} GeV$. At energies above the Planck mass, gravity is expected to become as strong as the other interactions. At energies well below M_P , as it happens in GUT's, the effects of gravity can be neglected. E_{GUT} is also predicted as the energy where the three running gauge coupling constants of the SM gauge group become equal. The value of E_{GUT} obtained experimentally by this matching condition predicts a proton lifetime, which contradicted the measurement already several years ago. Only the recent precision measurements at LEP and SLC could prove that the three running gauge couplings do not meet in one point if they run as predicted in the $SU(5)$ GUT. Therefore, one must add something else if one wants to describe all SM interactions by one simple gauge group. One popular direction of research is supersymmetry.

We are interested here in another solution of the problem, the consideration of larger unification groups. All GUT's with gauge groups larger than $SU(5)$ predict at least one extra neutral gauge boson (Z'). It was shown by H. Fritzsch and P. Minkowski in 1975 that the next interesting gauge group larger than $SU(5)$ is $SO(10)$. The $SO(10)$ theory predicts one extra neutral gauge boson because $rank[SO(10)] = 5$. It is a non-trivial fact that all SM fermions of one generation fit in only one multiplet of $SO(10)$. To complete the multiplet, one new fermion with the quantum numbers of the right-handed neutrino must be added. The $SO(10)$ GUT is not in contradiction with present experiments. GUT's with gauge groups larger than $SO(10)$ predict more than one extra neutral gauge bosons and many new fermions. These new (exotic) fermions must be heavy to make the theories consistent with present experiments.

The mass of the Z' is not constrained by theory. A priori, it can be anywhere between E_{weak} and E_{GUT} . As was shown in references [3, 4], it has naturally a mass of about one TeV in some supersymmetric GUT's. Then, a Z' can be observed at the next generation of colliders. An observation of a Z' would provide information on the GUT group and on its symmetry breaking. It is of special interest for experimental physicists because a Z' would serve as a calibration point for future detectors. The study of the Z' phenomenology is therefore an important part of the scientific program of every present and future collider.

As the SM Z boson, the Z' is expected to be a very short-lived particle. It can only be observed through its decay products or through indirect interference effects. It can be detected either in very high energy processes or in high precision experiments at lower energies. In the first kind of processes, the energy of the colliding particles must be high enough to produce a Z' . The decay products of the Z' must be then detected above the SM background. Such

a background is always present because the SM Z boson or the photon are produced by the same processes, which create a Z' . In precision experiments, the experimental errors and the errors due to the theoretical predictions of the observables must be smaller than the expected deviations due to a Z' .

There are several previous reviews on Z' physics. References [5, 6] give an overview of Z' physics in the E_6 GUT. In reference [7] the search for a Z' in high precision experiments is reviewed. A recent short review is given in [8].

In the recent years, extensive studies on the sensitivity of future e^+e^- [9], $pp(p\bar{p})$ [10] and $e^\pm p$ [11] colliders to a Z' have been completed. Among the new developments are

- the inclusion of radiative corrections, realistic experimental cuts and systematic errors in Z' studies and the development of codes allowing direct Z' fits to experimental data;
- the discussion of a Z' not only in the context of a model but also without model assumptions;
- the experimental successes during the last years of precision measurements, heavy flavour tagging and highly polarized beams allow the investigation of new observables.

In this paper, we review the main results of these new developments. Special attention is paid to the *mechanisms* leading to Z' limits in the different reactions. The resulting approximate formulae make the dependence of Z' constraints and Z' measurements on experimental conditions and model parameters transparent. The approximate formulae are compared with the existing results in the literature.

We divide the paper into five chapters and several appendices. In the first chapter, we introduce the parameters describing extra neutral gauge bosons. The E_6 GUT is considered as an example of a theory containing extra neutral gauge bosons. Far below the Z' resonance, the Z' can be described as a special case of four fermion contact interactions. A general formalism of the inclusion of Z' effects in Standard Model cross sections are form factors. We emphasize that it is necessary to distinguish between model dependent and model independent Z' analyses. We conclude the first chapter with some general remarks on the data analysis.

In the second chapter, we list Z' constraints at e^+e^- , e^-e^- and $\mu^+\mu^-$ colliders. The constraints from various reactions are considered in individual sections. Every section is organized in the same pattern. First, the relevant observables are discussed in the Born approximation. It is followed by a discussion of radiative corrections. Finally, different Z' constraints are considered. If necessary, different cases of the center-of-mass energy are distinguished.

In the third chapter, the Z' constraints obtained at hadron colliders are considered.

Z' constraints from other experiments; electron-proton collisions, atomic parity violation, neutrino scattering and cosmology are mentioned in chapter four.

Chapter five contains our summary and conclusions.

Two appendices complete this paper. The main notation is collected in appendix A. Appendix B contains an overview of the available FORTRAN codes suitable for Z' fits in different experiments.

Chapter 1

Preliminary considerations

1.1 Parameters describing extra neutral gauge bosons

Information on extra neutral gauge bosons can be obtained through experimental constraints *on* or measurements *of* its parameters. These Z' parameters are introduced in this section.

After fixing our assumptions and notation, we consider effects of gauge boson mixing. We then deal with the Z' couplings to SM fermions and with Z' decays to SM particles.

1.1.1 Assumptions and limitations

Suppose that a Z' exists in nature. Then, its parameters depend on many unknown details of the theory.

We assume that at most one extra neutral gauge boson is light enough to give the first signal in future experiments and that no other signals from a GUT are found at that time. In the case where there are additional signals of new physics, they would give interesting extra information on the parameters of the new theory.

We assume that the underlying effective gauge group at low energies is

$$SU(3)_c \times SU(2)_L \times U(1)_Y \times U'(1). \quad (1.1)$$

We further assume that the couplings of the Z' to fermions are universal for all generations. In models where this is not the case, one has to be careful about the suppression of flavour changing neutral currents. See reference [12] for recent constraints on such models and for further references.

A GUT containing a Z' predicts many new particles as, for example, additional (exotic) fermions, additional charged gauge bosons or additional Higgs bosons. In the simplest case of a $SO(10)$ GUT, the only additional fermion is one right-handed neutrino. The number of exotic fermions rises drastically for larger gauge groups. The couplings of these fermions to gauge bosons are fixed in the GUT but their masses are not constrained by the theory. Under our assumption that the Z' gives the only signal of the GUT, the decays of the Z' to exotic fermions and Higgs bosons are kinematically suppressed [13].

We neglect the mixing of SM fermions with exotic fermions [14] and possible simultaneous mixing of gauge bosons and fermions [15].

In a SUSY GUT, many interactions involving supersymmetric particles are predicted. We do not consider these effects [16].

We do not discuss either the special case of leptophobic Z' models [17, 18], which were constructed to explain the discrepancy of R_b at LEP with the SM expectations.

BESS models [19] also predict extra neutral gauge bosons. The corresponding Z' limits derived for hadron [20, 21] and lepton [20, 22, 23] colliders will not be discussed here.

1.1.2 Mixing

There are no quantum numbers which forbid a mixing of neutral gauge bosons. However, the ZZ' mixing arises naturally in many models.

1.1.2.1 Kinetic mixing

We first consider the case where all neutral gauge bosons are *massless*. Assume diagonal kinetic terms of the gauge fields. The general tree level parametrization of the neutral current Lagrangian for the gauge group (1.1) is then [24, 25]

$$- \mathcal{L}_{NC} = \bar{f}\gamma^\beta \left\{ gT_3^f W_{3\beta} + g'_{11} Y^f B'_\beta + g'_{12} Y^f Z'_{2\beta} + g'_{21} Q'^f B'_\beta + g'_{22} Q'^f Z'_{2\beta} \right\} f, \quad (1.2)$$

where the summation over the fermions f is understood, T_3^f is the third component of the SM isospin, Y^f is the hypercharge and Q'^f is the charge due to the new $U'(1)$. The particles associated with the $U(1)_Y$ and $U'(1)$ gauge groups are denoted as B' and Z'_2 , correspondingly. $W_{3\beta}$ is the same field as defined in the SM.

The non-zero contributions proportional to g'_{12} and g'_{21} can arise during the evolution from GUT energies to the weak scale. The two by two matrix g'_{ij} can be made triangular by a rotation of the two abelian gauge bosons around the angle θ_K , $c_K = \cos \theta_K$, $s_K = \sin \theta_K$,

$$\begin{pmatrix} B'_\beta \\ Z'_{2\beta} \end{pmatrix} = \begin{pmatrix} c_K & -s_K \\ s_K & c_K \end{pmatrix} \begin{pmatrix} B_\beta \\ Z'_\beta \end{pmatrix}. \quad (1.3)$$

The angle θ_K describes the kinetic mixing. After the mixing (1.3), the Lagrangian (1.2) transforms to

$$- \mathcal{L}_{NC} = \bar{f}\gamma^\beta \left\{ gT_3^f W_{3\beta} + g_{11} Y^f B_\beta + g_{12} Y^f Z'_\beta + g_{22} Q'^f Z'_\beta \right\} f \quad (1.4)$$

with $g_{11} = g'_{11}c_K + g'_{12}s_K$, $g_{12} = -g'_{11}s_K + g'_{12}c_K$, $g_{21} = g'_{21}c_K + g'_{22}s_K \equiv 0$ and $g_{22} = -g'_{21}s_K + g'_{22}c_K$.

If there is no additional symmetry requiring $g_{12} = 0$, the term proportional to g_{12} is needed to ensure the renormalizability of the theory [25].

Kinetic mixing plays an important role in some leptophobic models [26] and can communicate SUSY-breaking to the visible sector [27].

Kinetic mixing between the gauge bosons $W_{3\beta}$ and B_β is forbidden in the SM by $SU(2)_L$ gauge invariance.

1.1.2.2 Mass mixing

Gauge symmetry must be broken at low energies to describe massive gauge bosons.

In the SM, the entries of the mass matrix

$$\mathcal{L}_M = \frac{1}{2}(B, W_3)M_{SM}^2 \begin{pmatrix} B \\ W_3 \end{pmatrix}, \quad M_{SM}^2 = \begin{pmatrix} M_B^2 & -M_W M_B \\ -M_W M_B & M_W^2 \end{pmatrix} \quad (1.5)$$

are related to the vacuum expectation value v of the Higgs field,

$$\Phi = \begin{pmatrix} \phi^+ \\ \phi^0 \end{pmatrix}, \quad \langle \phi^0 \rangle = \frac{gv}{\sqrt{2}}, \quad M_W = \frac{gv}{2}, \quad M_B = \frac{g_{11}v}{2}. \quad (1.6)$$

M_{SM}^2 is diagonalized by a rotation of the symmetry eigenstates around the Weinberg angle θ_W , $c_W = \cos \theta_W$, $s_W = \sin \theta_W$ leading to the well-known mass eigenstates of the photon and the Z boson,

$$\begin{pmatrix} \gamma \\ Z \end{pmatrix} = \begin{pmatrix} c_W & s_W \\ -s_W & c_W \end{pmatrix} \begin{pmatrix} B \\ W_3 \end{pmatrix}. \quad (1.7)$$

The masses of the mass eigenstates are

$$M_Z^2 = M_W^2 + M_B^2, \quad M_\gamma^2 = 0. \quad (1.8)$$

The mass of the photon is zero due to the exact $U(1)_{em}$ gauge symmetry at low energies reflecting charge conservation. This symmetry protects the photon from further mixing.

The Weinberg angle is related to the entries of the mass matrix (1.5),

$$\tan 2\theta_W = \frac{2M_W M_B}{M_W^2 - M_B^2}. \quad (1.9)$$

We get the following relations between the Weinberg angle and the mass values,

$$t_W^2 = \frac{s_W^2}{c_W^2} = \frac{M_B^2 - M_\gamma^2}{M_Z^2 - M_B^2} = \frac{M_B^2}{M_W^2}, \quad \text{and} \quad M_B M_W = s_W c_W (M_Z^2 - M_\gamma^2) = s_W c_W M_Z^2. \quad (1.10)$$

In a theory with the gauge group (1.1), the mass matrix of the Z and Z' receives non-diagonal entries δM^2 , which are again related to the vacuum expectation values of the Higgs fields,

$$\mathcal{L}_M = \frac{1}{2}(Z, Z')M_{ZZ'}^2 \begin{pmatrix} Z \\ Z' \end{pmatrix}, \quad M_{ZZ'}^2 = \begin{pmatrix} M_Z^2 & \delta M^2 \\ \delta M^2 & M_{Z'}^2 \end{pmatrix}. \quad (1.11)$$

We assume that the vacuum expectation values of the Higgs fields are real. The mass matrix (1.11) is diagonalized by a rotation of the fields Z and Z' around the mixing angle θ_M , $c_M = \cos \theta_M$, $s_M = \sin \theta_M$ leading to the mass eigenstates Z_1 and Z_2 ,

$$\begin{pmatrix} Z_1 \\ Z_2 \end{pmatrix} = \begin{pmatrix} c_M & s_M \\ -s_M & c_M \end{pmatrix} \begin{pmatrix} Z \\ Z' \end{pmatrix}. \quad (1.12)$$

The masses M_1 and M_2 of the mass eigenstates Z_1 and Z_2 are

$$M_{1,2}^2 = \frac{1}{2} \left[M_Z^2 + M_{Z'}^2 \pm \sqrt{(M_Z^2 - M_{Z'}^2)^2 + 4(\delta M^2)^2} \right]. \quad (1.13)$$

It follows that

$$M_1 < M_Z < M_2, \quad \text{and hence} \quad \rho_{mix} = \frac{M_W^2}{M_1^2 c_W^2} > \frac{M_W^2}{M_Z^2 c_W^2} = \rho_0 = 1. \quad (1.14)$$

We have $M_Z = M_1$ and $M_{Z'} = M_2$ for $\theta_M = 0$. LEP 1 and SLC performed precision measurements of the mass eigenstate Z_1 .

Similar to the SM, the mixing angle θ_M is related to the entries of the mass matrix (1.11),

$$\tan 2\theta_M = \frac{2\delta M^2}{M_Z^2 - M_{Z'}^2}. \quad (1.15)$$

We get the following relations between θ_M and the mass values,

$$t_M^2 = \frac{s_M^2}{c_M^2} = \frac{M_Z^2 - M_1^2}{M_2^2 - M_Z^2} \quad (1.16)$$

and

$$\delta M^2 = s_M c_M (M_1^2 - M_2^2). \quad (1.17)$$

For fixed M_1 and M_Z , equation (1.16) relates θ_M and M_2 independently of the Higgs sector. This constraint on θ_M is called the mass constraint [5, 6]. It predicts $\theta_M \sim 1/M_2$ for large M_2 . For a fixed Higgs sector, δM^2 is also fixed leading to the constraint on θ_M given in equation (1.17). It is called the Higgs constraint [5, 6]. For large M_2 , it is stronger than the mass constraint predicting the asymptotic behaviour $\theta_M \sim 1/M_2^2$ [5, 6].

1.1.2.3 Alternative parametrization of the mixing

In left-right models [28] with the gauge group

$$SU(2)_L \times SU(2)_R \times U(1)_{B-L}, \quad (1.18)$$

the mass eigenstates γ, Z_1 and Z_2 are obtained by a one-step mixing through an orthogonal 3 by 3 matrix [29],

$$\begin{pmatrix} Z_1 \\ Z_2 \\ \gamma \end{pmatrix} = \begin{pmatrix} c_W c_M & s_W c_M c_{LR} + s_M s_{LR} & s_W c_M s_{LR} - s_M c_{LR} \\ -c_W s_M & -s_W s_M c_{LR} + c_M s_{LR} & -s_W s_M s_{LR} - c_M c_{LR} \\ -s_W & c_W c_{LR} & c_W s_{LR} \end{pmatrix} \begin{pmatrix} W_{3L} \\ W_{3R} \\ Y_{B-L} \end{pmatrix}, \quad (1.19)$$

depending on the three mixing angles θ_W, θ_M and θ_{LR} with $s_{LR} = \sin \theta_{LR}, c_{LR} = \cos \theta_{LR}$. In equation (1.19), we adapted the notation to our definitions. Note that the fields W_{3L}, W_{3R}, Y_{B-L} commute in the gauge group (1.18).

In previous sections, we described the mixing of the neutral gauge bosons associated with the gauge group (1.1) by two mixing angles θ_W and θ_M . To apply this procedure to left-right models, one has to first break the gauge group (1.18) to $SU(2)_L \times U(1)_Y \times U'(1)$. This breaking will generate non-diagonal terms in the associated gauge fields through fermion loops [26] if $\sum_{\text{chiral fermions } f} (Q^f Q'^f) \neq 0$. These non-diagonal terms can be described by a non-zero g_{12} in equation (1.4). In the case $g_R = g_L$, no non-diagonal terms exist ($g_{12} = 0$) and the mass matrix can be diagonalized by the two angles θ_W and θ_M [28] in both mixing procedures.

In this paper, we prefer the two-step mixing procedure. It has advantages in the model independent approach where one starts with the gauge group (1.1) and the corresponding symmetry eigenstates B and Z' .

1.1.3 Couplings to SM fermions

The couplings of the symmetry eigenstate Z' to fermions are fixed in a GUT. Experiments are sensitive to the couplings of the mass eigenstates Z_1 and Z_2 .

1.1.3.1 Couplings of the Symmetry Eigenstates

The Lagrangian (1.4) can be written in the form

$$-\mathcal{L}_{NC} = eA_\beta J_\gamma^\beta + g_1 Z_\beta J_Z^\beta + g_2 Z'_\beta J_{Z'}^\beta. \quad (1.20)$$

It contains the currents

$$J_\gamma^\beta = \sum_f \bar{f} \gamma^\beta v_f(0) f, \quad J_Z^\beta = \sum_f \bar{f} \gamma^\beta [v_f - \gamma_5 a_f] f, \quad J_{Z'}^\beta = \sum_f \bar{f} \gamma^\beta [v'_f - \gamma_5 a'_f] f. \quad (1.21)$$

To fix the notation, we give here the coupling constants of the photon and the SM Z boson to the SM fermion f ,

$$\begin{aligned} g_0 &\equiv e = \sqrt{4\pi\alpha} = g_{SW}, & v_f(0) &= Q^f, & a_f(0) &= 0, \\ g_1 &= \frac{e}{2s_W c_W} = (\sqrt{2}G_\mu M_Z^2)^{1/2}, & v_f &= T_3^f - 2Q^f s_W^2, & a_f &= T_3^f, \end{aligned} \quad (1.22)$$

with $T_3^e = -\frac{1}{2}$, $Q^e = -1$. Differently from the SM, it is useful to define the electric charge as $Q^f \equiv T_3^f + \sqrt{\frac{5}{3}}Y^f$ in GUT's. The comparison of the two Lagrangians (1.4) and (1.20) then gives $g_{11} = \sqrt{\frac{3}{5}}e/c_W$.

The couplings g_2 , v'_f and a'_f depend on the particular Z' model. In the Sequential Standard Model (SSM), all couplings of the Z' to SM fermions are equal to those of the SM Z boson, $g_2 = g_1$, $v'_f = v_f$, $a'_f = a_f$. Although it is hard to obtain the SSM in GUT's, it is a popular benchmark model, which is limited in different experiments.

Starting from the Lagrangian (1.4) and identifying $g_2 = g_{22}$, one obtains v'_f and a'_f as a function of the charge $Q^{f'}$ and the hypercharge Y^f [25],

$$\begin{aligned} v'_f &= Q^{f'L} + Q^{f'R} + \frac{g_{12}}{g_{22}}(Y^{fL} + Y^{fR}) = Q^{f'L} + Q^{f'R} + \frac{g_{12}}{g_{22}}\sqrt{\frac{3}{5}}(-T_3^f + 2Q^f), \\ a'_f &= Q^{f'L} - Q^{f'R} + \frac{g_{12}}{g_{22}}(Y^{fL} - Y^{fR}) = Q^{f'L} - Q^{f'R} + \frac{g_{12}}{g_{22}}\sqrt{\frac{3}{5}}(-T_3^f). \end{aligned} \quad (1.23)$$

We define the couplings to left- and right-handed fermions as

$$L'_f = \frac{1}{2}(v'_f + a'_f), \quad R'_f = \frac{1}{2}(v'_f - a'_f). \quad (1.24)$$

A possible charge $Q^{\nu_L^c} = -Q^{\nu_R}$ is not considered here because we count the right handed neutrino as an exotic fermion, which is assumed to be heavy. Therefore, $v_\nu - a_\nu$ does not enter our analysis. Hence, only *seven* of the eight couplings v'_f and a'_f are independent.

For extra neutral gauge bosons arising in the gauge group (1.1), we have

$$[Q^{f'}, T_3^f] = 0. \quad (1.25)$$

Then, the two relations

$$Q'^{uL} = Q'^{dL} \equiv Q'^{qL} \quad \text{and} \quad Q'^{eL} = Q'^{\nu L} \equiv Q'^{lL} \quad (1.26)$$

must be fulfilled to preserve $SU(2)_L$ gauge invariance. Relations similar to (1.26) are fulfilled for the hypercharges Y^f in the SM. Therefore, the relations (1.26) remain valid if the charges Q'^f are replaced by the corresponding Z' couplings to fermions. It follows that v'_f and a'_f can be parametrized by the following *five* independent couplings,

$$L'_u = L'_d \equiv L'_q, \quad L'_e = L'_\nu \equiv L'_l, \quad R'_u, \quad R'_d, \quad R'_e. \quad (1.27)$$

1.1.3.2 Couplings of the Mass eigenstates

From equations (1.23) and (1.12), we deduce the couplings of the mass eigenstates Z_1 and Z_2 to fermions,

$$\begin{aligned} a_f(1) &= c_M a_f + \frac{g_2}{g_1} s_M a'_f \equiv a_f(1 - y_f), \\ v_f(1) &= c_M v_f + \frac{g_2}{g_1} s_M v'_f \equiv a_f(1) \left[1 - 4|Q^f|s_W^2(1 - x_f) \right], \\ a_f(2) &= c_M a'_f + \frac{g_1}{g_2} s_M a_f, \\ v_f(2) &= c_M v'_f + \frac{g_1}{g_2} s_M v_f. \end{aligned} \quad (1.28)$$

The functions x_f and y_f give the ZZ' mixing in terms of form factors,

$$\begin{aligned} x_f &= (1 - v_f/a_f)^{-1} \left(\frac{v_f + t_M v'_f g_2/g_1}{a_f + t_M a'_f g_2/g_1} - \frac{v_f}{a_f} \right) \approx \theta_M \frac{g_2}{g_1} \frac{a'_f v'_f/a'_f - v_f/a_f}{1 - v_f/a_f}, \\ y_f &= -s_M \frac{g_2 a'_f}{g_1 a_f} + (1 - c_M) \approx -\theta_M \frac{g_2 a'_f}{g_1 a_f}. \end{aligned} \quad (1.29)$$

They are convenient for a simultaneous description of ZZ' mixing and electroweak corrections at the Z_1 peak [30]. We neglect terms of higher order in the mixing angle in the last approximation in equation (1.29). For small mixings, x_f and y_f are small being proportional to θ_M .

1.1.4 Decay width

We consider here only Z' decays to SM particles. We refer, for example, to reference [6] for the decay widths to other particles present in a GUT and to [31] for Z' decays to bosons.

1.1.4.1 Born approximation

The partial decay width of the Z_n , $n = 1, 2$ to a fermion pair $f\bar{f}$ is [32]

$$\Gamma(Z_n \rightarrow f\bar{f}) \equiv \Gamma_n^{f0} = N_f \mu M_n \frac{g_n^2}{12\pi} \left\{ [v_f(n)^2 + a_f(n)^2] \left(1 + 2\frac{m_f^2}{M_n^2} \right) - 6a_f(n)^2 \frac{m_f^2}{M_n^2} \right\}, \quad (1.30)$$

N_f is the color coefficient, i.e. $N_f = 1(3)$ for $f = l(q)$. μ is the phase space factor due to the massive final fermions, $\mu = \sqrt{1 - 4m_f^2/M_n^2}$.

A Z'_2 originating from the gauge group $U'(1)$ given in (1.1) or the Z' arising after kinetic mixing (1.3) have no couplings to W bosons. However, in the case of a non-zero mass mixing, the Z component contained in the mass eigenstates Z_1 and Z_2 interacts with W bosons, $g_{WWZ_1} = g_{WWZ}c_M$, $g_{WWZ_2} = g_{WWZ}s_M$, where $g_{WWZ} = ec_W/s_W$ is the SM coupling between W 's and the SM Z boson. The structure of the interaction is essentially the same as in the SM. The partial decay width of the Z_2 to a W^+W^- pair is then [31]

$$\begin{aligned} \Gamma(Z_2 \rightarrow W^+W^-) &\equiv \Gamma_2^{W0} \\ &= \frac{g_{WWZ}^2 M_2}{192\pi} s_M^2 \left(\frac{M_2}{M_Z}\right)^4 \left(1 - 4\frac{M_W^2}{M_2^2}\right)^{3/2} \left(1 + 20\frac{M_W^2}{M_2^2} + 12\frac{M_W^4}{M_2^4}\right). \end{aligned} \quad (1.31)$$

In GUT's, $\Gamma(Z_2 \rightarrow W^+W^-)$ is kept in a reasonable range for $M_2 \rightarrow \infty$ because the potentially dangerous factor M_2^4 is compensated by small mixing angles $s_M^2 \approx 1/M_2^4$, due to the Higgs constraint (1.17).

The decays $Z_2 \rightarrow f\bar{f}V$, $V = Z, W$ are of higher order. However, they are logarithmically enhanced by soft and collinear radiation. In the limit $M_Z^2/M_2^2 \ll 1$, the decay width becomes [33]

$$\begin{aligned} \Gamma(Z_2 \rightarrow f\bar{f}Z) &\equiv \Gamma_2^{ffZ0} \\ &= \frac{M_2 g_1^2 g_2^2}{192\pi^3} \left[R_f^2(2)R_f^2(1) + L_f^2(2)L_f^2(1) \right] \left[\ln^2\left(\frac{M_Z^2}{M_2^2}\right) + 3\ln\left(\frac{M_Z^2}{M_2^2}\right) + 5 - \frac{\pi^2}{3} + O\left(\frac{M_Z^2}{M_2^2}\right) \right]. \end{aligned} \quad (1.32)$$

The decay width $\Gamma(Z_2 \rightarrow f\bar{f}W) \equiv \Gamma_2^{ffW0}$ can be obtained from equation (1.32) by an appropriate replacement of the couplings and masses. The decays $Z_2 \rightarrow f\bar{f}\gamma$ and $Z_2 \rightarrow W^+W^- \gamma$ are considered as radiative corrections to the decays $Z_2 \rightarrow f\bar{f}$ and $Z_2 \rightarrow W^+W^-$.

All other decays of the Z_2 to SM particles are expected to be small. Decays of the Z_2 to non-standard particles depend on additional model parameters. We assume that they are kinematically suppressed.

The total decay width Γ_n of the Z_n is defined as the sum over all partial decay widths. It is convenient to combine M_n and Γ_n in the complex mass,

$$m_n^2 = M_n^2 - iM_n\Gamma_n. \quad (1.33)$$

1.1.4.2 Higher order effects

The Z' width can be neglected in experiments with typical energy transfers much lower than M_2 as far as $\Gamma_2 \ll M_2$. Γ_2 can be measured in $pp(p\bar{p})$ collisions for $s > 2(3)M_2^2$ or in e^+e^- collisions for $s \geq M_2^2$. To reach the experimental accuracy, the inclusion of higher order effects is necessary in these experiments. Radiative corrections to Γ_2 are absolutely necessary for precision measurements at the Z_2 peak in e^+e^- or $\mu^+\mu^-$ collisions.

Of course, tree level decays to non-standard particles have to be included if they are not suppressed. In this case, the corresponding parameters must be measured in independent experiments. We concentrate here on known higher order effects of the decays to SM particles.

Radiative corrections Radiative corrections to Γ_2^{f0} can be deduced from the results known for SM Z decays [34],

$$\begin{aligned}
\Gamma_n^f &= \Gamma_n^{f0} R_{\text{QED}} R_{\text{QCD}}, \quad n = 1, 2, \\
R_{\text{QED}} &= \left(1 + \frac{3\alpha}{4\pi} (Q^f)^2 \right), \\
R_{\text{QCD}} &= 0 \quad \text{for } f = l, \\
R_{\text{QCD}} &= 1 + \frac{\alpha_s(M_1^2)}{\pi} + 1.405 \frac{\alpha_s^2(M_1^2)}{\pi^2} - 12.8 \frac{\alpha_s^3(M_1^2)}{\pi^3} - \frac{(Q^f)^2 \alpha \alpha_s(M_1^2)}{4\pi^2} \quad \text{for } f = q.
\end{aligned} \tag{1.34}$$

For Γ_2^t , the top mass should also be taken into account in the radiative corrections [35]. See reference [36] for $O(\alpha\alpha_s)$ corrections in that case.

The SM weak corrections to SM Z decays are calculated in reference [37] in terms of form factors. See also section 2.1.2.4. The concept can be generalized to SM weak corrections of Z_2 decays to SM fermions. The full one-loop corrections in the GUT depend on the details of the theory. They can only be calculated if all relevant new parameters are known from independent experiments.

The main corrections to Γ_2^{W0} are QED corrections from radiation off the final state and the Coulomb singularity. See section 2.3.2 or [38] for further details and references.

Radiative corrections to Γ_2^{fV0} are expected to be a small correction to a small quantity. The known SM corrections to four fermion final states are summarized in reference [39].

Mass mixing Mass mixing changes the partial decay widths of the Z_2 because it induces changes in the couplings. The effect is of the order θ_M and is therefore small due to the present experimental limits on the mixing. It is interesting for precision measurements in e^+e^- or $\mu^+\mu^-$ collisions at $s \approx M_2^2$. It must be taken into account together with weak corrections of the full GUT.

Energy dependent width effects At lowest order, a particle has no width. It is obvious that a width is needed to describe a resonance. The simplest approximation is to use the constant width in the propagator, which is calculated in the previous sections. The next step of precision is to take into account that the width is a function of the energy.

In general, the inclusion of a finite width violates gauge invariance because it partially takes into account effects, which are of higher order in perturbation theory. It is shown in [40] that the gauge violating terms can be enhanced by large kinematic factors $\sim s/m_e^2$ in some processes with four fermion final states, i.e. in $e^+e^- \rightarrow e^+W^-\nu_e$. The problem can be cured by the inclusion of additional higher order contributions, which restore the gauge invariance, see [40, 41] for further details.

The effect is under control in fermion pair production where one should take the s -dependent width [42]. It is $\Gamma_2(s) \approx \frac{s}{M_2^2} \Gamma_2(M_2^2)$ if the vector boson can decay only into light particles.

The s -dependence of Γ_2 leads to a shift $\Delta E_{peak} = \frac{1}{2}(\Gamma_2/M_2)^2 M_2$ of the Z_2 peak position [42]. For $s > M_2^2$ the width should be taken s -dependent too because it influences the radiative tail as explained in section 2.1.2.1.

1.1.5 Summary of Z' parameters

Under the assumptions of section 1.1.1, we are left with the following Z' parameters,

$$\begin{aligned}
M_2, \Gamma_2 & \quad \text{the mass and width of the mass eigenstate } Z_2, \\
\theta_M & \quad \text{the } ZZ' \text{ mixing angle,} \\
g_2 & \quad \text{the coupling strength,} \\
v_f(2), a_f(2) & \quad \text{the vector and axial vector couplings to fermions.}
\end{aligned} \tag{1.35}$$

One can choose [43] the following quantities to parametrize the five independent Z_2 couplings (1.27) describing $v_f(2)$ and $a_f(2)$,

$$\begin{aligned}
\epsilon_A & \equiv [L_l(2) - R_e(2)]^2 \frac{g_2^2}{4\pi\alpha M_{Z'}^2 - s} = a_e^2(2) \frac{g_2^2}{4\pi\alpha M_{Z'}^2 - s}, \\
P_V^e & \equiv \frac{L_l(2) + R_e(2)}{L_l(2) - R_e(2)} = \frac{v_e(2)}{a_e(2)}, \\
P_L^q & \equiv \frac{L_q(2)}{L_l(2) - R_e(2)} = \frac{v_q(2) + a_q(2)}{2a_e(2)}, \\
P_R^i & \equiv \frac{R_i(2)}{L_q(2)} = \frac{v_i(2) - a_i(2)}{v_i(2) + a_i(2)}, \quad i = u, d.
\end{aligned} \tag{1.36}$$

In collisions of unpolarized protons, one is insensitive to the relative sign of the Z' couplings. Then, an alternative set of parameters is convenient [44],

$$\begin{aligned}
\gamma_L^l & \equiv \frac{L_l^2(2)}{L_l^2(2) + R_e^2(2)} = \frac{(v'_l + a'_l)^2}{2(v_e'^2 + a_e'^2)}, \\
\gamma_L^q & \equiv \frac{L_q^2(2)}{L_l^2(2) + R_e^2(2)} = \frac{(v'_q + a'_q)^2}{2(v_e'^2 + a_e'^2)}, \\
\tilde{U} & \equiv \frac{R_u^2(2)}{L_q^2(2)} = \frac{(v'_u - a'_u)^2}{(v'_q + a'_q)^2}, \\
\tilde{D} & \equiv \frac{R_d^2(2)}{L_q^2(2)} = \frac{(v'_d - a'_d)^2}{(v'_q + a'_q)^2}.
\end{aligned} \tag{1.37}$$

ϵ_A can be added to equation (1.37) as the fifth parameter.

Both parameter sets are related, see reference [45].

1.2 Extra neutral gauge bosons in E_6 models

In an E_6 GUT [6, 46], the five independent charges Q'^f are constrained [45] in addition to (1.26),

$$Q'^{e\tilde{L}} = Q'^{u\tilde{L}} = Q'^{qL}, \quad Q'^{lL} = Q'^{d\tilde{L}}. \tag{1.38}$$

Therefore, the charges Q'^f of a general Z' in an E_6 GUT can be parametrized by two independent parameters. However, the three conditions (1.38) lead to only two relations between the Z' couplings [45] as far as the ratio g_{12}/g_{22} in equation (1.23) is unknown,

$$2L'_q + R'_u + R'_e = 0, \quad L'_q - R'_d - L'_l + R'_e = 0. \quad (1.39)$$

The experimental check of the conditions (1.39) allows to determine whether a Z' can belong to the E_6 breaking scheme or not.

There are many breakings possible in the E_6 group. See [47] for an extensive discussion. Let us not consider the general E_6 case but restrict ourselves to the gauge breaking scheme

$$E_6 \rightarrow SO(10) \times U(1)_\psi \rightarrow SU(5) \times U(1)_\chi \times U(1)_\psi, \quad (1.40)$$

where the linear combination

$$Z'(\beta) = \chi \cos \beta + \psi \sin \beta \quad (1.41)$$

is assumed to be light. The special case $\eta = Z'(-\arctan \sqrt{5/3})$ is often considered. β is the free parameter in the breaking scheme (1.40). For the χ arising in the breaking of the $SO(10)$ [28, 32, 48, 49] to $SU(5)$ [50] and the ψ arising in the breaking of the E_6 to $SO(10)$, we get

$$-Q'_\chi{}^{qL} = \frac{1}{3}Q'^{lL}_\chi = \frac{1}{\sqrt{40}}, \quad Q'^{qL}_\psi = Q'^{lL}_\psi = \frac{1}{\sqrt{24}}, \quad g_2 = g_1 \sqrt{\frac{5}{3}} s_W, \quad g_{12} = 0. \quad (1.42)$$

Equation (1.23) now defines the couplings of the Z' to SM fermions as given in table 1.1.

| f | E_6 : | a'_f | v'_f | LR: | a'_f | v'_f |
|-------|---------|--|--|-----|---------------------|---|
| ν | | $3\frac{\cos\beta}{\sqrt{40}} + \frac{\sin\beta}{\sqrt{24}}$ | $3\frac{\cos\beta}{\sqrt{40}} + \frac{\sin\beta}{\sqrt{24}}$ | | $\frac{1}{2\alpha}$ | $\frac{1}{2\alpha}$ |
| e | | $\frac{\cos\beta}{\sqrt{10}} + \frac{\sin\beta}{\sqrt{6}}$ | $2\frac{\cos\beta}{\sqrt{10}}$ | | $\frac{\alpha}{2}$ | $\frac{1}{\alpha} - \frac{\alpha}{2}$ |
| u | | $-\frac{\cos\beta}{\sqrt{10}} + \frac{\sin\beta}{\sqrt{6}}$ | 0 | | $-\frac{\alpha}{2}$ | $-\frac{1}{3\alpha} + \frac{\alpha}{2}$ |
| d | | $\frac{\cos\beta}{\sqrt{10}} + \frac{\sin\beta}{\sqrt{6}}$ | $-2\frac{\cos\beta}{\sqrt{10}}$ | | $\frac{\alpha}{2}$ | $-\frac{1}{3\alpha} - \frac{\alpha}{2}$ |

Table 1.1 The vector and axial vector couplings of the Z' to SM fermions in the E_6 and LR models.

One has to be careful with the different notations for β in the literature. For example, the model parameter θ in reference [6] is related to our β as $\beta = \theta + \pi/2$.

Consider the gauge breaking scheme [51, 52]

$$SO(10) \rightarrow SU(3)_c \times SU(2)_L \times SU(2)_R \times U(1)_{B-L} \quad (1.43)$$

as a second example. Now the Z' couples to the current

$$J_{LR}^\beta = \sqrt{\frac{5}{3}} \left(\alpha J_{3R}^\beta - \frac{1}{2\alpha} J_{B-L}^\beta \right), \quad \alpha \equiv \sqrt{\frac{c_W^2 g_R^2}{s_W^2 g_L^2} - 1}, \quad (1.44)$$

where g_L and g_R are the couplings to the left- and right handed gauge groups. J_{3R} is the current associated with the $SU(2)_R$ group and B and L are baryon and lepton numbers, $B - L = 2(Q - T_{3L} - T_{3R})$. α is constrained to lie in the range $\sqrt{2/3} \leq \alpha \leq \sqrt{c_W^2/s_W^2 - 1}$. Within our conventions, we have

$$Q'_{LR}{}^f = Q'_\chi{}^f \sqrt{\frac{2}{5}} \frac{\alpha^2 + 1}{\alpha}, \quad g_2 = g_1 s_W, \quad \frac{g_{12}}{g_2} = \frac{1}{\sqrt{15}} \frac{3\alpha^2 - 2}{\alpha}. \quad (1.45)$$

The case $\alpha = \sqrt{2/3}$ is identical to $Z = \chi$. Again, equation (1.23) gives all Z' couplings to SM fermions shown in table 1.1.

The decay width of a Z' to fermion pairs is small in E_6 theories. Typical values for $\sum_f \Gamma_2^f/M_{Z'}$ are between 0.5% and 2% if only decays to SM fermions are kinematically allowed. If the decays to all exotic fermions and Higgs bosons are possible, Γ_2 becomes roughly three times larger [31, 51].

The entries of the mass matrix (1.11) are completely defined in a fixed model. For example, in a model with a gauge symmetry breaking by two Higgs doublets and one Higgs singlet [31],

$$\Phi_1 = \begin{pmatrix} \phi_1^0 \\ \phi_1^- \end{pmatrix}, \quad \Phi_2 = \begin{pmatrix} \phi_2^+ \\ \phi_2^0 \end{pmatrix}, \quad \Phi_3 = \phi_3^0, \quad \langle \phi_i^0 \rangle = \frac{g v_i}{\sqrt{2}}, \quad i = 1, 2, 3, \quad v^2 = v_1^2 + v_2^2, \quad (1.46)$$

one gets [31]

$$\delta M^2 = 2M_{Z'SW}^2 \frac{Q'(\phi_1)v_1^2 - Q'(\phi_2)v_2^2}{v^2}, \quad M_{Z'}^2 = 4M_{Z'SW}^2 \frac{1}{v^2} \sum_{i=1}^3 [Q'(\phi_i^0)v_i]^2. \quad (1.47)$$

Q'_1 and Q'_2 are the $U'(1)$ charges of the two Higgs doublets. The entry $M_{Z'}^2$ of the mass matrix (1.11) is known from the SM. Equation (1.47) gives an example for the Higgs constraint (1.17). The values of $Q'(\phi_1)$ and $Q'(\phi_2)$ depend on the particular symmetry breaking [53].

The Higgs constraint can be combined with the formula for Γ_2^W . It gives $\Gamma_2^W \approx \Gamma_2^e$ in left-right models [54].

1.3 Extra neutral gauge bosons and contact interactions

Far below the resonance, Z' effects can be described by four fermion contact interactions. The interaction of a Z' with the massless fermions f and F is then given by the amplitude

$$\begin{aligned} \mathcal{M}(Z') = \frac{g_2^2}{M_{Z'}^2} \sum_{f,F} & \left(L'_f L'_F \bar{u}_{f,L} \gamma_\beta u_{f,L} \bar{u}_{F,L} \gamma^\beta u_{F,L} + R'_f R'_F \bar{u}_{f,R} \gamma_\beta u_{f,R} \bar{u}_{F,R} \gamma^\beta u_{F,R} \right. \\ & \left. + R'_f L'_F \bar{u}_{f,R} \gamma_\beta u_{f,R} \bar{u}_{F,L} \gamma^\beta u_{F,L} + L'_f R'_F \bar{u}_{f,L} \gamma_\beta u_{f,L} \bar{u}_{F,R} \gamma^\beta u_{F,R} \right). \end{aligned} \quad (1.48)$$

This can be compared with four fermion contact interactions [55],

$$\begin{aligned} \mathcal{M}(\text{contact}) = 4\pi \sum_{f,F} & \left[\frac{\eta_{LL}^{fF}}{(\Lambda_{LL}^{fF})^2} \bar{u}_{f,L} \gamma_\beta u_{f,L} \bar{u}_{F,L} \gamma^\beta u_{F,L} + \frac{\eta_{RR}^{fF}}{(\Lambda_{RR}^{fF})^2} \bar{u}_{f,R} \gamma_\beta u_{f,R} \bar{u}_{F,R} \gamma^\beta u_{F,R} \right. \\ & \left. + \frac{\eta_{RL}^{fF}}{(\Lambda_{RL}^{fF})^2} \bar{u}_{f,R} \gamma_\beta u_{f,R} \bar{u}_{F,L} \gamma^\beta u_{F,L} + \frac{\eta_{LR}^{fF}}{(\Lambda_{LR}^{fF})^2} \bar{u}_{f,L} \gamma_\beta u_{f,L} \bar{u}_{F,R} \gamma^\beta u_{F,R} \right]. \end{aligned} \quad (1.49)$$

Λ_{ij}^{fF} , $i, j = L, R$ are the scales of the new physics and $\eta_{ij}^{fF} = \pm 1$.

Constraints on four fermion contact interactions can always be interpreted as constraints on extra neutral gauge bosons,

$$\frac{g_2^2 L'_m L'_n}{4\pi M_{Z'}^2} \equiv \frac{L_m^N L_n^N}{s} = \frac{\eta_{LL}^{mn}}{(\Lambda_{LL}^{mn})^2}, \quad m, n = f, F. \quad (1.50)$$

We use the definition

$$L_f^N \equiv L'_f \frac{g_2}{\sqrt{4\pi}} \frac{\sqrt{s}}{M_{Z'}}. \quad (1.51)$$

Relations similar to (1.50) can be written for the other helicity combinations. Note that Z' interactions far below the Z' peak can only constrain the ratios L_f^N, R_f^N and not the Z' couplings and the Z' mass separately.

Interactions of extra neutral gauge bosons are not as general as 4 fermion contact interactions. The Lagrangian (1.48) describes the interaction between fermions of flavours f and F by the *four* couplings L_f^N, L_F^N, R_f^N and R_F^N . The same process is described in contact interactions by the *twelve* parameters Λ_{ij}^{mn} , $i, j = L, R$, $mn = ff, fF, FF$.

If a future helicity conserving experiment shows small deviations from the SM predictions, one can always parametrize the deviation in terms of contact interactions. If the new interaction is due to a Z' , the parameters of the contact interactions fulfill the relations

$$\begin{aligned} \eta_{LL}^{mn} = \eta_{RR}^{mn} = 1, \quad \eta_{LR}^{mn} = \eta_{RL}^{mn}, \quad (\Lambda_{LR}^{mn})^2 = (\Lambda_{RL}^{mn})^2 = \sqrt{(\Lambda_{LL}^{mn})^2 (\Lambda_{RR}^{mn})^2}, \quad mn = ff, fF, FF, \\ (\Lambda_{ii}^{fF})^2 = \sqrt{(\Lambda_{ii}^{ff})^2 (\Lambda_{ii}^{FF})^2}, \quad i = L, R. \end{aligned} \quad (1.52)$$

The normalized Z' couplings can then be calculated according to equation (1.50). Under the assumption of the gauge group (1.1), the Z' couplings must satisfy the additional relations (1.27).

Of course, Z_2 effects near the Z_2 resonance cannot be described by contact interactions.

1.4 Four fermion interactions and form factors

In many experiments, a Z' can be detected through four fermion interactions. In addition to the Z' exchange, we always have the SM contributions where the Z' is replaced by the photon or the Z boson. The contributions due to the exchange of extra neutral gauge bosons can be absorbed into the couplings of the SM Z boson [56]. The following discussion is general for four fermion interactions. It can be directly applied to Bhabha and Møller scattering, $pp, p\bar{p}$ or ep scattering.

Consider the four fermion interaction $e^+e^- \rightarrow f\bar{f}$ ($f \neq e$) as an example. The amplitude for this process is

$$\mathcal{M} = \sum_n \frac{g_n^2}{s - m_n^2} \bar{v}(e) \gamma_\beta \left[v_e(n) - \gamma_5 a_e(n) \right] u(e) \cdot \bar{u}(f) \gamma^\beta \left[v_f(n) - \gamma_5 a_f(n) \right] v(f). \quad (1.53)$$

In the SM, the summation runs over the photon and the Z boson ($n = 0, 1$). In a theory including a Z' , the extra amplitude with the Z' exchange, $\mathcal{M}_E = \mathcal{M}(n = 2)$, has to be added.

It is important that \mathcal{M}_E has the same structure as the SM amplitude. Then one can formally include the contribution of \mathcal{M}_E in the couplings of the SM Z boson leaving the couplings of the photon unchanged.

Consider the amplitude with Z and Z' exchange only,

$$\begin{aligned}
\mathcal{M} &= \sum_{n=1,2} \frac{g_n^2}{s - m_n^2} \bar{v}(e) \gamma_\beta \left[v_e(n) - \gamma_5 a_e(n) \right] u(e) \cdot \bar{u}(f) \gamma^\beta \left[v_f(n) - \gamma_5 a_f(n) \right] v(f) \\
&\equiv \frac{g_1^2}{s - m_1^2} \bar{v}(e) \gamma_\beta u(e) \cdot \bar{u}(f) \gamma^\beta v(f) \cdot v_e(1) v_f(1) (1 + \epsilon_{vv}) \\
&\quad - \bar{v}(e) \gamma_\beta u(e) \cdot \bar{u}(f) \gamma^\beta \gamma_5 v(f) \cdot v_e(1) a_f(1) (1 + \epsilon_{va}) \\
&\quad - \bar{v}(e) \gamma_\beta \gamma_5 u(e) \cdot \bar{u}(f) \gamma^\beta v(f) \cdot a_e(1) v_f(1) (1 + \epsilon_{av}) \\
&\quad + \bar{v}(e) \gamma_\beta \gamma_5 u(e) \cdot \bar{u}(f) \gamma^\beta \gamma_5 v(f) \cdot a_e(1) a_f(1) (1 + \epsilon_{aa}), \\
\text{with} \quad \epsilon_{xy} &= \chi_{Z/Z'} \frac{x_e(2) y_f(2)}{x_e(1) y_f(1)}, \quad x, y = a, v, \quad \chi_{Z'/Z} = \frac{g_2^2 (s - m_1^2)}{g_1^2 (s - m_2^2)}. \tag{1.54}
\end{aligned}$$

The coefficients ϵ_{xy} contain all information of the amplitude \mathcal{M}_E . Various additional amplitudes \mathcal{M}_E arising, for example, from weak corrections or ZZ' mixing, can be written in the form (1.54) if the quantities ϵ_{xy} are specified [57].

Following the tradition of electroweak corrections, we want to parametrize the contributions ϵ_{xy} by (complex) form factors $\rho_{ef}, \kappa_e, \kappa_f, \kappa_{ef}$, which are introduced by replacements of the couplings,

$$\begin{aligned}
v_e(1) v_f(1) &\rightarrow a_e(1) a_f(1) \left[1 - 4|Q^e| s_W^2 \kappa_e - 4|Q^f| s_W^2 \kappa_f + 16|Q^e Q^f| s_W^4 \kappa_{ef} \right], \\
v_e(1) &\rightarrow a_e(1) \left[1 - 4|Q^e| s_W^2 \kappa_e \right], \\
v_f(1) &\rightarrow a_f(1) \left[1 - 4|Q^f| s_W^2 \kappa_f \right], \\
a_e(1), a_f(1) &\rightarrow \text{unchanged}, \\
g_1^2 = &\rightarrow g_1^2 \rho_{ef}. \tag{1.55}
\end{aligned}$$

Comparing with equation (1.54), the form factors can be expressed through ϵ_{xy} ,

$$\begin{aligned}
\rho_{ef} &= 1 + \epsilon_{aa} \\
\kappa_f &= \frac{1}{\rho_{ef}} \left[1 + \frac{\epsilon_{av} v_f(1) - \epsilon_{aa} a_f(1)}{v_f(1) - a_f(1)} \right] \\
\kappa_{ef} &= \frac{1}{\rho_{ef}} \left[1 + \frac{\epsilon_{vv} v_e(1) v_f(1) + \epsilon_{aa} a_e(1) a_f(1) - \epsilon_{av} a_e(1) v_f(1) - \epsilon_{va} v_e(1) a_f(1)}{[v_e(1) - a_e(1)][v_f(1) - a_f(1)]} \right]. \tag{1.56}
\end{aligned}$$

In particular, the additional Z' amplitude can be included in the Z couplings specifying ϵ_{xy} as given in equation (1.54),

$$\begin{aligned}
\rho_{ef} &= 1 + \chi_{Z'/Z} \frac{a_e(2) a_f(2)}{a_e(1) a_f(1)}, \\
\kappa_f &= \frac{1}{\rho_{ef}} \left[1 + \chi_{Z'/Z} \frac{a_e(2) [v_f(2) - a_f(2)]}{a_e(1) [v_f(1) - a_f(1)]} \right],
\end{aligned}$$

$$\kappa_{ef} = \frac{1}{\rho_{ef}} \left[1 + \chi_{Z'/Z} \frac{a_e(2)[v_f(2) - a_f(2)][v_e(2) - a_e(2)]}{a_e(1)[v_f(1) - a_f(1)][v_e(1) - a_e(1)]} \right]. \quad (1.57)$$

The result agrees with the formulae given in reference [58]. As mentioned there, this method of the inclusion of the Z' contributions has the advantage that it can be easily implemented in computer codes designed for SM calculations. The form factors (1.56) and (1.57) work equally well for any four fermion process. They include the Z' contribution without any approximation. Of course, they are s -dependent, in general not small and even resonating near the Z' peak.

Consider the case where two additional amplitudes are added to \mathcal{M}_{SM} ,

$$\mathcal{M} = \mathcal{M}_{SM} + \mathcal{M}_1 + \mathcal{M}_2. \quad (1.58)$$

Suppose that both additional amplitudes are parametrized in the way described above, i.e. assume that the form factors $\rho_{ef}^i, \kappa_e^i, \kappa_f^i, \kappa_{ef}^i$, $i = 1, 2$ are known. Then, the combined form factors can be calculated by taking into account $\epsilon_{xy}^\Sigma = \epsilon_{xy}^1 + \epsilon_{xy}^2$,

$$\rho_{ef}^\Sigma = \rho_{ef}^1 + \rho_{ef}^2 - 1, \quad \kappa_f^\Sigma = \frac{\kappa_f^1 \rho_{ef}^1 + \kappa_f^2 \rho_{ef}^2 - 1}{\rho_{ef}^1 + \rho_{ef}^2 - 1}, \quad \kappa_{ef}^\Sigma = \frac{\kappa_{ef}^1 \rho_{ef}^1 + \kappa_{ef}^2 \rho_{ef}^2 - 1}{\rho_{ef}^1 + \rho_{ef}^2 - 1}. \quad (1.59)$$

The summation rules (1.59) are exact. In many applications, the form factors are not very different from one. In this case, the approximate summation rules

$$\rho_{ef}^\Sigma = \rho_{ef}^1 \rho_{ef}^2, \quad \kappa_f^\Sigma = \kappa_f^1 \kappa_f^2, \quad \kappa_{ef}^\Sigma = \kappa_{ef}^1 \kappa_{ef}^2 \quad (1.60)$$

are often used. In their derivation, contributions proportional to $\epsilon_{xy}\epsilon_{x'y'}$ are neglected.

The case (1.58) arises, for example, in the simultaneous description of ZZ' mixing and electroweak corrections. The functions ϵ_{xy}^m describing the ZZ' mixing are

$$\begin{aligned} \epsilon_{xy}^m &= \chi_{Z_1/Z} \left(c_M + \frac{g_{Z'}}{g_Z} s_M \frac{x'_e}{x_e} \right) \left(c_M + \frac{g_{Z'}}{g_Z} s_M \frac{y'_f}{y_f} \right) - 1, \quad x, y = a, v, \\ \chi_{Z_1/Z} &= \frac{s - m_Z^2}{s - m_1^2}. \end{aligned} \quad (1.61)$$

Again, the resulting form factors can be calculated [57] using equation (1.56),

$$\begin{aligned} \rho_{ef}^m &= \chi_{Z_1/Z} \left(c_M + \frac{g_{Z'}}{g_Z} s_M \frac{a'_e}{a_e} \right) \left(c_M + \frac{g_{Z'}}{g_Z} s_M \frac{a'_f}{a_f} \right), \\ \kappa_f^m &= \frac{1 + \frac{s_M g_{Z'}}{c_M g_Z} \frac{v'_f - a'_f}{v_f - a_f}}{1 + \frac{s_M g_{Z'}}{c_M g_Z} \frac{a'_f}{a_f}}, \\ \kappa_{ef}^m &= \kappa_e^m \kappa_f^m. \end{aligned} \quad (1.62)$$

The form factors ρ_{ef}^m, κ_f^m and κ_{ef}^m are related to the functions x_f and y_f introduced in equation (1.28),

$$\rho_{ef}^m = (1 - y_e)(1 - y_f), \quad \kappa_f^m = 1 - x_f. \quad (1.63)$$

1.5 Model dependence of Z' constraints

Future experiments will either be consistent with the SM or show deviations from the SM predictions. In the first case, the data can be used to constrain extensions of the SM, for example, contact interactions or theories predicting extra neutral gauge bosons. In the case of a deviation, one can try to interpret it in terms of Z' parameters. This procedure could either fail or favor some Z' models compared to others. The analysis can be done with or without assumptions on the Z' model. We call these procedures *model dependent* and *model independent* analyses.

Of course, there are several steps from the model independent Z' analysis to the model dependent Z' analysis. As far as the model assumptions are consistent with the experimental data, a model dependent analysis is justified and welcome to learn more details about the underlying theory.

For example, helicity conserving processes can be parametrized by four fermion contact interactions. Only little can be learned about the origin of the new interaction in this case. If there are deviations from the SM and the conditions (1.52) and (1.27) are fulfilled, the new interaction is consistent with a Z' coming from the gauge group (1.1). This theoretical assumption increases our knowledge about the origin of the new interaction. If the couplings fulfill the relations (1.39), the new interaction is consistent with a Z' coming from the E_6 group. The subsequent assumption that the new interaction *is* due to a Z' from an E_6 breaking, increases the model dependence but allows to probe further details of the assumed model. The experimental verification that $-3L'_q = L'_l$ is also fulfilled supports the hypothesis that the interaction is due to a Z' from a $SO(10)$ breaking. Finally, the new interaction could be tested for compatibility with a definite Z' , e.g. $Z' = \chi$. This hypothesis contains most model assumptions but allows more detailed tests of the theory and the best fits to the remaining free parameters.

Examples of model dependent Z' constraints are the lower bounds on $M_{Z'}$ or the regions of θ_M allowed for certain E_6 models quoted in the Particle Data Book.

For a *model independent* analysis, one has to pay a price. Usually, one cannot constrain single Z' parameters but only certain combinations of them. Often, only a limited set of observables is useful for the model independent analysis. Examples of model independent Z' constraints are the allowed regions of $v_f^M = v_f' \theta_M$ and $a_f^M = a_f' \theta_M$ from LEP 1 data [59, 60, 61], the constraints on $v_i^N \approx v_i' / M_{Z'}$ and $a_i^N \approx a_i' / M_{Z'}$ from LEP2 data [62] or the constraints on $\sigma_T^l = \sigma(p\bar{p} \rightarrow Z') \cdot Br_2^l$ from Tevatron data [63].

Model independent Z' constraints can always be converted into model dependent Z' constraints specifying the Z' model. The constraints on model parameters obtained in such a two-step procedure are in general weaker than the constraints that would be obtained by a direct model dependent fit to the same data.

Model dependent and model independent Z' analyses are complementary. Both analyses have advantages and disadvantages, which are summarized in table 1.2. Throughout this paper, we explicitly mention whether a constraint is obtained in a model dependent or in a model independent analysis.

| Model dependent Z' analysis | Model independent Z' analysis |
|--|--|
| – The constraints are a mixture of experimental results and theoretical assumptions. | + The constraints result from data only. They are not biased by theoretical assumptions. |
| – A separate data analysis is needed for every new Z' model. | + Z' limits for a new Z' model can be deduced without a new data analysis. |
| + Single Z' parameters can be constrained. | – Only combinations of Z' parameters can be constrained. |
| + Z' limits from different experiments can always be compared. | – Z' limits from different experiments cannot always be compared. |

Table 1.2 Advantages (+) and disadvantages (–) of a model dependent and model independent Z' analysis.

1.6 Extracting Z' limits from data

In any analysis, one selects observables O_i from the data and compares them with the predictions $O_i(\text{SM}+Z')$ in a theory including a Z' . This allows to exclude or to confirm Z' models at a given confidence level. The procedure is different in experiments with indirect and with direct Z' limits.

1.6.1 Indirect Z' limits

In experiments with indirect Z' signals, for example in $e^+e^- \rightarrow \mu^+\mu^-$ below the Z' resonance, the SM already predicts a large number of events of the given signature. A Z' gives a signal in the observable O_i if it produces a deviation $\Delta^{Z'}O_i$ from the SM prediction $O_i(\text{SM})$, which is larger than the experimental error ΔO_i . Here and in the following, ΔO_i stands for the error of an asymmetry, the error of a ratio of cross sections or for the relative error of a cross section. Because of the large number of events, these errors can be assumed to be Gaussian distributed. Neglecting correlations, we define

$$\chi^2 = \sum_i \left[\frac{O_i - O_i(\text{SM} + Z')}{\Delta O_i} \right]^2. \quad (1.64)$$

For $\chi^2 > \chi_{min}^2 + \chi_{cl}^2$, the considered model is excluded at a certain confidence level depending on χ_{cl} .

In a real experiment, all possible observables would be measured and contribute to the final result. In a *theoretical* analysis, the additional information due to measurements of two observables O_1 and O_2 related by theory (i.e. $O_1(\text{SM} + Z') = O_2(\text{SM} + Z')$) could be taken into account by the inclusion of *one* of these observables but with a smaller effective error

ΔO_Σ . This error can be estimated as

$$\begin{aligned}\chi^2 &= \sum_{i=1,2} \left[\frac{O_i - O_i(\text{SM} + Z')}{\Delta O_i} \right]^2 = \left[\frac{O_1 - O_1(\text{SM} + Z')}{\Delta O_\Sigma} \right]^2, \\ \frac{1}{(\Delta O_\Sigma)^2} &= \sum_{i=1,2} \frac{1}{(\Delta O_i)^2}.\end{aligned}\tag{1.65}$$

The generalization to more observables is straight forward.

Experimental errors consist of statistical and systematic contributions. We assume in the estimates of the following sections that the combined error is the quadratic sum,

$$\Delta O = \sqrt{(\Delta^{stat} O)^2 + (\Delta^{syst} O)^2} = \Delta^{stat} O \sqrt{1 + r^2}.\tag{1.66}$$

We define the ratio $r = \Delta^{syst} O / \Delta^{stat} O$.

Optimal observables [64, 65] can be constructed to get the maximum sensitivity to Z' parameters. To measure (small) Z' parameters $\lambda(Z')$ in indirect Z' analyses, one can look for deviations in differential cross sections,

$$d\sigma(\phi) = d\sigma_{SM}(\phi) + d(\Delta^{Z'} \sigma(\phi)) = d\sigma_{SM}(\phi) + \lambda(Z') d\tilde{\sigma}(\phi).\tag{1.67}$$

Examples for $\lambda(Z')$ are θ_M or \sqrt{s}/M_2 . The Z' parameter is measured by an integration over the phase space $d\phi$ with a weight function $f(\phi)$ [64],

$$f^{(1)}(\lambda(Z')) = \int f(\phi) d\sigma(\phi).\tag{1.68}$$

The weight function can be chosen in such a way that the sensitivity to $\lambda(Z')$ becomes maximum. For one parameter, one gets [64], $f(\phi) = \Delta^{Z'} \sigma(\phi) / \sigma_{SM}(\phi)$. The generalization to several parameters is given in reference [65].

1.6.2 Direct Z' limits

Direct Z' production is possible in e^+e^- or $\mu^+\mu^-$ collisions for $s \approx M_2^2$ or in hadron collisions for $s > M_2^2$.

In direct production in e^+e^- or $\mu^+\mu^-$ collisions, many Z' events are expected at future colliders. It can be assumed that the events are Gaussian distributed allowing a χ^2 analysis (1.64). In contrast to indirect Z' limits, the number of Z' events at the Z_2 peak is much larger than the SM background allowing precision measurements.

In direct Z' production at hadron colliders, the number of SM background events is expected to be very small or zero. A few Z' events serve as a signal. Then, one cannot assume that these events are Gaussian distributed. Constraints on Z' models at a given confidence level are obtained for all models, which predict the same number of Z' events. For example, in the case where the signal is Poisson distributed, the SM background is zero and zero events are observed, all theories predicting $N_{Z'} = 3$ events are excluded at 95% confidence [66]. For a non-zero background, $N_{Z'}$ depends on it [66].

Chapter 2

Z' search at e^+e^- , e^-e^- and $\mu^+\mu^-$ colliders

Lepton colliders have the advantage that different observables can be detected above a small background. As has been shown by the LEP and SLC experiments, different fermions as e, μ, τ, c, b can be tagged in the final state. The polarization of τ 's and likely of top quarks can be measured. Highly polarized electron beams are available. One can also hope for a reasonable positron polarization. At muon colliders, one expects some polarization of both beams [67].

e^+e^- and $\mu^+\mu^-$ collisions yield several interesting reactions which can probe different properties of extra Z bosons.

Fermion pair production allows for a measurement of a large number of different observables. It is assumed that the final fermions are not electrons or electron neutrinos. All couplings of the Z' to charged SM fermions can be constrained separately. This is a unique property of this reaction.

Bhabha and *Møller scattering* have much larger event rates than fermion pair production. In addition, Møller scattering could profit from two highly polarized electron beams. Of course, these reactions are sensitive to gauge boson couplings to electrons only. The sensitivity to these couplings competes with fermion pair production.

W pair production is very sensitive to ZZ' mixing. This sensitivity is enhanced for large energies because a non-zero ZZ' mixing destroys the gauge cancellation between the different amplitudes present in the SM. The sensitivity to other Z' parameters cannot compete with fermion pair production.

All *other reactions* in e^+e^- or e^-e^- collisions can not add useful information on extra neutral gauge bosons.

Although we will explicitly mention mostly e^+e^- and e^-e^- collisions, all results presented in this chapter are also applicable to $\mu^+\mu^-$ or $\mu^-\mu^-$ collisions. One important difference arises for measurements on and beyond the Z_2 peak. As known from Z_1 physics, a precise measurement of the mass and the width of the resonance relies crucially on the accurate monitoring of the beam energy. Here, a muon collider would have clear advantages compared to an electron collider [67] because the latter suffers from a large beam energy spread.

2.1 Z' search in $e^+e^- \rightarrow f\bar{f}$

The sensitivity of fermion pair production to different Z' parameters depends crucially on the ratio of the center-of-mass energy \sqrt{s} to the masses M_1 and M_2 of the gauge bosons Z_1 and Z_2 . We distinguish four different cases,

$$\begin{aligned}
 \text{case 1:} & \quad s \approx M_1^2, \\
 \text{case 2:} & \quad M_1^2 \neq s < M_2^2, \\
 \text{case 3:} & \quad s \approx M_2^2, \\
 \text{case 4:} & \quad s > M_2^2,
 \end{aligned} \tag{2.1}$$

where $s \approx M_n^2$ means $(M_n - \Gamma_n)^2 < s < (M_n + \Gamma_n)^2$.

Case 1 is very important in setting constraints on the ZZ' mixing angle. The Z_2 propagator, i.e. the sensitivity to M_2 is usually suppressed by a factor Γ_1/M_1 .

Case 2 would give the first signals of a Z' in e^+e^- collisions. The SM parameters are already precisely known from measurements at the Z_1 peak leading to accurate predictions for observables at higher energies. Information about a Z' is obtained from the differences to these predictions. If there is agreement with the SM predictions, lower bounds on the Z' mass can be set for a fixed model. The sensitivity to the ZZ' mixing angle is suppressed by a factor Γ_1/M_1 compared to measurements at the Z_1 peak.

Case 3 is certainly the best possibility to get precise and detailed information about a Z' . The corresponding measurements have much in common with the LEP and SLC experiments at the Z_1 peak.

Case 4 is interesting because it can constrain a Z' with couplings to SM fermions much weaker than predicted in the usual GUT's. Such a Z' could escape detection in experiments below its resonance.

This section is organized as follows. After giving the relevant observables in the Born approximation, we discuss the different radiative corrections. A discussion of constraints on Z' parameters in the four cases (2.1) follows in different subsections. Model dependent and model independent constraints are distinguished.

Every subsection on Z' constraints is organized by the same pattern. For every constrained Z' parameter, the physical origin of the constraint is explained first and a simple estimate is given. The estimate is then confronted with Z' constraints obtained from present experiments and with constraints obtained in theoretical analyses for future colliders.

2.1.1 Born Approximation

2.1.1.1 Amplitude

The amplitude for $e^+e^- \rightarrow (\gamma, Z, Z', \dots) \rightarrow f\bar{f}$, $f \neq e$ is

$$\mathcal{M} = \sum_n \frac{g_n^2}{s - m_n^2} \bar{v}(e) \gamma_\beta \left[v_e(n) - \gamma_5 a_e(n) \right] u(e) \bar{u}(f) \gamma^\beta \left[v_f(n) - \gamma_5 a_f(n) \right] v(f). \tag{2.2}$$

The summation runs over the exchanged gauge bosons. In contrast to equation (1.48), we use here the parametrization in vector and axial vector couplings. This is useful because the

photon has a pure vector coupling while the Z boson has almost a pure axial vector coupling to the e^+e^- pair in the initial state.

Only products of an *even* number of couplings of the Z' to fermions appear in the amplitude (2.2). Hence, the process $e^+e^- \rightarrow f\bar{f}$ cannot distinguish between Z' models, which differ only by the signs of all Z' couplings to fermions.

Measurements at one energy point sufficiently far away from the Z_1 and Z_2 resonances can only restrict the normalized couplings a_f^N and v_f^N [68],

$$a_f^N \equiv a_f(2) \sqrt{\frac{g_2^2 s}{4\pi m_2^2 - s}} \quad \text{and} \quad v_f^N \equiv v_f(2) \sqrt{\frac{g_2^2 s}{4\pi m_2^2 - s}} \quad (2.3)$$

and not the Z_2 couplings $a_f(2), v_f(2)$ and the Z_2 mass m_2 separately. Therefore, a heavy Z_2 with large couplings cannot be distinguished from a light Z_2 with small couplings as far as $M_2^2 \gg s$. Below the resonance, fermion pair production by a Z' can be described by effective four fermion contact interactions, see section 1.3. Note that the definition (2.3) differs slightly from the definition (1.51). We will use definition (2.3) in this section because it is natural in fermion pair production. For comparisons with other reactions the definition (1.51) must be used. Note that the difference between the two definitions is $O(s/M_2^2)$. This is a small quantity for Z' masses at the detection limit $M_{Z'} \approx 3\sqrt{s}$ to $7\sqrt{s}$.

Several widths Γ_2 below the M_2 resonance, the width Γ_2 does not influence the Z' limits and can be neglected. Therefore, the indirect Z' limits from fermion pair production remain valid for extra Z bosons which have for some reason a width much larger than predicted in usual GUT's. This is an important difference with Z' limits from hadron colliders, which depend on Γ_2 through branching ratios as Br_2^μ .

The amplitude can be decomposed as $\mathcal{M} = \mathcal{M}_{SM} + g_2\theta_M\mathcal{M}_M$ on the Z_1 resonance in the limit of small ZZ' mixing. According to equation (1.28), \mathcal{M}_M is proportional to either a'_f or v'_f . Therefore, measurements at the Z_1 peak constrain the combinations

$$a_f^M = \theta_M g_2 a'_f \quad \text{and} \quad v_f^M = \theta_M g_2 v'_f, \quad (2.4)$$

and not a'_f, v'_f and θ_M separately [18]. Similar to the off-resonance case, a Z' with large couplings and small ZZ' mixing cannot be distinguished from a Z' with small couplings and large ZZ' mixing as far as $\theta_M \ll 1$.

2.1.1.2 Cross section

The total and the forward-backward cross sections are defined as

$$\sigma_T = \int_{-1}^1 dc \frac{d\sigma}{dc}, \quad \sigma_{FB} = \int_0^1 dc \frac{d\sigma}{dc} - \int_{-1}^0 dc \frac{d\sigma}{dc}, \quad c = \cos \theta. \quad (2.5)$$

θ is the angle between the outgoing anti-fermion \bar{f} and the incoming positron. At the Born level, the cross sections σ_A^f , $A = T, FB$ are

$$\sigma_A^f = d_A \sum_{m,n=0}^N \sigma_A^0(s; m, n) = d_A N_f \frac{\pi\alpha^2}{s} \sum_{m,n=0}^N C_A(m, n) \chi_m(s) \chi_n^*(s) \quad (2.6)$$

with $d_T = \frac{4}{3}$ and $d_{FB} = 1$. N_f is due to color, $N_f = 1(3)$ for $f = l(q)$.

The summation runs over all interferences. $\chi_n(s)$ is the propagator of the vector boson Z_n with the invariant energy squared s ,

$$\chi_n(s) = \frac{g_n^2}{4\pi\alpha} \frac{s}{s - m_n^2}. \quad (2.7)$$

$C_T(m, n)$ and $C_{FB}(m, n)$ contain the vector and axial vector couplings of the gauge boson Z_n to the fermion f , $v_f(n)$ and $a_f(n)$, and the helicities of the initial (λ_+, λ_-) and final (h_+, h_-) fermions,

$$\begin{aligned} C_T(m, n; \lambda_1, \lambda_2, h_1, h_2) &= C_T(\text{initial fermions}) \times C_T(\text{final fermions}), \\ C_T(\text{initial fermions}) &= \lambda_1[v_e(m)v_e^*(n) + a_e(m)a_e^*(n)] + \lambda_2[v_e(m)a_e^*(n) + a_e(m)v_e^*(n)], \\ C_T(\text{final fermions}) &= h_1[v_f(m)v_f^*(n) + a_f(m)a_f^*(n)] + h_2[v_f(m)a_f^*(n) + a_f(m)v_f^*(n)], \\ C_{FB}(m, n; \lambda_1, \lambda_2, h_1, h_2) &= C_T(m, n; \lambda_2, \lambda_1, h_2, h_1) \end{aligned} \quad (2.8)$$

with

$$\begin{aligned} \lambda_1 &= 1 - \lambda_+\lambda_-, & \lambda_2 &= \lambda_+ - \lambda_-, \\ h_1 &= \frac{1}{4}(1 - h_+h_-), & h_2 &= \frac{1}{4}(h_+ - h_-). \end{aligned} \quad (2.9)$$

The unpolarized case corresponds to $\lambda_+ = \lambda_- = h_+ = h_- = 0$, i.e. $\lambda_1 = h_1 = 1$ and $\lambda_2 = h_2 = 0$. The couplings of the vector bosons to fermions are given in section 1.1.3.

The left–right cross sections are defined as

$$\begin{aligned} \sigma_{LR} &= \sigma_T(\lambda_- = -1, \lambda_+ = 0) - \sigma_T(\lambda_- = +1, \lambda_+ = 0), \\ \sigma_{LR,FB} &= \sigma_{FB}(\lambda_- = -1, \lambda_+ = 0) - \sigma_{FB}(\lambda_- = +1, \lambda_+ = 0), \end{aligned} \quad (2.10)$$

where a summation over the polarizations of the final states is assumed. The cross section

$$\sigma_{pol} = \sigma_T(h_- = -1, h_+ = 0) - \sigma_T(h_- = +1, h_+ = 0) \quad (2.11)$$

is useful if the polarization of the final state can be measured.

The differential cross section can be calculated from σ_T and σ_{FB} as

$$\frac{d\sigma}{dc} = \frac{3}{8}(1 + c^2) \cdot \sigma_T + \frac{1}{2}c \cdot \sigma_{FB}. \quad (2.12)$$

We would like to mention here that cross sections depending on transverse polarizations can be considered if the polarization of the final state is measurable or if transverse beam polarization is available, see [69] for a general discussion and [70] for applications to LEP 1. Simple transverse asymmetries are suppressed as m_f/\sqrt{s} , where m_f is the mass of the polarized particle, while double transverse asymmetries don't have such a suppression. We do not consider these potentially interesting observables here because they suffer from experimental difficulties.

For b - and top quark production, the finite fermion mass m_f must be taken into account in the cross section (2.8),

$$\begin{aligned} C_T(\text{final fermions}) &= [v_f(m)v_f^*(n) + a_f(m)a_f^*(n)] \left[1 + \frac{1}{2}h_1 + \frac{\beta^2}{2}(-2 + h_1) \right] \beta \\ &\quad - a_f(m)a_f^*(n) \frac{1}{2}(2 + h_1)(1 - \beta^2)\beta + [v_f(m)a_f^*(n) + a_f(m)v_f^*(n)]h_2\beta^2, \\ C_{FB}(\text{final fermions}) &= [v_f(m)a_f^*(n) + a_f(m)v_f^*(n)]h_1\beta^2 + v_f(m)v_f^*(n)h_2\beta - a_f(m)a_f^*(n)h_2\beta^3. \end{aligned} \quad (2.13)$$

We have $\mu^2 = 4m_f^2/s$ and $\beta = \sqrt{1 - \mu^2}$.

2.1.1.3 ZZ' mixing

The effect of ZZ' mixing is already included in the couplings $v_f(n), a_f(n), n = 1, 2$ by definition (1.28). One can rewrite equation (2.8) in terms of the unmixed couplings and form factors x_f, y_f , which take into account the mixing,

$$\begin{aligned} v_f(1) &\rightarrow a_f(1) \left[1 - 4|Q^f|s_W^2(1 - x_f) \right], \\ a_f(1) &\rightarrow a_f, \\ \frac{\pi\alpha}{2s_W^2c_W^2} &\rightarrow \frac{\pi\alpha}{2s_W^2c_W^2}(1 - y_e)(1 - y_f). \end{aligned} \quad (2.14)$$

This formalism is very useful at the Z_1 peak where ZZ' mixing and electroweak corrections must be described simultaneously [30]. The replacements (2.14) must also be applied to the couplings in the total width Γ_1 appearing in the propagator.

2.1.1.4 Observables

Helicity conservation allows non-zero cross sections for only the four different spin configurations $\lambda_+ = -\lambda_- = \pm 1$ and $h_+ = -h_- = \pm 1$. Furthermore, we see from equation (2.8) that the forward–backward cross section σ_{FB} is uniquely related to the total cross section σ_T . Therefore, only four of the cross sections and asymmetries, which one can construct from σ_T^f and σ_{FB}^f , are independent. An example of independent observables are the total cross section and simple asymmetries,

$$\begin{aligned} \sigma_T^f &\quad \text{total cross section,} \\ A_{FB}^f = \frac{\sigma_{FB}^f}{\sigma_T^f} &\quad \text{forward–backward asymmetry,} \\ A_{LR}^f = \frac{\sigma_{LR}^f}{\sigma_T^f} &\quad \text{left–right asymmetry,} \\ A_{pol}^f = \frac{\sigma_{pol}^f}{\sigma_T^f} &\quad \text{polarization asymmetry of the final state.} \end{aligned} \quad (2.15)$$

They can be constructed for every final fermion flavour f .

Not all observables listed above are measurable. All four observables require the detection of the flavour f . Forward–backward asymmetries require discrimination between particles and antiparticles. Left–right asymmetries require beam polarization. A_{pol}^f requires a measurement of the polarization of one final particle.

One can measure combined asymmetries for some final states.

$$\begin{aligned} A_{LR,FB}^f &\quad \text{combined left–right forward–backward asymmetry,} \\ A_{pol,FB}^f &\quad \text{combined polarization forward–backward asymmetry,} \\ A_{LR,pol}^f &\quad \text{combined left–right polarization asymmetry.} \end{aligned} \quad (2.16)$$

As mentioned above, the combined asymmetries must be related to simple asymmetries,

$$A_{LR,pol}^f = \frac{4}{3}A_{FB}^f, \quad A_{pol,FB}^f = \frac{3}{4}A_{LR}^f, \quad A_{LR,FB}^f = \frac{3}{4}A_{pol}^f. \quad (2.17)$$

Assuming lepton universality, we find a further relation between observables with leptons in the final state,

$$A_{LR}^l = A_{pol}^l. \quad (2.18)$$

Of course, the relations (2.17) and (2.18) do not hold for $m_f \neq 0$. They are modified by radiative corrections. However, as we will see in the next section, they are a good approximation for light final state fermions and radiative corrections with appropriate kinematic cuts.

In a theoretical analysis, the additional information due to measurements of several related observables as A_{LR}^l and A_{pol}^l could be taken into account by the inclusion of only *one* of these observables but with a smaller effective error, see equation (1.65).

Optimal observables [64, 65] can be constructed to enhance the sensitivity to Z' parameters.

Two parameters, the axial vector and the vector coupling of the Z' to charged *leptons*, a'_l, v'_l , are measured by three independent observables. Contradictory signals in all three observables could disprove a Z' as the origin of these signals. A consistent measurement of non-zero a'_l or v'_l allows the measurement of couplings to the other fermions f by the four additional independent observables (2.15). Therefore, two additional relations between the four observables must be fulfilled if the interaction is due to a Z' . At the Z' peak, they are $A_{FB}^f = \frac{3}{4}A_{pol}^f A_{LR}^e$ and $A_{LR}^f = A_{LR}^e$ for $m_f = 0$ in the Born approximation. Again, the hypothesis of a new vector boson could be disproved. If the deviation turns out to be inconsistent with Z' interactions, one can try to describe the new physics in the more general framework of four fermion contact interactions (1.49).

To eliminate the systematic errors from the luminosity measurement and flavour detection and to reduce the sensitivity to radiative corrections, ratios of total cross sections are considered as well as observables depending on the sum of all light 5 quark flavours,

$$R^{had} = \frac{\sigma_T^{u+d+s+c+b}}{\sigma_T^\mu}, \quad A_{LR}^{had} = A_{LR}^{u+d+s+c+b}, \quad R_b = \frac{\sigma_T^b}{\sigma_T^{u+d+s+c+b}}, \quad R_c = \frac{\sigma_T^c}{\sigma_T^{u+d+s+c+b}}. \quad (2.19)$$

Similar observables are defined by the sum over all lepton flavours (considering only the s -channel contribution for final electrons). We denote them with the flavour index l .

At the peak of a gauge boson Z_n , the partial decay widths $\Gamma_n^f = \Gamma(Z_n \rightarrow f\bar{f})$ are important additional observables.

As mentioned before, we do not consider asymmetries involving transverse polarizations. There is one potentially interesting observable, the P and T odd transverse-normal spin correlation, which is proportional to the imaginary part of the product of the propagators of the exchanged gauge bosons. This observable gives bounds on M_2 from measurements at the Z_1 peak, which are not suppressed by the factor Γ_1/M_1 . Unfortunately, this potential sensitivity is completely killed by the loss of statistics in the measurements of the two transverse correlations of the final τ 's [71]. Contributions proportional to the imaginary part of the Z_1 propagator are suppressed as Γ_1/M_1 off the Z_1 peak.

2.1.2 Radiative corrections

All observables entering the Z' search must be predicted with theoretical errors smaller than the expected experimental error. This demands the inclusion of radiative corrections. Fortunately, not all radiative corrections are of equal importance. This allows simplifying approximations. The $O(\alpha)$ corrections to the SM process are presented in references [72, 73, 74, 75, 76], for a review see [77].

2.1.2.1 QED corrections

Among the complete $O(\alpha)$ corrections to $e^+e^- \rightarrow (\gamma, Z, Z', \dots) \rightarrow f\bar{f}$, the numerically largest QED corrections are a gauge invariant subset. Furthermore, initial state corrections, final state corrections, and the interference between them are separately gauge invariant. The QED corrections can be calculated in a model independent way. They depend on the kinematics as the scattering angles and the energies of all final particles. We focus here on QED corrections to light fermion production.

The final state corrections and the interference between initial and final state corrections to the new Z' interferences can be obtained from the SM result. The initial state corrections to the Z' interferences are calculated in [78] and [79] for massless and in [80] for massive final fermions.

We discuss here the initial state radiation because it is of major importance for Z' tagging. Initial state corrections can be calculated in the structure function approach [81],

$$\sigma^{ISR}(s) = \int_{x_1^-}^1 dx_1 \int_{x_2^-}^1 dx_2 D(x_1, s) D(x_2, s) \sigma^0(x_1 x_2 s). \quad (2.20)$$

The structure function approach assumes that the colliding electron and positron have energies degraded by radiated photons, which is described by the structure function $D(x, s)$. The structure function is independent of the particular observable. To calculate the corrections to distributions, one has to boost the final particle pair to the laboratory system for every choice of x_1 and x_2 . This is easy in Monte Carlo algorithms but impossible in analytical calculations.

Alternatively, initial state corrections can be calculated in the flux function approach,

$$\sigma_A^{ISR}(s) = \left[1 + S(\epsilon) \right] \sigma_A^0(s) + \int_{\epsilon}^{\Delta} dv \sigma_A^0 \left(s(1-v) \right) H_A^e(v). \quad (2.21)$$

The flux functions $H_A^e(v)$ depend on the particular observable. They describe the probability of the emission of a photon with a certain energy fraction. v is the energy of the emitted photon in units of the beam energy. For σ_T, σ_{FB} and $d\sigma/dc$ they can be found in references [73], [82] and [76]. To order $O(\alpha)$, we have

$$\begin{aligned} H_T^e(v) &= \bar{H}_T^e(v) + \frac{\beta_e}{v} = \beta_e \frac{1 + (1-v)^2}{2v}, \\ H_{FB}^e(v) &= \bar{H}_{FB}^e(v) + \frac{\beta_e}{v} = \frac{\alpha}{\pi} (Q^e)^2 \frac{1 + (1-v)^2}{v} \frac{1-v}{(1-\frac{v}{2})^2} \left[L_e - 1 - \ln \frac{1-v}{(1-\frac{v}{2})^2} \right], \\ \beta_e &= \frac{2\alpha}{\pi} (Q^e)^2 (L_e - 1), \quad L_e = \ln \frac{s}{m_e^2}, \quad Q^e = -1. \end{aligned} \quad (2.22)$$

The quantity $[1 + S(\epsilon)]$ in equation (2.21) describes the Born term plus corrections due to soft and virtual photons. To order $O(\alpha)$, we have

$$S(\epsilon) = \bar{S} + \beta_e \ln \epsilon = \beta_e \left(\ln \epsilon + \frac{3}{4} \right) + \frac{\alpha}{\pi} (Q^e)^2 \left(\frac{\pi^2}{3} - \frac{1}{2} \right). \quad (2.23)$$

The structure function and the flux function approach give an equivalent description of QED corrections. See references [38, 83] for an extensive discussion and further references.

Starting from the convolution (2.21), the origin of the radiative tail and its magnitude can be estimated. We do this ignoring details of the radiator functions $S(\epsilon)$ and $H_A^e(v)$. The s' dependence of the Born cross section is

$$\sigma_A \approx \frac{1}{s'} \chi_m(s') \chi_n^*(s') = \frac{s}{m_n^{*2} - m_n^2} \frac{1}{s} \left[\frac{s'}{s' - m_n^{*2}} - \frac{s'}{s' - m_n^2} \right]. \quad (2.24)$$

For $m = n$, the first factor of the last expression becomes

$$\frac{s}{m_n^{*2} - m_n^2} = -\frac{i M_n}{2 \Gamma_n} \frac{s}{M_n^2}. \quad (2.25)$$

This imaginary quantity must be met by another imaginary multiplier to give contributions to the cross section. Because we average over transverse polarizations, it can arise only from the v integration (2.21) over the remaining factors of equation (2.24). Keeping only the relevant term after partial fraction decomposition, one gets

$$\sigma_T^{ISR}(s) - \sigma_T^0(s) \approx \frac{i M_n}{2 \Gamma_n} \frac{s}{M_n^2} \frac{1}{s} \int_0^\Delta dv \frac{1}{1 - v - m_n^{*2}/s} \approx \frac{i M_n}{2 \Gamma_n} \ln \frac{m_n^{*2}/s - 1 + \Delta}{m_n^{*2}/s - 1}. \quad (2.26)$$

The real part of the argument of the logarithm is negative for $s > M_n^2$ and $\Delta > 1 - M_n^2/s$. These are the necessary conditions for the development of the radiative tail; the center-of-mass energy must be larger than the mass of the resonance, and the radiation of photons must be allowed, which are sufficiently hard to ensure a ‘‘radiative return’’ to the resonance.

We now estimate the magnitude of the radiative tail by restoring the missing factors,

$$\text{rad. tail} \approx \sigma_T^{ISR}(s) - \sigma_T^0(s) \approx \sigma_T^0(s; n, n) \cdot \beta_e \frac{\pi M_n}{2 \Gamma_n}. \quad (2.27)$$

Only the contribution of the exchange of the vector boson n appears in equation (2.27). Therefore, the other interferences are not enhanced by the radiative tail. Putting $s_W^2 = \frac{1}{4}$ and $M_n/\Gamma_n = M_1/\Gamma_1$, one gets $\sigma_T^l(s; 0, 1) = 0$ and $\sigma_T^l(s; 1, 1)/\sigma_T^l(s; 0, 0) = 1/9$ in the limit $s \gg M_Z^2$. This gives

$$\text{rad. tail} \approx 7 \cdot \sigma_T^l(s; 1, 1) \approx 7/10 \cdot \sigma_T^l, \quad (2.28)$$

which is in reasonable agreement with the exact calculation and with figure 2.1. For b quark production, where the Z boson exchange $\sigma_T^b(s; 1, 1)$ dominates over the photon exchange $\sigma_T^b(s; 0, 0)$, the effect of the radiative tail is much more pronounced.

The radiative tail enhances SM cross sections, while for $M_{Z'} > \sqrt{s}$ the Z' signal is not enhanced. Therefore, the radiative tail must be removed for a Z' search below the Z' resonance. This can be done by removing events with hard photons by demanding $\Delta < 1 - M_1^2/s$.

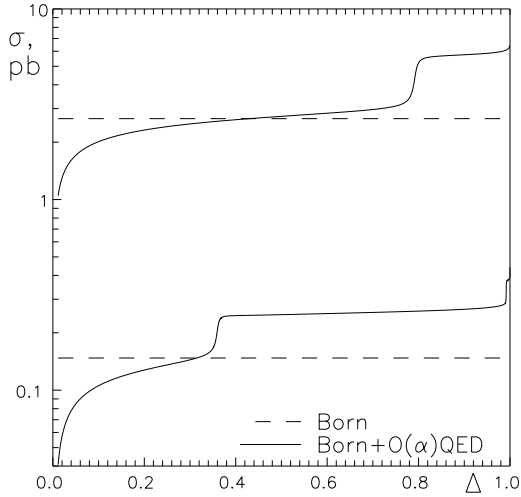


Figure 2.1 The total cross section σ_T^μ as function of the cut on the photon energy Δ in units of the beam energy for $M_{Z'} = M_\eta = 800 \text{ GeV}$. The upper (lower) set of curves corresponds to $\sqrt{s} = 200(1000) \text{ GeV}$. This is figure 1 from reference [57].

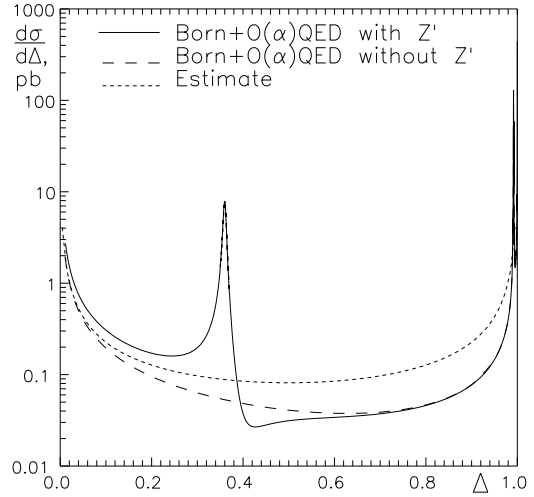


Figure 2.2 $d\sigma_T^\mu/d\Delta$ as function of the photon energy Δ in units of the beam energy. For the solid line, we choose $M_{Z'} = M_\eta = 800 \text{ GeV}$ and $\sqrt{s} = 1000 \text{ GeV}$. The dashed line is the SM. The dotted line is the function $\sigma_T^{\mu 0} \beta_e / [\Delta(1 - \Delta)]$, compare estimate (2.85).

The dependence of the cross section on Δ is shown in figure 2.1 for two different energies. The upper curve corresponds to an energy above the Z peak but below the Z' peak, the lower curves to an energy above the Z and Z' peaks. One recognizes the step-like behaviour for photon energies where the radiative tail(s) are “switched on”. We see that the radiatively corrected cross section is numerically similar to the Born prediction only for a certain cut, which rejects all hard photons from the radiative returns to resonances. This is the reason why Z' analyses at the Born level give limits, which are numerically similar to those obtained with radiative corrections and appropriate kinematic cuts. Of course, radiative corrections must be included in fits to real data.

The radiative tail is due to the emission of photons with energies E_γ in the (narrow) interval

$$\Delta^- = 1 - \frac{M_n^2}{s} - \frac{M_n \Gamma_n}{s} < \frac{E_\gamma}{E_{beam}} < 1 - \frac{M_n^2}{s} + \frac{M_n \Gamma_n}{s} = \Delta^+. \quad (2.29)$$

Therefore, experiments with energies above resonances have sharp peaks in the photon energy spectrum. This is illustrated in figure 2.2. There, the Z_1 and Z_2 resonances are represented by peaks at $E_\gamma/E_{beam} = \Delta_n = 1 - M_n^2/s$ with $\Delta_1 = 0.992$ and $\Delta_2 = 0.36$. All final states $f\bar{f}$ contribute to the peaks. Their heights and widths depend on the width of the related gauge boson as indicated in equations (2.26) and (2.29).

2.1.2.2 Weak corrections

The precision of present and future e^+e^- colliders is high enough to be sensitive to weak corrections. They can be implemented by form factors [58, 84, 85] applying the following formal replacements of the coupling constants in the Born cross section,

$$\begin{aligned}
v_f(0) &\rightarrow v_f(0)F_A(q^2), \\
v_e(1)v_f(1) &\rightarrow a_e(1)a_f(1) \left[1 - 4|Q^e|s_W^2\kappa_e - 4|Q^f|s_W^2\kappa_f + 16|Q^eQ^f|s_W^4\kappa_{ef} \right], \\
v_e(1) &\rightarrow a_e(1) \left[1 - 4|Q^e|s_W^2\kappa_e \right], \\
v_f(1) &\rightarrow a_f(1) \left[1 - 4|Q^f|s_W^2\kappa_f \right], \\
a_e(1), a_f(1) &\rightarrow \text{unchanged}, \\
g_1^2 = \frac{4\pi\alpha}{2s_W^2c_W^2} &\rightarrow \sqrt{2}G_\mu M_Z^2 \rho_{ef}.
\end{aligned} \tag{2.30}$$

The complex functions $\rho_{ef}, \kappa_e, \kappa_f$ and κ_{ef} contain all information about the SM weak corrections, while the complex function $F_A(q^2)$ takes into account the effects of the vacuum polarization of the photon. Although the largest contribution to $F_A(q^2)$ comes from QED, we feel that it should be mentioned in this section. If the new functions are set to one, we recover the Born formulae. κ_{ef} is different from $\kappa_e\kappa_f$ due to box contributions, which enforce the additional replacement rule for the combination $v_e(1)v_f(1)$. The conjugated couplings in the Born cross section have to be replaced with the corresponding complex conjugated relations (2.30). The functions κ_e, κ_f and κ_{ef} can be absorbed in effective Weinberg angles.

ZZ' mixing effects and weak corrections have to be treated simultaneously for predictions at the Z_1 peak. According to equations (2.14) and (1.60), it can be done [30] by the following replacements in equation (2.30),

$$\begin{aligned}
\kappa_f &\rightarrow \kappa_f^M = \kappa_f(1 - x_f), \\
\kappa_{ef} &\rightarrow \kappa_{ef}^M = \kappa_{ef}(1 - x_e)(1 - x_f), \\
\rho_{ef} &\rightarrow \rho_{ef}^M = \rho_{ef}\rho_{mix}(1 - y_e)(1 - y_f), \\
M_Z^2 &\rightarrow M_1^2.
\end{aligned} \tag{2.31}$$

In (2.31), we have neglected terms, which are proportional to the SM weak corrections times the mixing angle θ_M . The multiplier $\rho_{mix} = M_Z^2/M_1^2$ takes into account that the replacement (2.30) of g_1^2 is valid only for the mass of the symmetry eigenstate M_Z . Alternatively, one could calculate the form factors (2.31) by the sum rule (1.59) where $\kappa_f^1, \kappa_{ef}^1$ and ρ_{ef}^1 are the weak form factors κ_f, κ_{ef} and ρ_{ef} and $\kappa_f^2, \kappa_{ef}^2$ and ρ_{ef}^2 are the mixing form factors $\kappa_f^m, \kappa_{ef}^m$ and ρ_{ef}^m given in equation (1.62). The replacements (2.31) must also be made to the Z_1 width entering the propagator of the mass eigenstate.

Non-standard one loop corrections cannot be calculated without knowledge about the underlying theory. If the Z' is the first signal of physics beyond the SM, these corrections will probably not play an important role. They are expected to be a small correction to a small deviation from the SM prediction.

See references [25, 86] for the renormalization of $SU(2)_L \times U(1)_Y \times U'(1)$ gauge theories.

2.1.2.3 QCD corrections

QCD corrections have to be taken into account in the case of hadronic final states. They don't feel the gauge boson exchanged before. Therefore, the known SM results for massless [34] and massive [35, 87, 88] final state fermions can be used. The $O(\alpha_s)$ QCD corrections can be obtained from the $O(\alpha)$ final state QED corrections by the replacement $\alpha \rightarrow \frac{4}{3}\alpha_s$. They depend on the mass of the final state fermion and on the maximal allowed energy $E_g = \Delta_g\sqrt{s}/2$ of the radiated gluon. For $m_f = 0$ and $\Delta_g = 1$, the lowest order QCD corrections vanish for forward-backward asymmetries and reduce to the well known factor $1 + \alpha_s/\pi$ for total cross sections.

As known from SM calculations, radiative corrections due to spin asymmetries of the final state need special care. Due to spin-flip contributions induced by gluon radiation, the result of a calculation with zero fermion masses $m_f = 0$ does not coincide with the result calculated for $m_f \neq 0$ in the limit $m_f \rightarrow 0$ [89]. The problem also arises in final state QED corrections, however, it is numerically less important because α is numerically smaller than α_s .

2.1.2.4 Corrections to Γ_1

As is known from the experiments at LEP and SLC, the measurements on the Z_1 resonance are sensitive to radiative corrections to the Z_1 width. In contrast to the corrections to Γ_2 described in section 1.1.4.2, we give here the formulae including the weak corrections to Γ_1 ,

$$\Gamma_1^f = \frac{N_f G_\mu \sqrt{2} M_1^3}{12\pi} \rho_f^Z \mu R_{\text{QED}} R_{\text{QCD}}(M_1^2) \left\{ [v_f(1)^2 + a_f(1)^2] \left(1 + 2 \frac{m_f^2}{M_1^2} \right) - 6 a_f(1)^2 \frac{m_f^2}{M_1^2} \right\}. \quad (2.32)$$

The functions R_{QED} and R_{QCD} describing the QED and QCD corrections [34] are given in equation (1.34).

The function ρ_f^Z absorbs Δr arising during the replacement of the weak coupling constant by the muon decay constant,

$$g_1^2 = \frac{4\pi\alpha}{s_W^2 c_W^2} = \frac{G_\mu \sqrt{2} M_Z^2}{1 - \Delta r} = \frac{G_\mu \sqrt{2} M_W^2}{(1 - \Delta r) c_W^2}. \quad (2.33)$$

As in $e^+e^- \rightarrow f\bar{f}$, the remaining weak corrections can be taken into account [37] by a replacement of the vector couplings,

$$v_f(1) \rightarrow a_f(1) [1 - 4|Q^f|s_W^2\kappa_f]. \quad (2.34)$$

The functions κ_f are often absorbed in s_W^2 defining effective Weinberg angles. In comparison to the weak corrections to $e^+e^- \rightarrow f\bar{f}$, we have no box contributions in the Z_1 decay. Therefore, a special replacement rule (2.30) for the product $v_e(1)v_f(1)$ is absent.

In the case of a non-zero ZZ' mixing, we have to apply additional replacements similar to the rule (2.31),

$$\begin{aligned} \rho_Z^f &\rightarrow \rho_Z^f \rho_{\text{mix}}(1 - y_f)^2, \\ \kappa_f &\rightarrow \kappa_f = \kappa_f(1 - x_f). \end{aligned} \quad (2.35)$$

2.1.3 Z' constraints at $s \approx M_1^2$

The Z' signal in measurements at the Z_1 peak is a deviation of the couplings of the mass eigenstate Z_1 to fermions from the SM prediction. This prediction depends on the SM parameters, which are also defined by measurements at the Z_1 peak. If one wants to constrain Z' parameters from the same data, the cleanest analysis would be a simultaneous fit of SM and Z' parameters. We call this procedure *direct Z' analysis*.

Alternatively, the data distributed around the Z_1 peak can be fitted first in a model independent procedure. The results of such a fit are M_1 , partial and total decay widths Γ_1^f and cross sections and asymmetries at the peak. This output is the input of a second fit, which determines the SM and Z' parameters. We call this procedure *indirect Z' analysis*. The first direct analysis was done in [30]. The indirect analyses are shown to agree with this direct analysis.

As mentioned in the introduction, we will not consider the mixing of the new fermions with SM fermions. See reference [90] for such an analysis based on LEP 1 data.

In the following subsections, we discuss different Z' constraints. We always start with a derivation of a simple estimate. This estimate shows the scaling of the constraint with different parameters of the experiment as integrated luminosity, center-of-mass energy and systematic errors. We then discuss present constraints and possible constraints from future experiments and prove the quality of our estimates.

2.1.3.1 Model independent constraints on v_f^M and a_f^M

Estimate The quantities v_f^M and a_f^M defined in equation (2.4) can be constrained at the Z_1 peak independently of the Z' model.

Consider the partial decay width and different asymmetries at the Z_1 peak,

$$\begin{aligned}\Gamma_1^f &= M_1 \frac{g^2}{12\pi} \left[v_f^2(1) + a_f^2(1) \right] N_f \approx \Gamma_1^{f0} \left\{ 1 + 2 \frac{v_f v_f^M + a_f a_f^M}{g_1(v_f^2 + a_f^2)} \right\} = \Gamma_1^{f0} + \Delta^{Z'} \Gamma_1^f, \\ A_{FB}^f &= \frac{3}{4} A_e A_f \approx A_{FB}^{f0} + \frac{3}{4} A_e^0 \Delta A_e + \frac{3}{4} A_e^0 \Delta A_f = A_{FB}^{f0} + \Delta^{Z'} A_{FB}^f, \\ A_{LR}^f &= A_e \approx A_e^0 + \Delta A_e = A_{LR}^0 + \Delta^{Z'} A_{LR}, \\ A_{pol}^f &= \frac{4}{3} A_{LR,FB} = A_f \approx A_f^0 + \Delta A_f = A_{pol}^{f0} + \Delta^{Z'} A_{pol}^f\end{aligned}\tag{2.36}$$

$$\text{with } A_f \equiv \frac{2a_f(1)v_f(1)}{a_f(1)^2 + v_f(1)^2}, \text{ and } \Delta A_f \approx 2 \frac{v_f a_f^M + a_f v_f^M}{g_1(v_f^2 + a_f^2)} - 4 \frac{a_f^2 v_f a_f^M + v_f^2 a_f v_f^M}{g_1(v_f^2 + a_f^2)^2}.\tag{2.37}$$

The index zero denotes the observables without mixing.

If the deviation $\Delta^{Z'} O_i$ in the observable O_i is larger than the experimental error ΔO_i ,

$$\Delta^{Z'} \Gamma_1^f > \Delta \Gamma_1^f, \quad \Delta^{Z'} A_{FB}^f > \Delta A_{FB}^f, \quad \Delta^{Z'} A_{LR}^f > \Delta A_{LR}^f, \quad \Delta^{Z'} A_{pol}^f > \Delta A_{pol}^f,\tag{2.38}$$

one can see a signal. The relations (2.38) and (1.60) predict that the different observables are blind to Z' models predicting v_f^M and a_f^M between two parallel lines. Neglecting systematic

errors, the Z' constraints (2.38) scale like $1/\sqrt{L}$. For $f = e, \nu$ and $s_W^2 = \frac{1}{4}$, equations (2.36) and (2.38) transform to

$$|a_e^M| > \frac{g_1}{4} \frac{\Delta\Gamma_1^e}{\Gamma_1^{e0}}, \quad |a_\nu^M + v_\nu^M| > \frac{g_1}{2} \frac{\Delta\Gamma_1^\nu}{\Gamma_1^{\nu0}}, \quad |v_e^M| > \frac{g_1}{6} \frac{\Delta A_{FB}^e}{A_e^0}, \quad |v_e^M| > \frac{g_1}{4} \Delta A_{LR}^e. \quad (2.39)$$

The constraint from A_{FB}^e linear in θ_M exists only for $s_W^2 \neq \frac{1}{4}$ leading to $A_e^0 \neq 0$. The equations (2.39) allow an independent constraint or measurement of $a_\nu^M + v_\nu^M = L_\nu^M$ and L_e^M and therefore an experimental check [59, 60] of the relations (1.27).

Present constraints Model independent Z' constraints based on the combined data of LEP and SLC [91] are discussed in references [23, 59, 60, 61]. Before confronting Γ_1^f, A_{FB}^f and A_{LR}^f with the data, radiative corrections have to be included. This implies a substitution of g_1^2 with G_μ in the expression (2.30) for Γ_1^f . The substitution induces a dependence on $\rho_{mix} = M_Z^2/M_1^2$. This spoils the model independent limits on v_f^M, a_f^M making them dependent on the additional Z' parameter M_2 .

The problem is solved in references [59, 60] by considering special *combinations* of observables where the leading dependence on ρ_{ef} and ρ_{mix} drops out. As a result, these special combinations are also much less sensitive to the top and the Higgs mass.

With the recent experimental data [91] on $M_W, G_\mu, s_W^2, \alpha(M_Z^2)$ and M_t , one can follow another procedure and calculate ρ_{mix} according to equation (2.33). One gets $\rho_{mix} = 1 \pm 0.003$, compare [92]. The main sources of the uncertainty of ρ_{mix} are the experimental error of the M_W measurement and the theoretical error of Δr arising due to the unknown Higgs mass and to a less extent due to the experimental error of the top mass. In the two- σ errors, the experimental error in the M_W measurement dominates because the theoretical error in Δr is not doubled. We assumed that the symmetry is broken by one Higgs doublet only. In general, one would obtain different results for extended Higgs sectors. In this sense, the error of ρ_{mix} still contains a model dependence, which is expected to be small. The expression of Γ_1^f is now independent of M_2 . The price one has to pay is that the uncertainty of ρ_{mix} must be added to the experimental error of Γ_1^f .

Figure 2.3 illustrates the constraints on a_i^M and v_i^M obtained from the data [91], $\Gamma_1^l = (83.91 \pm 0.11) MeV$, $A_{FB}^l = 0.0174 \pm 0.0010$, $A_\tau = 0.1401 \pm 0.0067$. In the SM, we have $A_\tau = A_{pol}^\tau = A_{LR}^\tau$. The plotted regions correspond to a $\chi^2 = \chi_{min}^2 + 5.99$. In contrast to the demonstration in reference [61], we take into account the deviations of the measurements from the theoretical prediction in figures 2.3 and 2.4. The constraints from Γ_l and from A_{FB}^l and A_τ combined are shown separately for $\rho_{mix} = 1$. The quantitative agreement with the estimates (2.39) is very good. The excluded regions are slightly rotated relative to the axes because $s_W^2 \neq \frac{1}{4}$. The deviation of the experimental value from the theoretical prediction leads to a parallel shift of the exclusion region of the corresponding observable. All three observables combined cannot exclude the region inside the ellipse. The uncertainty of ρ_{mix} yields a shift of the ellipse, which results in the larger solid region. This shift is possible only in one direction because we always have $M_1 < M_Z$ according to equation (1.14). Future improved measurements of M_W and M_t and a determination of M_H would reduce the shift.

The present data are consistent with the assumption (1.25), i.e. with $L_e^M = L_\nu^M$. One could then interpret the constraint (2.39) from the invisible width as a constraint to L_e^M . Unfortunately, this gives no improvement to the combined region shown in figure 2.3.

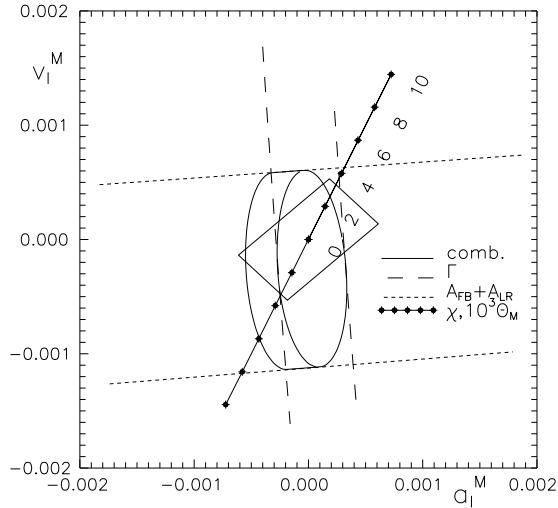


Figure 2.3 Areas of (a_1^M, v_1^M) , for which the extended gauge theory's predictions are indistinguishable from the SM (95% CL). Models between the dashed (dotted) lines cannot be detected with Γ_l , (A_{FB}^l and A_{LR}^l together). The regions surrounded by the solid lines cannot be resolved by all three observables combined, see text. The numbers at the straight line indicate the value of θ_M in units of 10^{-3} for the χ model. The dots for $\theta_M < 0$ are not labeled. The rectangle is calculated from figure 2.18.

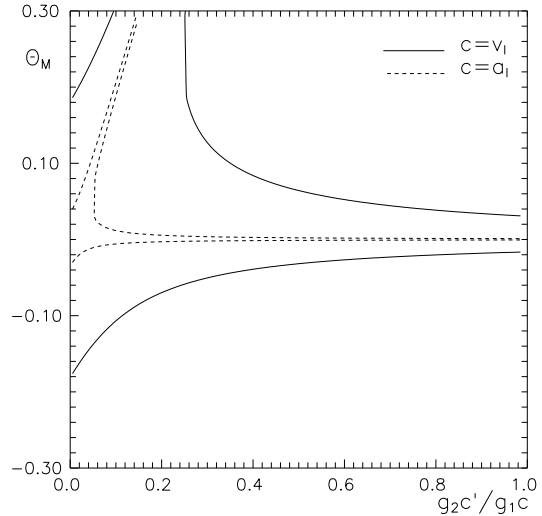


Figure 2.4 Areas of $(g_2 a_1' / (g_1 a_1), \theta_M)$ and $(g_2 v_1' / (g_1 v_1), \theta_M)$, for which the extended gauge theory's predictions are indistinguishable from the SM (95% CL). This figure is an update of figure 4 in reference [61].

The *model independent* constraint shown in figure 2.3 can be interpreted as a constraint on the ZZ' mixing angle θ_M for any fixed model with known couplings a_i' and v_i' . Varying the mixing angle, one moves on a straight line on figure 2.3. This line intersects the model independent exclusion limit for certain values of θ_M . The values of θ_M at the intersection points define the excluded regions of θ_M . Graphically, one obtains $-0.006 < \theta_M < 0.0025$ for the χ model. The model independent constraints obtained from a one-parameter fit are expected to be stronger.

Model independent limits on v_q^M, a_q^M can be obtained in a similar procedure, see reference [61].

A global fit to LEP data would allow to constrain the 5 independent couplings $L_i^M, R_e^M, L_q^M, R_u^M$ and R_d^M simultaneously. These couplings are defined in analogy to v_f^M, a_f^M ,

$$L_f^M = \theta_M g' L_f', \quad R_f^M = \theta_M g' R_f'. \quad (2.40)$$

Future constraints The present constraints on a_e^M and v_e^M obtained from LEP data can be improved by future measurements of the reaction $e^+e^- \rightarrow W^+W^-$. The rectangle in figure 2.3

is calculated from figure 1 of reference [93]. See section 2.3 for details.

The constraints on a_q^M and v_q^M from the Z_1 peak cannot be improved by measurements at $M_1^2 \neq s < M_2^2$. Future measurements at the Z_2 peak (if it exists) allow a separate measurement of the couplings a'_f, v'_f and of the mixing angle θ_M .

2.1.3.2 Model independent constraint on θ_M

Figure 2.3 is independent of θ_M as far as θ_M is small. This allows the derivation of a model independent constraint on θ_M . In the simplest approximation, where only the linear terms in θ_M are kept in equation (1.28), we obtain the estimate

$$|\theta_M| < \frac{\Delta c}{c} \frac{g_1 c}{g_2 c'}, \quad \text{where } c = a_l, v_l \text{ and } c' = a'_l, v'_l. \quad (2.41)$$

Δc is the bound on a_l^M or v_l^M taken from figure 2.3. In particular, the estimate (2.41) gives $|\theta_M| < 0.003$ for $g_2 a'_l / (g_1 a_l) = 0.62$ as it is the case in many GUT's.

The exact numerical result for θ_M as a function of $g_2 a'_l / (g_1 a_l)$ is shown in figure 2.4. The approximate bound (2.41) is recovered at large $g_2 c' / (g_1 c)$. In contrast to (2.41), the exact calculation gives a constraint on θ_M also for a Z' with zero coupling, i.e. for $g_2 c' / (g_1 c) = 0$. It is $|\theta_M| < 0.035$ for $c = a_l$. This can easily be understood from equation (1.28) where the deviations of the couplings $a_f(1)$ or $v_f(1)$ from a_f or v_f with increasing θ_M eventually become larger than the experimental error even for the case $g_2 = 0$.

If one allows a large ZZ' mixing, there is one particular Z' with *all* couplings proportional to those of the SM Z boson *and* a fine-tuned overall coupling strength,

$$g_2 c'_f = g_1 c_f \frac{1 - c_M}{s_M}, \quad c = a, v, \quad f = l, c, b, \quad (2.42)$$

which will not produce a deviation of $c_f(1)$ from c_f . The beginning of this region of insensitivity can be recognized in figure 2.4. Models with fine tuning (2.42) in all couplings can only be detected by effects of the Z' propagator.

2.1.3.3 Model dependent constraint on θ_M and M_2

Estimate θ_M can be much better constrained in particular Z' models because they link the Z' couplings to leptons and to quarks by model parameters. Assuming $v'_f \approx v_f$ and $a'_f \approx a_f$, we obtain from equation (2.39),

$$|\theta_M| < \theta_M^{lim} \approx \frac{g_1}{2g_2} \frac{\Delta\Gamma_1^f}{\Gamma_1^f}. \quad (2.43)$$

The constraint (2.43) scales with the integrated luminosity L as

$$\theta_M^{lim} \sim \left[\frac{1 + r^2}{L} \right]^{1/2}. \quad (2.44)$$

r is the ratio of the systematic and statistical error as defined in equation (1.66).

Consider now the sensitivity to M_2 . For simplicity, we assume $\theta_M = 0$ identifying $Z_2 = Z'$ and $Z_1 = Z$. Again, we assume that the Z and Z' couple with the strengths g_1 and g_2 to SM fermions setting $v'_f \approx v_f, a'_f \approx a_f$. Only the ZZ' interference is important near the Z resonance, Then, we can approximate the relative shift of cross sections, $\Delta^{Z'}O/O_{SM} = \Delta\sigma_T/\sigma_T$ by a ratio of propagators,

$$\frac{\Delta^{Z'}O}{O_{SM}} \approx \frac{g_2^2}{g_1^2} \frac{|\Re\chi_Z\chi_{Z'}^*|}{|\chi_Z|^2} = \frac{g_2^2}{g_1^2} \frac{s - M_Z^2}{M_{Z'}^2 - s}. \quad (2.45)$$

The deviation $\Delta^{Z'}O$ has to be compared with the experimental error ΔO . Choosing $\sqrt{s} = M_Z + \Gamma_Z/2$, we conclude that a Z' with a mass

$$M_{Z'} < M_{Z'}^{lim} = M_Z \left(1 + \frac{g_2^2}{g_1^2} \frac{O}{\Delta O} \frac{\Gamma_Z}{M_Z}\right)^{1/2} \equiv M_Z \left(1 + \frac{1}{\Delta o} \frac{\Gamma_Z}{M_Z}\right)^{1/2}, \quad \Delta o = \frac{g_1^2}{g_2^2} \frac{\Delta O}{O} \quad (2.46)$$

would be detected by the observable O . The factor Γ_Z/M_Z reflects the suppression of the ZZ' interference relative to the resonating contribution.

One exception is the transverse-normal spin asymmetry mentioned in section 2.1.1.4. It is proportional to the imaginary part of the product of the propagators. Hence, it has no suppression factor Γ_1/M_1 . Unfortunately, this potential sensitivity is compensated by the loss of statistics in the measurement of this asymmetry [71]. The result is a net sensitivity to M_2 weaker than (2.46).

Present constraints Measurements at the Z_1 resonance give the best present limits on ZZ' mixing [66].

The analysis of LEP data requires the inclusion of weak corrections. This induces a dependence of the limits on the Higgs and the top mass. Sometimes, θ_M and M_2 are fitted as independent parameters, which corresponds to a Higgs sector consisting of an arbitrary number of Higgs doublets and singlets. One should note that in this case the weak corrections calculated within the minimal SM are only approximate. For a specified Higgs sector, θ_M and M_2 are related by the Higgs constraint (1.17). This relation transforms the tight limits on θ_M to limits on M_2 , which are much better than those obtained for unconstrained Higgs sectors, compare also figure 7 in reference [94].

The present two-dimensional constraint of the parameter space θ_M, M_2 from L3 data is shown in figure 2.5. The figure is based on LEP data published in 1997 [95]. A χ^2 fit to the observables $\sigma_T^l, A_{FB}^l, A_{pol}^\tau, R_b$ and A_{FB}^b is performed. The bound on θ_M is dominated by the data from the Z_1 peak, while the bound on M_2 is dominated by the data above the Z_1 peak.

Constraints on θ_M for a Z' in E_6 models obtained in the same analysis [103] are shown in figure 2.6. We see that the data give tight constraints on θ_M for all models considered.

Several indirect [23, 59, 60, 90, 94, 96, 97, 98, 99] and direct [30, 62, 100, 101, 103] Z' analyses have been performed recently. We can only comment on some of them and compare the results with the naive estimates derived in the previous section.

Reference [94] , DELAGUILA92 This analysis is based on LEP data published in [104] and on $\nu q, \nu_\mu e, eH$ data [105], atomic parity violation data [106] and on data on M_W [105, 107], see table 1 of reference [94]. The limit on θ_M , see figure 7 of reference [94],

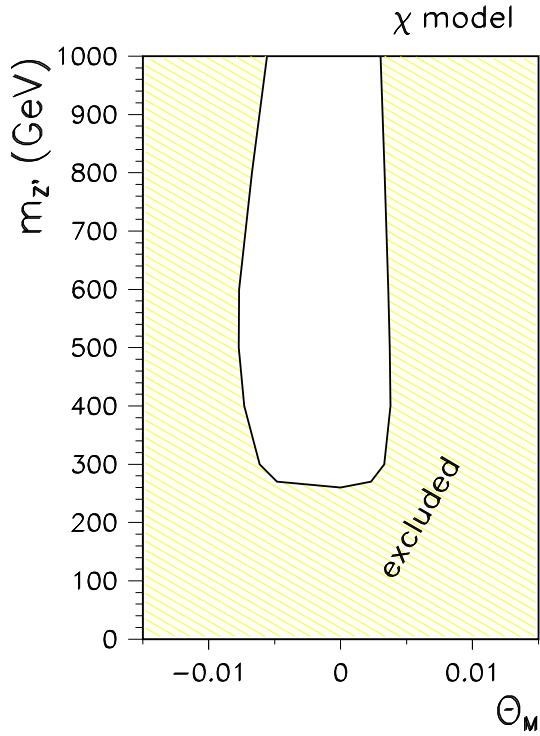


Figure 2.5 The 95% CL allowed regions in the $\theta_M - M_{Z'}$ plane for the χ model. The input of this figure is $M_Z = (91.1863 \pm 0.0019) \text{ GeV}$, $M_t = (175 \pm 6) \text{ GeV}$, $M_H = 150 \text{ GeV}$ and $\alpha_s = 0.118 \pm 0.003$. This figure is a preliminary result taken from reference [102].

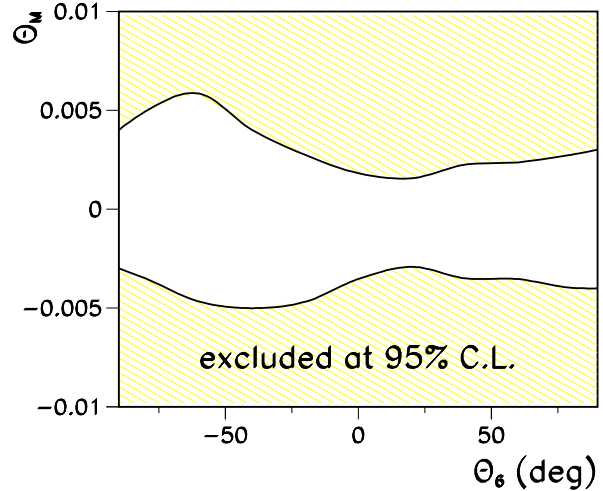


Figure 2.6 The 95% CL bounds on the ZZ' mixing angle, θ_M , as a function of the E_6 parameter $\beta = \theta_6$. The input of this figure is $M_Z = (91.1863 \pm 0.0019) \text{ GeV}$, $M_t = (175 \pm 6) \text{ GeV}$, $M_H = 150 \text{ GeV}$, $\alpha_s = 0.118 \pm 0.003$ and $M_{Z'} > 550 \text{ GeV}$. This is figure 1 from reference [103].

is dominantly set by the LEP data. Special attention is paid to the constraints on the breaking parameters of the E_6 theory by the data. Furthermore, the correlation between $M_{Z'}$ and M_t is considered in detail. We show in table 2.1 the bounds taken from figure 7 for $M_{Z'} = 700 \text{ GeV}$, $M_t = 130 \text{ GeV}$ and $M_H = 100 \text{ GeV}$. We select $\Gamma_1 = (2485 \pm 9) \text{ MeV}$ from the data [104] for the estimate (2.43) of θ_M . We multiply the 90% CL numbers given in [94] by 1.195 to estimate the 95% CL bounds.

Reference [30], LEIKE92 This analysis is based on the data from reference [108], which includes the LEP data from 1989 and 1990. It is the first *direct* Z' analysis. It is shown there that the results of earlier *indirect* analyses [60, 109, 110] agree with the results of the direct analysis. The values of θ_M given in table 2.1 are taken from figure 3 of [30] for $M_{Z'} = 700 \text{ GeV}$, $M_t = 150 \text{ GeV}$ and $M_H = 300 \text{ GeV}$. We use $\Gamma_Z = (2487 \pm 10) \text{ MeV}$ based on the data [108] for our estimate.

Reference [96], ALTARELLI93 This analysis is based on LEP data [111] and on CDF and UA2 data. The limits on θ_M are dominated by the LEP data. In addition, the data are interpreted in terms of the ϵ parameters defined in [112] and in models with specified Higgs sectors. Note that the angle θ_2 parametrizing the E_6 models introduced there is connected with β introduced in equation (1.41) by the relation $\beta = \theta_2 - \arctan \sqrt{5/3}$. We take θ_M from table 5 for $M_t = 150 \text{ GeV}$ and $M_H = 100 \text{ GeV}$ choosing $\theta_2 = 0, 50, -30$

degrees for $Z' = \eta, \chi, \psi$. These values θ_2 are only approximate for $Z' = \chi(\psi)$, where the exact values should be 52.2(-37.8) degrees. Furthermore, we exploited the insensitivity of the reaction $e^+e^- \rightarrow f\bar{f}$ relative to the simultaneous change of the signs of all Z' couplings to fermions, i.e. to a shift $\theta_2 \rightarrow \theta_2 + \pi$. We multiplied the numbers from table 5 in reference [96] by 1.96 to estimate 95% CL numbers from the values given at one- σ . We select $\Gamma_Z = (2489 \pm 7) MeV$ from the data [111] for our estimate.

Reference [101] , ABREU95 This *direct* Z' analysis of the DELPHI collaboration is based on LEP data from 1990 to 1992. The limits on θ_M are obtained for $M_t = 150 GeV$ and $M_H = 300 GeV$. The effect of α_s is small as far as it is chosen between 0.118 and 0.128.

Reference [3] , CVETIČ97 This analysis is based on LEP and SLD data [113], [114]. The CDF constraint $M_t = (175 \pm 6) GeV$ is included. We take the 95% CL bounds on θ_M from table 2. Our estimate is based on Γ_Z from the data [113], [114].

Reference [102] , S.RIEMANN97 This analysis is based on L3 data [115] and LEP data [116] published in 1996 and 1997. It includes the recent measurements beyond the Z_1 peak. The measurements on the Z_1 peak define the limits on θ_M , while the measurements beyond the Z_1 peak define $M_{Z'}^{lim}$. The values for θ_M shown in table 2.1 are obtained for $M_t = (175 \pm 6) GeV$, $\alpha_s(M_Z) = 0.118 \pm 0.003$ and $M_{Z_2} > 550 GeV$.

We now compare the results of the analyses listed above with the results on θ_M obtained from a model independent analyses based on leptonic observables only and specified to specific models in a second step.

Reference [60] , LAYSSAC92 This analysis is based on LEP data published in [117]. We show in table 2.1 the bounds on θ_M taken from figure 3. We multiply the bounds given there at one- σ with 1.96 to estimate the 95% CL bounds.

This paper , section 2.1.3.1 This analysis is based on combined LEP and SLC data from 1990 to 1995 published in [91]. We show in table 2.1 the bounds on θ_M obtained from figure 2.3 by the same procedure as explained for the χ model.

The limits from the model independent analyses are weaker than those obtained in the model dependent analyses. The main reason of this difference is that the model independent analyses are based on data from leptons in the final state only. In the model dependent analyses, all couplings of the Z' to fermions are linked by model parameters. This allows the inclusion of leptonic and hadronic observables in the analysis.

We list only the results of one analysis on M_2 because the limits from precision measurements at the Z_1 peak alone are rather poor in the case of an unconstrained Higgs sector.

Reference [30] , LEIKE92 See description of limits on θ_M above for details of this analysis. We show in table 2.2 the limits on $M_{Z'}$ quoted in section 4.2 of reference [30]. The estimate (2.46) is based on $\Gamma_Z = (2487 \pm 10) MeV$ selected from the data [108] used in [30].

We see that the predictions of the formulae (2.43) and (2.46) are in reasonable agreement with the numbers obtained in the exact analyses of real data. Of course, they cannot reproduce details of the different models.

| Analysis | χ | ψ | η | LR | θ_M^{lim} |
|----------------|-----------------|-----------------|-----------------|-----------------|------------------|
| [94] | -0.007 , 0.005 | -0.007 , 0.006 | -0.006 , 0.008 | -0.008 , 0.003 | ± 0.006 |
| [30] | -0.006 , 0.008 | -0.009 , 0.006 | -0.011 , 0.009 | -0.004 , 0.008 | ± 0.007 |
| [96] | -0.0035, 0.0035 | -0.0051, 0.0043 | -0.013 , 0.0090 | -0.0029, 0.0033 | ± 0.005 |
| [101] | -0.0070, 0.0078 | -0.0075, 0.0095 | -0.029 , 0.029 | -0.0057, 0.0077 | ± 0.005 |
| [3] | -0.0029, 0.0011 | -0.0022, 0.0026 | -0.0055, 0.0021 | -0.0013, 0.0021 | ± 0.002 |
| [102] | -0.0036, 0.0017 | -0.0039, 0.0029 | -0.0049, 0.0055 | -0.0053, 0.0033 | ± 0.002 |
| [60] | -0.022 , 0.012 | -0.008 , 0.014 | -0.024 , 0.040 | -0.006 , 0.011 | |
| 2.1.3.1 | -0.006 , 0.003 | -0.011 , 0.006 | -0.018 , 0.014 | -0.008 , 0.005 | |

Table 2.1 The 95% CL ranges of the ZZ' mixing angle θ_M for different Z' models obtained in the analyses listed in the text. The estimate θ_M^{lim} is calculated using equation (2.43) with $g_2/g_1 = \sqrt{\frac{5}{3}}s_W \approx 0.62$.

| Analysis | χ | ψ | η | LR | $M_{Z'}^{lim}$ |
|----------|--------|--------|--------|------|----------------|
| [30] | 148 | 122 | 118 | - | 138 |

Table 2.2 The lower bounds on Z' masses $M_{Z'}^{lim}$ in GeV excluded with 95% CL by the analysis explained in the text. The estimate $M_{Z'}^{lim}$ from (2.46) is added with $g_2/g_1 = \sqrt{5/3}s_W \approx 0.62$.

Future constraints The limits on θ_M from the data [91] could be improved only by future measurements of the reaction $e^+e^- \rightarrow W^+W^-$. For details, we refer to section 2.3.

The present limits on M_2 for models with unconstrained Higgs sectors are much weaker than those from LEP 2 or from the Tevatron. Future e^+e^- and $pp(pp\bar{p})$ experiments will further improve the limits on M_2 . With constrained Higgs sectors, the indirect limits on M_2 from the measurements at the Z_1 peak compete with the limits from the other experiments [66].

2.1.4 Z' limits at $M_1^2 \neq s < M_2^2$

Below the Z_2 resonance and off the Z_1 peak, different cross sections and asymmetries are predicted by the SM. The SM parameters are known very precisely from the measurements at the Z_1 peak. If future measurements differ from these predictions, one can try to interpret the differences as effects due to an extra Z boson. The Z' signal arises through interferences of the Z_2 with the photon or Z_1 boson. The deviations due to these interferences can be detected if they are larger than the experimental error.

Compared to measurements at the Z_1 peak, the sensitivity to θ_M is suppressed by a factor

Γ_1/M_1 due to statistics. Therefore, the dependence on θ_M can be neglected putting $\theta_M = 0$ and identifying $Z_2 = Z'$ and $Z_1 = Z$.

Early Z' analyses can be found in references [32, 46, 118, 119]. We consider here results for Z' constraints obtained by different recent analyses.

2.1.4.1 Model independent constraints on v_i^N and a_i^N

Estimate As shown in section 2.1.1, the amplitude of off-resonance fermion pair production depends only on the normalized couplings v_f^N and a_f^N and not on a'_f, v'_f and $M_{Z'}$ separately.

Consider the constraints arising from the independent observables σ_T^l , A_{FB}^l and A_{LR}^l introduced in section 2.1.1. The measurement of each of these observables excludes a certain domain of the Z' couplings v_i^N and a_i^N . This domain can be calculated analytically in the Born approximation taking into account the contributions of the $\gamma Z'$ and $Z Z'$ interferences, neglecting the $Z' Z'$ contribution. For simplicity, we set $s_W^2 = \frac{1}{4}$. The three considered observables detect a signal if the following conditions are fulfilled [68],

$$\begin{aligned} \sigma_T^l : & \quad \left| \left(\frac{v_i^N}{H_T} \right)^2 + \left(\frac{a_i^N}{H_T} \right)^2 \frac{\chi_Z(s)}{4} \right| \geq 1, & H_T &= \sqrt{\frac{\alpha \chi_{cl}}{2} \frac{\sigma_T^l}{\sigma_T^l(QED)} \frac{\Delta \sigma_T^l}{\sigma_T^l}}, \\ A_{FB}^l : & \quad \left| \left(\frac{v_i^N}{H_{FB}} \right)^2 - \left(\frac{a_i^N}{H_{FB}} \right)^2 \frac{(3 - A_{FB}^l \chi_Z(s)) \frac{1}{4}}{A_{FB}^l - \frac{3}{16} \chi_Z(s)} \right| \geq 1, & H_{FB} &= \sqrt{\frac{\frac{\alpha \chi_{cl}}{2} \frac{\sigma_T^l}{\sigma_T^l(QED)} \Delta A_{FB}^l}{A_{FB}^l - \frac{3}{16} \chi_Z(s)}}, \\ A_{LR}^l : & \quad \left| \left(\frac{v_i^N}{H_{LR}''} \right) \left(\frac{a_i^N}{H_{LR}} \right) \right| \geq 1, & H_{LR} &= \sqrt{\frac{\frac{\alpha \chi_{cl}}{2} \frac{\sigma_T^l}{\sigma_T^l(QED)} \Delta A_{LR}}{1 + \frac{1}{4} \chi_Z(s)}}. \end{aligned} \quad (2.47)$$

$\chi_Z(s)$ is defined in (2.7) and $\sigma_T^l(QED) = \frac{4\pi\alpha^2}{3s}$. σ_T^l detects a Z' with couplings outside an ellipse above the Z_1 peak and outside a set of hyperbolas below the Z_1 peak. The forward-backward asymmetry is sensitive to a Z' with couplings outside a set of hyperbolas above the Z_1 peak and to a Z' with couplings outside an ellipse below the Z_1 peak. The left-right asymmetry detects a Z' with couplings outside a different set of hyperbolas for all energies. As explained in section 2.1.2.1, the quantitative prediction (2.47) is only changed a little by radiative corrections if appropriate kinematic cuts are applied. The axes of the ellipse and the hyperbolas H_T, H_{FB} and H_{LR} do not depend on the Z' model. They are proportional to the root of the experimental errors $\Delta \sigma_T^l$, ΔA_{FB}^l and ΔA_{LR}^l . For further details, we refer to [68].

Alternatively, the *differential* cross sections of left- and right-handed beams can be considered. The Cramer-Rao bound [120] for the reaction $e^+e^- \rightarrow \mu^+\mu^-$ is derived in the second reference of [121] in the limit $M_{Z'}^2 \gg s \gg M_Z^2$ and $s_W^2 = \frac{1}{4}$. In our notation, we have

$$\chi_\infty^2 \approx \frac{L}{s} \pi [10(v_e^N)^4 + 22(v_e^N)^2(a_e^N)^2 + 7(a_e^N)^4]. \quad (2.48)$$

The bound (2.48) gives the theoretical limit of a constraint of the Z' parameters by the observables considered.

For comparison, we give the bound (2.47) deduced from σ_T^l in the same limit as (2.48),

$$\chi^2 \approx \frac{L}{s} \pi \frac{24}{5} [(v_e^N)^2 + \frac{1}{3}(a_e^N)^2]^2. \quad (2.49)$$

As it should be, it is worse than (2.48).

To conclude, we remark that expressions similar to (2.47) were obtained some time ago in reference [122] to constrain the interactions of the SM Z boson.

Present Constraints Present constraints on v_i^N and a_i^N are available from measurements at TRISTAN and at LEP 2.

Reference [123] , OSLAND97 This analysis is based on measurements of σ_T^μ and A_{FB}^μ at TRISTAN [124] ($L = 300 pb^{-1}$, $\sqrt{s} = 58 GeV$) and LEP1.5 ($L = 5 pb^{-1}$, $\sqrt{s} = 130 - 140 GeV$). The constraints on a_i^N and v_i^N are shown in figure 2.7. The constraints from future measurements at LEP2 ($L = 150(500) pb^{-1}$, $\sqrt{s} = 190 GeV$) are predicted too. The systematic error of both observables is assumed to be 1% at all colliders (see table 1 in reference [123]). The conventions are $A_i = a_i^N$, $V_i = v_i^N$.

Reference [103] , S.RIEMANN97 This analysis is based on LEP data published in 1997 [95]. A χ^2 fit to the observables σ_T^l , A_{FB}^l and A_{pol}^r is performed to give the allowed regions in the $a_i' - v_i'$ plane. The resulting constraints are shown in figure 2.8. All radiative corrections and systematic errors are included in this analysis.

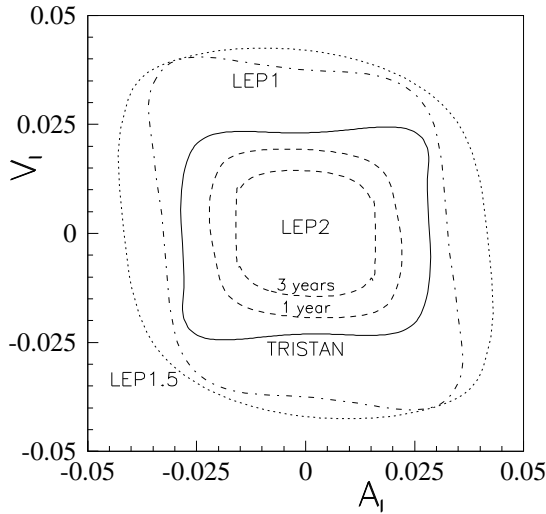


Figure 2.7 Combined regions allowed by σ_T^μ and A_{FB}^μ for $\chi^2 = \chi_{min}^2 + 4$ in the (A_i, V_i) plane for TRISTAN, LEP1, LEP1.5 and LEP2 colliders. Two bounds are shown for LEP2 corresponding to $L = 150 pb^{-1}$ (one year of running) and $L = 500 pb^{-1}$ (three years of running). Radiative corrections are included. This is figure 4 of reference [125].

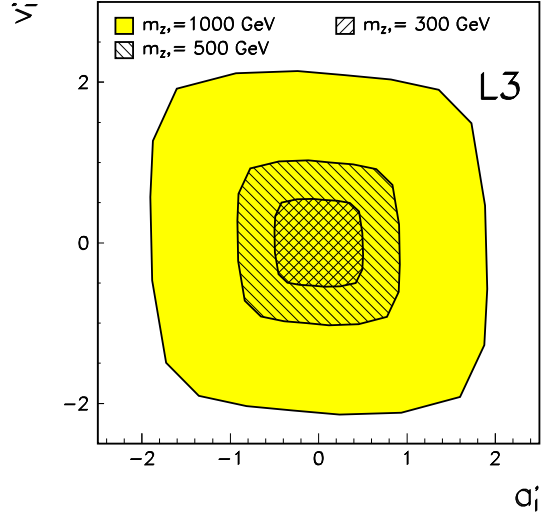


Figure 2.8 The 95% CL allowed regions in the a_i', v_i' plane from L3 data now (large region) and at the end of LEP2 (small region). The input of this figure is $M_Z = (91.1863 \pm 0.0019) GeV$, $M_t = (175 \pm 6) GeV$, $M_H = 150 GeV$, $\alpha_s = 0.118 \pm 0.003$ and $M_{Z'}$ = 500 GeV. This is figure 2 of reference [103].

Future Constraints Predictions for future constraints on a_i^N and v_i^N of a 500 GeV collider including radiative corrections are shown in figure 2.9. The analysis includes statistical and systematic errors. The resulting combined errors of the observables entering figure 2.9 are $\Delta\sigma_T^l/\sigma_T^l = 1\%$, $\Delta A_{FB}^l = 1\%$ and $\Delta A_{LR}^l = 1.2\%$. We refer to [126] for further details. As predicted by the Born analysis (2.47), the regions indistinguishable from the SM are approximately ellipses for σ_T^l and areas between hyperbolas for A_{FB}^l and A_{LR}^l . The remaining two parts of the hyperbolas from A_{FB}^l are outside the figure. A_{LR} gives only a marginal improvement to the Z' exclusion limits.

A quantitative comparison with (2.47) shows that the error of the Born prediction for the exclusion regions is below 10%. Of course, this number depends on the kinematic cuts as explained in section 2.1.2.1. The equations (2.47) can be used to predict the changes in figure 2.9 for different errors of the observables.

The model independent exclusion region predicted for final LEP2 data ($\sqrt{s} = 190$ GeV, $L = 0.5$ fb $^{-1}$) is shown in figure 3a of reference [126]. It looks very similar to figure 2.9 and agrees with figure 2.7.

For illustration purposes, the domains of the normalized couplings a_i^N, v_i^N are shown in figure 2.10 for E_6 models. For a fixed Z' model, i.e. known couplings v_i^l and a_i^l , the limits on a_i^N and v_i^N transform to Z' mass limits. This is illustrated in figure 2.10 for $Z = \chi$. Superimposing figures 2.9 and 2.10, we predict $M_\chi^{lim} \approx 4\sqrt{s}$. For a fixed $M_{Z'}$, figure 2.9 can be drawn for a_i^l and v_i^l as done in figure 2.8.

The couplings of the Z' to quarks a_q^N and v_q^N can only be constrained if the Z' couplings to leptons are non-zero. This is different from the constraints on a_q^M and v_q^M at the Z_1 peak, which were possible also in the case $v_i^M = a_i^M = 0$.

In models, where the couplings of the Z' to leptons are considerably smaller than those to quarks, one can have a signal in the quarkonic observables without a signal in leptonic observables. See reference [127] for a discussion of such a possibility.

Assuming the relations (1.27), the measurements at future colliders would constrain the five couplings

$$L_l(2), R_e(2), L_q(2), R_u(2), R_d(2). \quad (2.50)$$

In the case of an agreement of these measurements with the SM predictions, the allowed regions of the couplings (2.50) contain zero.

The *measurement* of non-zero couplings in the case of a Z' signal is investigated in the literature and will be discussed in section 2.1.4.4.

Finally, we mention that a_f^N, v_f^N and a_f^M, v_f^M are uniquely related by the Higgs constraint (1.17) in models where the Higgs sector is specified. An appropriate scaling and a superposition of figures 2.3 and 2.9 would then allow a direct comparison of the model independent limits from $e^+e^- \rightarrow f\bar{f}$ for $s \approx M_1^2$ and for $M_1^2 \neq s < M_2^2$.

2.1.4.2 Model dependent constraints on $M_{Z'}$

Estimate To obtain an estimate for $M_{Z'}$, we fix the Z' couplings $v_f' \approx v_f$, $a_f' \approx a_f$. Consider the $\gamma Z'$ interference in σ_T^f . We derive

$$\frac{\Delta^{Z'} O}{O_{SM}} \approx \frac{g_2^2 |\Re \chi_\gamma \chi_{Z'}^*|}{g_1^2 |\chi_\gamma|^2} \approx \frac{g_2^2 s}{g_1^2 M_{Z'}^2 - s}, \quad \text{which gives} \quad M_{Z'}^{lim} = \sqrt{s} \left(1 + \frac{1}{\Delta o}\right)^{1/2}. \quad (2.51)$$

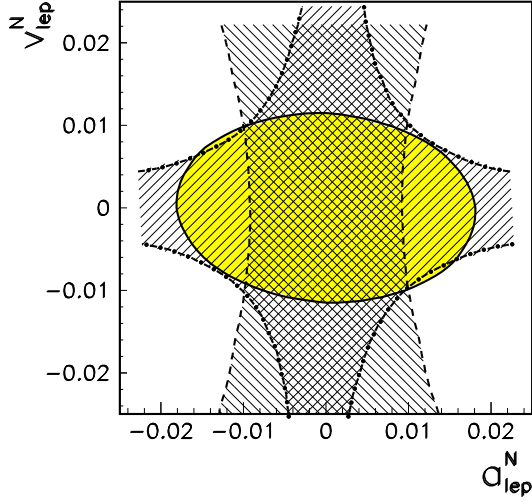


Figure 2.9 Areas of (a_l^N, v_l^N) values, for which the extended gauge theory's predictions are indistinguishable from the SM (95% CL) for $\sqrt{s} = 500 \text{ GeV}$ and $L = 20 \text{ fb}^{-1}$. Models inside the ellipse cannot be detected with σ_T^l measurements. Models inside the hatched areas with falling (rising) lines cannot be resolved with A_{FB}^l (A_{LR}^l). I thank S. Riemann for providing this figure.

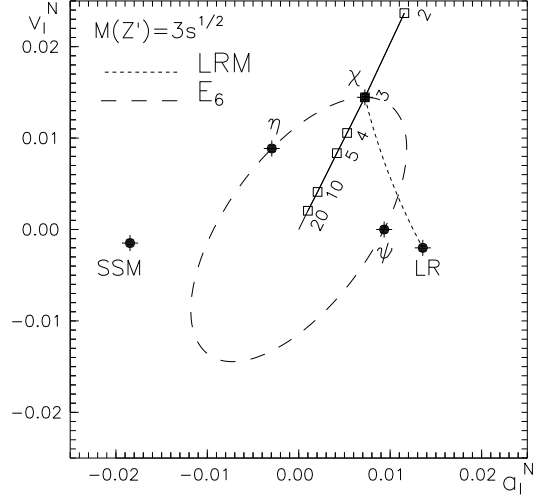


Figure 2.10 The normalized leptonic vector and axial vector couplings v_l^N and a_l^N for $M_{Z'} = 3\sqrt{s}$ in typical GUT's. For the χ model, $M_{Z'}$ is varied in units of \sqrt{s} .

Models with $M_{Z'} < M_{Z'}^{lim}$ would give a signal in the observable O . Comparing the two expressions for measurements on and off the Z peak given by the equations (2.46) and (2.51), we see that (2.46) has an additional suppression factor Γ_Z/M_Z .

We usually have $1/\Delta o \equiv g_2^2/g_1^2 \cdot O/\Delta O \gg 1$. This allows the further approximation in (2.51),

$$M_{Z'}^{lim} \approx \sqrt{\frac{s}{\Delta o}}. \quad (2.52)$$

The approximation (2.52) is in agreement with the estimates(2.47), which contains more details of the model. Taking into account the scaling of the error $\Delta o \sim \sqrt{s/L}$, one obtains the well known scaling law of the Z' mass limit [68, 128, 129], $M_{Z'}^{lim} \approx (sL)^{1/4}$. It is valid in the absence of systematic errors. A scaling including the systematic errors is obtained substituting L by $L/(1+r^2)$,

$$M_{Z'}^{lim} \sim \left[\frac{sL}{1+r^2} \right]^{1/4}. \quad (2.53)$$

The influence of (not too large) systematic errors on Z' exclusion limits is therefore rather moderate.

Radiative corrections give cross sections depending on kinematic cuts. We already noticed

the moderate dependence of cross sections on the photon energy cut Δ in the case where the radiative return is forbidden, see figure 2.1. The influence of Δ on $M_{Z'}^{lim}$ is further reduced by the fourth root in equation (2.53).

Present Constraints The best present mass limits on extra neutral gauge bosons predicted in E_6 models come from proton collisions. As an example of limits on $M_{Z'}$ from e^+e^- collisions, we quote the numbers in table 2.3 read off from reference [102] S. RIEMANN97. More details of the analysis are given in section 2.1.4.1. The estimate of $M_{Z'}^{lim}$ is calculated using the statistical error of σ_T^l . Formula (2.51) must be used because of the small numbers of events.

| Analysis | χ | ψ | η | LR | SSM | $M_{Z'}^{lim}$ |
|----------|--------|--------|--------|-----|-----|----------------|
| [102] | 300 | 220 | 230 | 310 | 520 | 240 |

Table 2.3 The lower bound on Z' masses $M_{Z'}^{lim}$ excluded with 95% CL by the analysis explained in the text.

Future Constraints Many analyses investigate the Z' mass limits reachable at future colliders. The minimal input of these analyses are assumptions about the center-of-mass energy, the integrated luminosity and a list of observables used in the fit. Optionally, systematic errors are included. Radiative corrections have to be included into fits to real data. However, they introduce only small changes in theoretical investigations, where the “data” can be generated in the Born approximation and then be fitted by Born formulae [68, 130]. See section 2.1.2 for the reasons why this works well.

We now comment on the recent theoretical analyses, the results of which are collected in Table 2.4.

Reference [126] , LEIKE97 Theoretical analysis for LEP 2 and a future linear collider. The observables

$$\sigma_T^l, A_{FB}^l, A_{LR}^l, A_{pol}^\tau, R^{had}, A_{LR}^{had}, R_b = \sigma_T^b/\sigma_T^{had}, A_{FB}^b, A_{LR}^b \quad (2.54)$$

are included in the fit. 80% polarization of the electron beam is assumed. The efficiency of flavour tagging is included in the systematic errors. The full SM radiative corrections are included. The numbers giving limits at 95% CL are taken from table 3 of reference [126]. The mass limits without and with inclusion of systematic errors are shown. We take the error of the most accurately measured observable for our estimate of $M_{Z'}^{lim}$, i.e. ΔA_{LR}^{had} in all scenarios. The one- σ errors of ΔA_{LR}^{had} with and without systematic errors are 0.8% and 0.6% (0.7% and 0.5%) for LEP2 (LC500).

Reference [131] , RIZZO96 Theoretical analysis for new gauge boson searches at different future colliders. The observables

$$\sigma_T^f, A_{FB}^f, A_{LR}^f, A_{LR,FB}^f, A_{pol}^\tau \text{ and } A_{pol,FB}^\tau \quad (2.55)$$

for different final state fermions $f = l, c, b, t$ are included in the fit. 90% polarization of the electron beam is assumed. Initial state radiation, finite identification efficiencies and systematic errors associated with luminosity and beam polarization uncertainties are taken into account. We selected for table 2.4 the numbers given in table 3 of reference [131], which are given at 95% confidence.

Reference [132] , GODFREY96 Analysis of new gauge boson searches at different future colliders. Compared to the older analysis [133], more observables and the option of a $\mu^+\mu^-$ collider are included. The 18 observables

$$\sigma_f^\mu, A_{FB}^f, A_{LR}^f, f = \mu, \tau, c, b; A_{LR,FB}^f, f = \mu, c, b; A_{pol}^\tau, R^{had}, A_{LR}^{had} \quad (2.56)$$

are included in the fit for e^+e^- colliders. 90% electron polarization is assumed. Only the 10 observables, which do not demand beam polarization, are included for $\mu^+\mu^-$ colliders. Detection efficiencies are taken into account. Radiative corrections and systematic errors are not included. The numbers quoted in table 2.4 are taken from figure 1 of reference [133] multiplied with 1.15 to transform the 99% CL limits given there to 95% CL limits. The estimate (2.52) in table 2.4 is obtained with the statistical error of A_{LR}^{had} as input.

| Analysis | \sqrt{s}/TeV | Lfb | χ | ψ | η | LR | SSM | $M_{Z'}^{lim}(E_6)$ |
|--------------------|----------------|-------|--------|--------|--------|------|-------|---------------------|
| [126] +syst. | 0.19 | 0.5 | 0.99 | 0.56 | 0.62 | 1.10 | 1.50 | 0.95 |
| [126] stat. | 0.19 | 0.5 | 1.10 | 0.64 | 0.69 | 1.30 | 1.70 | 1.10 |
| [126] +syst. | 0.5 | 20 | 2.8 | 1.6 | 1.7 | 3.2 | 4.0 | 2.6 |
| [126] stat. | 0.5 | 20 | 3.1 | 1.8 | 1.9 | 3.8 | 4.7 | 3.1 |
| [131] | 0.5 | 50 | 3.2 | 1.8 | 2.3 | 3.7 | 4.0 | 2.6 |
| [132] e^+e^- | 0.5 | 50 | 5.2 | 2.5 | 2.9 | 4.2 | 6.9 | 3.9 |
| [132] $\mu^+\mu^-$ | 0.5 | 50 | 4.0 | 2.3 | 2.5 | 3.7 | 6.9 | 3.9 |

Table 2.4 The lower bound on Z' masses $M_{Z'}^{lim}$ in TeV excluded by the different analyses described in the text. The estimate (2.51) for $M_{Z'}^{lim}$ is calculated with $g_2/g_1 = 0.62$.

The estimate for $M_{Z'}^{lim}$ in table 2.4 gives a good prediction of the exact exclusion limits. Of course, it cannot describe the differences between the E_6 models. The scaling (2.53) predicts that systematic errors of the same magnitude as the statistical errors, i.e. $r = 1$, should change $M_{Z'}^{lim} \rightarrow M_{Z'}^{lim}/\sqrt[4]{2}$, which is a reduction of 16% only. This is in agreement with table 2.4. Observables, which require flavour tagging, have systematic errors, which usually dominate the statistical errors. However, these observables give only a moderate contribution to $M_{Z'}^{lim}$ keeping the dependence of $M_{Z'}^{lim}$ on their systematic errors small. For details, we refer to [126, 131].

The price one has to pay for model independent limits on v_i^N and a_i^N can be estimated comparing the exclusion limit for $M_\chi^{lim} = 2.8 TeV$ quoted in table 2.4 with the value $M_\chi^{lim} = 4\sqrt{s} = 2 TeV$ obtained in the model independent analysis explained in section 2.1.4.1. Both

analyses are based on the same assumptions on the data. The difference occurs because the model independent analysis is based on a two parameter fit to σ_T^l, A_{FB}^l and A_{LR}^l , while the numbers quoted in table 2.4 are based on a one-parameter fit to many more observables. The difference between the values for $M_{Z'}^{lim}$ from both analyses is not too large. This reflects the importance of σ_T^l, A_{FB}^l and A_{LR}^l in the $M_{Z'}^{lim}$ constraint.

2.1.4.3 Constraints on g_2

GUT's are the main motivation for the search for extra neutral gauge bosons. In GUT's, all gauge interactions are unified at high energies. In general, it is not expected that the renormalization group equations change the gauge couplings drastically during the evolution from GUT energies down to low energies. Therefore, one expects $g_2 \approx g_1$ at low energies. On the other hand, it is useful from the experimental stand point of view to find all possible constraints on new particles, which can be derived from the data. This is the reason why we consider limits on a Z' with small couplings to all SM fermions. The best present constraints on a Z' with small couplings in the case of a non-zero ZZ' mixing come from measurements at the Z_1 peak, see figure 2.4. Here, we assume that there is no ZZ' mixing.

Estimate Equation (2.51) can be inverted to give an estimate of the sensitivity to the coupling strength g_2 ,

$$g_2^{lim} = g_1 \sqrt{\frac{M_{Z'}^2 - s}{s} \frac{\Delta O}{O}}. \quad (2.57)$$

Models with couplings $g_2 > g_2^{lim}$ would give a signal in the observable O . Formula (2.57) is not true near the Z' resonance. If one assumes that measurements with an accuracy of 1% are performed at energies $\sqrt{s}, \sqrt{2s}, \sqrt{4s}, \dots$, a Z' with $g_2 > g_1/7$ is excluded below its resonance with 95% confidence .

Alternatively, the bounds on $a'_i g_2$ and $v'_i g_2$ follow from the model independent limits on a_i^N, v_i^N , compare definition (2.3),

$$a'_i g_2 = a_i^N \sqrt{4\pi} \sqrt{\frac{|m_2^2 - s|}{s}}. \quad (2.58)$$

The formula (2.58) is also valid for energies above the Z' resonance. As expected, the sensitivity to a weakly coupled Z' increases for the center-of-mass energies approaching the Z' mass. As it should be, the estimate (2.58) agrees with (2.57) after substituting a_f^N according to (2.47).

Present and future Constraints The present bounds on a_i^N and v_i^N from TRISTAN can be read off from figure 2.7, those from 1996 L3 data are given in references [62, 102],

$$\begin{aligned} \text{TRISTAN: } & a_i^N = 0.025 \quad v_i^N = 0.03, \\ \text{LEP 1.5, } \sqrt{s} \approx 130 \text{ GeV: } & a_i^N = 0.095 \quad v_i^N = 0.16, \\ \text{LEP 2, } \sqrt{s} = 170 \text{ GeV: } & a_i^N = 0.10 \quad v_i^N = 0.11. \end{aligned} \quad (2.59)$$

The bounds on a_i^N and v_i^N expected from a next linear collider can be taken from figure 2.9,

$$\text{NLC, } \sqrt{s} = 500 \text{ GeV, } L = 20 \text{ fb}^{-1} : \quad a_i^N = 0.0093, \quad v_i^N = 0.011. \quad (2.60)$$

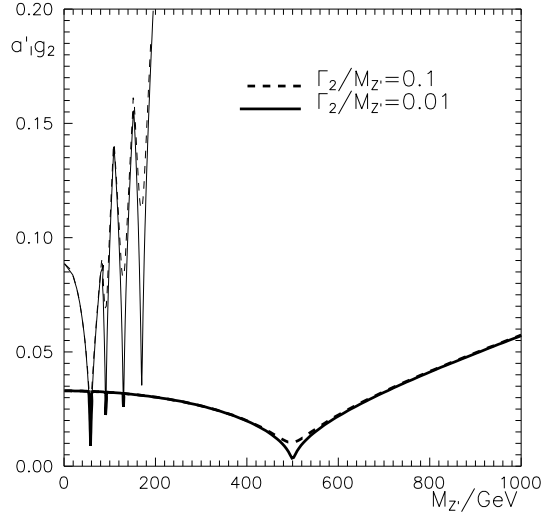


Figure 2.11 Present (thin lines) and future (thick lines) upper bounds (95% CL) on $a'_i g_2$ as function of the Z' mass. Every bound is shown for $\Gamma_2/M_2 = 0.01$ (solid lines) and $\Gamma_2/M_2 = 0.1$ (dashed lines). See text for the input.

The constraints on $a'_i g_2$ resulting from the input (2.59) and (2.60) are shown in figure 2.11. The limits on g_2 for models with other couplings are expected to be similar because the constraints on a_i^N and v_i^N are comparable. The inclusion of PEP and PETRA data would improve the bound on g_2 for small $M_{Z'}$.

Although, $\Gamma_{Z'}$ is related to g_2 in GUT's, we consider it as a free parameter in figure 2.11. This figure illustrates that the constraint is not very sensitive to Γ_2/M_2 . The same is true for the mass exclusion limits obtained in the previous section. This insensitivity to Γ_2/M_2 is an important difference to Z' limits from hadron collisions.

For models, where $a'_i g_2$ is known, mass limits $M_{Z'}^{lim}$ can be derived from figure 2.11. For example, $Z' = \psi$ has pure axial couplings to electrons, $a'_i = 1/\sqrt{6}$, ($a'_i g_2 \approx 0.094$). It follows that $M_{Z'}^{lim} = 180 \text{ GeV}$ from figure 2.11. The value $M_{Z'}^{lim} = 220 \text{ GeV}$ quoted in table 2.3 is based on the same data set. It is better because hadronic observables also enter this number, while only leptonic observables enter the limit from figure 2.11.

As we will see later, the limit on g_2 for $M_{Z'}^2 > s$ can be further improved for $M_{Z'} < s$ by searching for photons from the radiative return to the Z' resonance.

2.1.4.4 Errors of model measurements

In the case of deviations from the SM predictions, one has to prove experimentally that these deviations are due to an extra neutral gauge boson. If this is the case, the three observables σ_T^l , A_{FB}^l and A_{LR}^l depend on the two couplings a'_i and v'_i only. Therefore, there must be a relation between these observables. Z' theories occupy only a two-dimensional subspace of the three-dimensional space spanned by the values of these three observables. See reference

[134] for a detailed discussion of this point. If the new interaction is due to a Z' , its couplings to all fermions should be measured. These measurements can be done with or without model assumptions as far as these are consistent with the data. In contrast to the Z' exclusion limits, the systematic errors of future experiments have a significant influence on measurements of Z' model parameters.

Estimate Suppose that there exists a Z' with $M_{Z'} = f_m M_{Z'}^{lim} < M_{Z'}^{lim}$. We first estimate the experimental bounds on the Z' mass $M_{Z'}^- < M_{Z'} < M_{Z'}^+$, which can be set by the observable O . Considerations similar to those of the exclusion limits in section 2.1.4.2 give

$$M_{Z'}^\pm = M_{Z'} \left(\frac{1 \mp \Delta o (1 - \Delta o / f_m^2)}{1 \mp f_m^2 \pm \Delta o} \right)^{1/2} \approx \frac{M_{Z'}}{\sqrt{1 \mp f_m^2}}. \quad (2.61)$$

The last approximation is valid under the conditions $\Delta o \ll 1 - f_m^2 < 1$ and $\Delta o \ll f_m^2$, which are fulfilled in a reasonable model measurement. For small f_m^2 , we can further approximate,

$$\frac{M_{Z'}^+ - M_{Z'}^-}{M_{Z'}^+ + M_{Z'}^-} \approx \frac{\Delta M_{Z'}}{M_{Z'}} \approx \frac{1}{2} \left(\frac{M_{Z'}}{M_{Z'}^{lim}} \right)^2 \equiv \frac{1}{2} f_m^2. \quad (2.62)$$

Similar considerations can be used for a measurement of the coupling strength g_2 assuming that the Z' mass is known,

$$\frac{\Delta g_2}{g_2} \approx \frac{1}{2} [f_m^2 - \Delta o (1 - f_m^2)] \approx \frac{1}{2} f_m^2. \quad (2.63)$$

Again the last sequence of the approximations relies on $\Delta o \ll f_m^2$. In practice, the estimates (2.62) and (2.63) work satisfactorily for $f_m < \frac{1}{2}$.

The estimates (2.62) and (2.63) give a general relation between Z' exclusion limits and relative errors of Z' model measurements: They relate the amount of $(Ls)_{det}$ one has to pay for the detection of a Z' of a certain model to the amount of $(Ls)_\varepsilon$ which is necessary for a model measurement with the accuracy ε , of the same model by the same observables at the same confidence level [135],

$$(Ls)_\varepsilon \approx \frac{1}{4\varepsilon^2} \cdot (Ls)_{det}. \quad (2.64)$$

The influence of systematic errors on model measurements is predicted by the estimates (2.62), (2.63) and (2.53),

$$\frac{\Delta M_{Z'}}{M_{Z'}}, \frac{\Delta g_2}{g_2} \sim \left[\frac{1 + r^2}{sL} \right]^{1/2}. \quad (2.65)$$

Relations (2.65) are scaling laws similar to (2.53). Compared to exclusion limits, the influence of the systematic error is now more pronounced.

Present Measurements There are no experimental indications for extra neutral gauge bosons. However, in the PEP [136], PETRA [137] and TRISTAN [138] experiments the couplings (and the mass) of the SM Z boson were constrained by measurements below its resonance. These experimental results allow the test of our estimates (2.62) and (2.63). In

fact, these estimates give a correct prediction of the experimental error of the Z coupling measurement $\Delta a_\mu/a_\mu$ of *all* these experiments within a factor of two.

Let us demonstrate the estimates with the results of the AMY collaboration [138]. In the first step, we calculate $M_Z^{lim} \approx 350 \text{ GeV}$ using the estimate (2.51). We took the most accurate observable $A_{FB}^\mu = -0.303 \pm 0.028$ for Δo adding the statistical and systematic errors in quadrature. The estimates (2.62) and (2.63) predict $\Delta M_Z/M_Z, \Delta g/g \approx 3.4\%$. This can be compared with the result of the AMY analysis, $\Delta g/g = \Delta \sqrt{a_l^2 + v_l^2} / \sqrt{a_l^2 + v_l^2} \approx \Delta a_l/a_l = 0.024/0.476 \approx 5\%$.

Future Measurements Figure 2.12 shows typical results of a fit to a_i^N and v_i^N in the case of a Z' signal. It includes the full SM corrections and a cut on the photon energy. As in the case of exclusion limits shown in figure 2.9, different observables shrink different regions in the parameter space. A two-fold sign ambiguity remains as long as fermion pair production is the only process which detects the Z' . We would be left with a four-fold sign ambiguity without A_{LR}^l because only A_{LR}^l or related observables are sensitive to the sign of $v_i^N \cdot a_i^N$. This underlines the essential role of beam polarization in Z' model measurements.

A superposition of figure 2.12 and figure 2.10 allows us to estimate errors of model measurements. Assume a measurement of the overall coupling strength $c_i^N \approx \sqrt{(a_i^N)^2 + (v_i^N)^2}$ and $M_{Z'} = 1.5 \text{ TeV}$. One finds from figure 2.12 the errors $\Delta c_i^N/c_i^N = 0.27, 0.23$ and 0.11 for $Z' = LR, \chi$ and SSM . To compare this result with the estimate (2.62), one should take $M_{Z'}^{lim}$ obtained from leptonic observables only, which are $2.0, 2.6$ and 2.7 TeV according to table 2.4 in [126]. The errors predicted by the estimate (2.62) are then $0.28, 0.17$ and 0.15 . The agreement of the numbers is reasonable.

In reference [126], the couplings of the Z' to b quarks are constrained fixing the leptonic couplings to the values predicted in certain E_6 models. Assuming that the couplings to quarks are predicted by the same model, one can constrain the allowed region for a'_b, v'_b by observables with b quarks in the final state. The resulting regions are clearly off the point $(a'_b, v'_b) = (0, 0)$ as shown in figure 2.13. Compared to figure 2.12, the constraints on v_q^N and a_q^N have a larger error, which is due to the larger systematic errors of b -quark observables.

Alternatively, one can assume Z' couplings to leptons, which are inside the combined region of figure 2.9 for a 500 GeV collider. Such models don't give a signal in the leptonic observables. Taking different sets of leptonic couplings satisfying these conditions, one can estimate the limits on Z' couplings to quarks. Such an analysis is performed in reference [102] for LEP2 data and in references [127] for future colliders.

Assuming relation (1.25), all couplings of the Z' to SM fermions are described by the five parameters (1.36). One can then try to fit these parameters by all available observables simultaneously. This is done in reference [43] for an e^+e^- collider with $\sqrt{s} = 0.5 \text{ TeV}, L = 20 \text{ fb}^{-1}$ and $M_{Z'} = 1 \text{ TeV}$ for different models using the 18 different observables

$$\sigma_T^l, R^{had}, A_{LR}^{had}, R^f = \frac{\sigma_T^f}{\sigma_T^l}, A_{FB}^f, A_{LR}^f, A_{LR,FB}^f, f = l, c, b, t. \quad (2.66)$$

In references [43] and [8], one can find three dimensional figures of possible constraints. We select the result of such a fit from table 5 of the newer analysis [45] and present it in table 2.5. No radiative corrections and no systematic errors are included in the analysis [45]. The

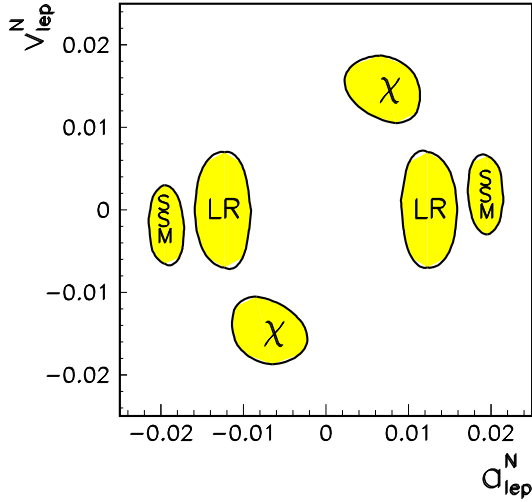


Figure 2.12 Resolution power of LC500 (95% CL) for different models and $M_{Z'} = 1.5 \text{ TeV}$ based on a combination of all leptonic observables. This is figure 4b from reference [126].

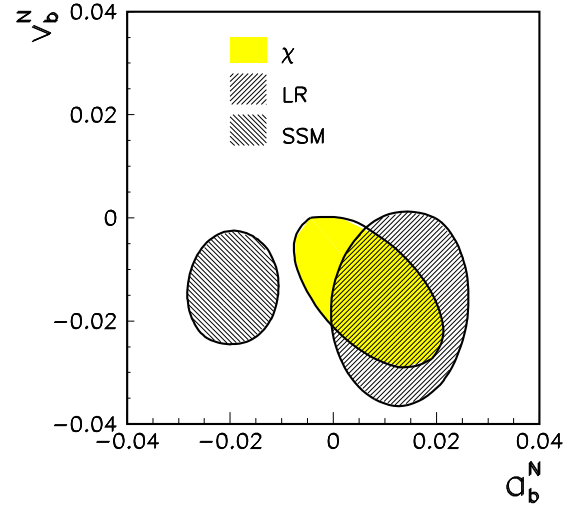


Figure 2.13 Resolution power of LC500 in the (a_b^N, v_b^N) plane (95% CL) based on a combination of all b -quark observables. Different Z' models are considered, $M_{Z'} = 1.5 \text{ TeV}$. This is figure 7 from reference [126].

complete table 4 in reference [45] underlines again the crucial role of beam polarization in model measurements. It is shown there that the errors of model measurements without beam polarization are several times larger.

Having made measurements of the Z' couplings, one can go one step further and check whether the signal is compatible with a Z' originating from an E_6 GUT, i.e. check whether the relations (1.39) are fulfilled. If this is the case, one can try to define the underlying parameters g_{12}/g_2 and β of the breaking of the E_6 group from the data [45]. Alternatively, one can try to constrain [45, 126, 130] the parameters α or β parametrizing the E_6 models as given in equations (1.40) and (1.44).

Influence of systematic errors Let us compare the scaling (2.65) with the results of an exact calculation shown in figure 2.14. We first note that the different scenarios change mainly the size of the constrained region but not its shape. The change of the size can be characterized by one number. Let us normalize the the size of the region without systematic errors to unity. Then the sizes of the regions of the five scenarios in figure 2.14 are (legend from top to down) 1.9, 5.6, 2.5, 1 and 2.9. Combining the curves with $\Delta^{syst} = 0$ and $\Delta^{syst} = 1.5\%$ for $L = 50 \text{ fb}^{-1}$ and using estimate (2.65), we calculate $\Delta^{syst}/\Delta^{stat} = r = 2.3$, and therefore $\Delta^{stat} = 0.65\%$. This is exactly the value, which would follow from the expected number of b quark events. We now estimate (2.65) the sizes of all remaining curves in figure 2.14 as 1.8, 4.2, 2.5, 1, 2.8. The agreement except for the second curve is surprisingly good. The disagreement of the second curve arises because the accuracy ϵ of the model measurement is well above $\frac{1}{8}$, which means

| Analysis | χ | ψ | η | LR |
|-----------------|-------------------|-------------------|-------------------|--------------------|
| P_V^l | 2.00 ± 0.08 | 0.00 ± 0.04 | -3.0 ± 0.5 | -0.148 ± 0.018 |
| $P_L^q = P_l^b$ | -0.50 ± 0.04 | 0.50 ± 0.10 | 2.0 ± 0.3 | -0.143 ± 0.037 |
| P_R^u | -1.00 ± 0.15 | -1.00 ± 0.11 | -1.00 ± 0.15 | -6.0 ± 1.4 |
| $P_R^d = P_R^b$ | 3.00 ± 0.24 | -1.00 ± 0.21 | 0.50 ± 0.09 | 8.0 ± 1.9 |
| ϵ_A | 0.071 ± 0.005 | 0.121 ± 0.017 | 0.012 ± 0.003 | 0.255 ± 0.0016 |

Table 2.5 Values of the couplings (1.36) for typical models and statistical errors as determined from probes at the NLC ($\sqrt{s} = 500 \text{ GeV}$, $L = 20 \text{ fb}^{-1}$, $M_{Z'} = 1 \text{ TeV}$). 100% heavy flavour tagging efficiency and 100% longitudinal polarization of the electron beam is assumed. The numbers are taken from table 4 of reference [45].

that (2.65) is a bad approximation. In a similar way, the different scenarios of the other figures in reference [139] are reproduced by the relation (2.65).

| | χ | ψ | η | LR |
|-------------------------------|------------------------|-------------------------|-------------------------|----------------------------|
| P_V^l , no syst. err. | 2.00 ± 0.11 | 0.00 ± 0.064 | $-3.00^{+0.53}_{-0.85}$ | $-0.148^{+0.020}_{-0.024}$ |
| P_V^l , syst. err. included | 2.00 ± 0.15 | 0.00 ± 0.13 | $-3.00^{+0.73}_{-1.55}$ | $-0.148^{+0.023}_{-0.026}$ |
| P_L^b , no syst. err. | -0.500 ± 0.018 | 0.500 ± 0.035 | $2.00^{+0.33}_{-0.31}$ | -0.143 ± 0.033 |
| P_L^b , syst. err. included | -0.500 ± 0.070 | 0.500 ± 0.130 | $2.00^{+0.64}_{-0.62}$ | -0.143 ± 0.066 |
| P_R^b , no syst. err. | $3.00^{+0.15}_{-0.14}$ | -1.00 ± 0.29 | 0.50 ± 0.11 | $8.0^{+2.5}_{-1.5}$ |
| P_R^b , syst. err. included | $3.00^{+0.65}_{-0.50}$ | $-1.00^{+0.26}_{-0.34}$ | $0.50^{+0.23}_{-0.22}$ | $8.0^{+6.7}_{-2.4}$ |

Table 2.6 Z' coupling combinations P_V^l , P_L^b and P_R^b and their one- σ errors derived from all observables with and without systematic errors for $\sqrt{s}=500 \text{ GeV}$ and $M_{Z'}=1 \text{ TeV}$. This is table 5 of reference [126].

The estimate (2.65) can be confronted with the measurements of model parameters quoted in table 2.6. The influence of systematic errors is predicted by (2.65). For $r = 1$, as expected for leptonic observables in reference [126], ΔP_V^l are predicted to relax by $\sqrt{2}$, which reproduces the tendency in table 2.6. P_L^b given in table 2.6 is only measured by observables with b quarks in the final state. It is therefore dominated by the systematic errors of b quark observables. In reference [126], these systematic errors are roughly four times as large as the statistical errors. According to the estimate (2.65), $r = 4$ should enlarge ΔP_L^b and ΔP_R^b by a factor $\sqrt{17}$. Indeed this happens for some models in table 2.6.

To conclude, the systematic errors have a *large* influence on errors of *model measurements*.

Combining Measurements at several Energies The estimates obtained above for measurements at *one* energy point can be generalized to measurements, which are distributed over

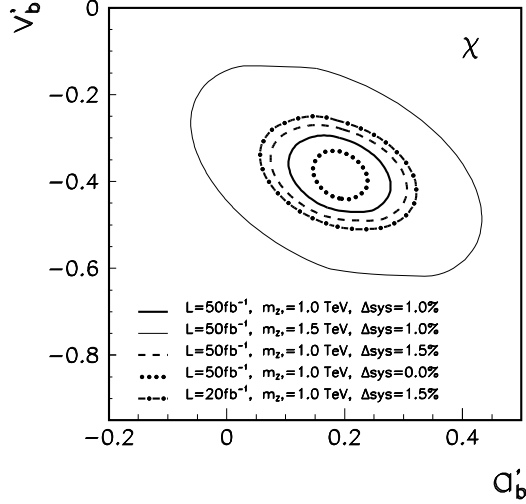


Figure 2.14 Influence of luminosity, Z' mass, and systematic error on contours of $Z' b\bar{b}$ couplings. A Z' in the χ model is assumed; $\sqrt{s} = 500 \text{ GeV}$. This is figure 3 of reference [139].

several energy points s_i with integrated luminosities L_i . Observing that only the combination sL enters all estimates, one can rescale all measurements to one energy s_0 with the luminosity $L_0 = \sum_i s_i L_i / s_0$ and assume *one* measurement at s_0 with L_0 .

A difference occurs, if one wants to use several energy points for a *simultaneous* measurement of the Z' mass and the Z' couplings by a fit to the line shape as proposed in references [140, 141]. Such a measurement was demonstrated historically for the SM Z boson at the PEP and PETRA colliders. It demands measurements of high accuracy at several well separated energy points. The luminosities L_i should be chosen in such a way that the statistical significance

$$\Delta^{Z'} O / \Delta O \approx \sqrt{s_i L_i} \quad (2.67)$$

is about equal for the different energy points s_i .

Although the error of the simultaneous fit of $M_{Z'}$, v'_i , a'_i scales with the product sL like the error of a fit to v_i^N , a_i^N , the prefactor is very different. One needs much more luminosity to measure the couplings and the Z' mass separately compared to a measurement of v_f^N and a_f^N only. Here is one example of the amount of sL needed for different experiments ($\sqrt{s} < M_\chi = 1.6 \text{ TeV}$, 95% CL):

| | |
|--|-------------------------------------|
| Detection: | $sL \approx 0.7 \text{ TeV}^2 / fb$ |
| measurement of $g_2^2 / M_{Z'}^2$, or v_i^N , a_i^N with 15% error: | $sL \approx 8 \text{ TeV}^2 / fb$ |
| measurement of g_2^2 and $M_{Z'}^2$, separately with 15% error: | $sL \approx 260 \text{ TeV}^2 / fb$ |

The first two numbers are obtained from table 2.4 using the scalings (2.53) and (2.62) with $r = 0$, the third number is taken from reference [140].

2.1.5 Z' measurements at $s \approx M_2^2$

A precision measurement on top of the Z_2 resonance in e^+e^- or $\mu^+\mu^-$ collisions would be the best experiment to study the properties of an extra neutral gauge boson. See for example [6, 142, 143, 144] for related studies. Such an experiment would have much in common with the measurements at the Z_1 -peak at LEP 1 and SLC, however, there are also important differences.

In the case of a non-zero ZZ' mixing, in addition to the decay $Z_2 \rightarrow f\bar{f}$ other decay modes such as $Z_2 \rightarrow W^+W^-$ or $Z_2 \rightarrow Z_1H$ are allowed. Because there are no experimental hints for a non-zero ZZ' mixing, we discuss the decay to W^+W^- in a different section. If Z_2 -decays to exotic fermions are kinematically allowed, the number of observables at the Z_2 -peak is even larger than that at the Z_1 -peak yielding important additional information on the breaking scheme of the underlying GUT.

A second difference to the Z_1 -peak is the effect of beamstrahlung. The resulting energy spread of the beams is expected to be between 0.6 and 2.5% for the discussed 500 GeV e^+e^- colliders and even larger for higher energies [145]. Some precision measurements would demand an energy spread as low as 0.2% [146]. A precision scan of the Z_2 peak is among these measurements. Here, a $\mu^+\mu^-$ collider would have clear advantages over an e^+e^- collider. In $\mu^+\mu^-$ collisions, the energy spread of the beams is naturally between 0.04 and 0.08% [67]. It is expected that it can be further reduced to 0.01% [67]. The absolute calibration of the center-of-mass energy is expected to be of the same accuracy.

As in the previous cases, Z' measurements at the Z_2 peak can also be made with or without model assumptions.

2.1.5.1 Model independent Z' measurements

A model independent measurement on the Z_2 resonance can be done generalizing the model independent approach to the Z_1 resonance [147, 148]. It has the advantage that no unknown radiative corrections are needed. We follow here a notation close to reference [149], where also a more extensive discussion and further references may be found. The ansatz for the four helicity amplitudes is

$$\mathcal{M}^{fi}(s) = e^2 s \sqrt{\frac{4}{3}} \left[\frac{R_\gamma^f}{s} + \frac{R_Z^{fi}}{s - \bar{m}_1} + \frac{R_{Z'}^{fi}}{s - \bar{m}_2} + F^{fi}(s) \right], \quad i = 0, 1, \dots, 3. \quad (2.68)$$

$F^{fi}(s)$ is an analytic function without poles. In general, the expression (2.68) is not unique. However, it makes sense, if the resonances are well separated. This is the case because we have $m_1 \ll m_2$ due to the present experimental constraints. The QED parameter R_γ^f can be measured at such a low energy that all other contributions are unimportant. Therefore, a model independent fit to the Z_1 resonance can be performed *fixing* the QED term. See reference [148] for a first fit and [150] for recent experimental results. There are no hints for a Z_2 at the Z_1 resonance. Therefore the fits to the Z_1 resonance are independent of a possible term of the Z_2 pole. By the same scheme, a model independent fit of the Z_2 resonance can be performed with the amplitude (2.68) *fixing* the QED *and* the Z_1 terms. Such a procedure is as unique as are the present model independent fits to the Z_1 resonance.

The complex constants R_γ^f and R_Z^{fi} can be derived within a given theory to a certain order

of perturbation series. At the Born level, we have

$$\begin{aligned}
R_\gamma^f &= Q^e Q^f, \\
R_Z^{f0} &= 4L_e L_f \frac{g_1^2}{e^2}, \quad R_Z^{f1} = 4L_e R_f \frac{g_1^2}{e^2}, \quad R_Z^{f2} = 4R_e R_f \frac{g_1^2}{e^2}, \quad R_Z^{f3} = 4R_e L_f \frac{g_1^2}{e^2}, \\
R_{Z'}^{f0} &= 4L'_e L'_f \frac{g_2^2}{e^2}, \quad R_{Z'}^{f1} = 4L'_e R'_f \frac{g_2^2}{e^2}, \quad R_{Z'}^{f2} = 4R'_e R'_f \frac{g_2^2}{e^2}, \quad R_{Z'}^{f3} = 4R'_e L'_f \frac{g_2^2}{e^2}.
\end{aligned} \tag{2.69}$$

The complex mass $\bar{m}_i = \bar{M}_i^2 - i\bar{M}_i\bar{\Gamma}_i$ is slightly different from the on-shell mass m_i because it contains a constant width defining the complex pole in the ansatz (2.68). If the vector boson Z_n can only decay into light fermion pairs, we have [42]

$$\bar{M}_n = M_n - \frac{\Gamma_n^2}{2M_n}, \quad \bar{\Gamma}_n = \Gamma_n - \frac{\Gamma_n^3}{2M_n^2}. \tag{2.70}$$

From the amplitude (2.68), total cross sections can be calculated by the standard procedure,

$$\sigma_i^f = \frac{1}{2s} \int |\mathcal{M}^{fi}(s)|^2 d\Gamma = |\mathcal{M}^{fi}(s)|^2 \frac{1}{(4\pi)^2} \frac{\pi}{s}. \tag{2.71}$$

The four Born cross sections σ_T^{f0} , σ_{FB}^{f0} , σ_{LR}^{f0} and σ_{pol}^{f0} introduced in (2.10) and (2.11) are obtained by linear combinations of σ_i^f ,

$$\begin{aligned}
\sigma_T^f &= +\sigma_0^f + \sigma_1^f + \sigma_2^f + \sigma_3^f, \\
\frac{4}{3}\sigma_{FB}^f &= +\sigma_0^f - \sigma_1^f + \sigma_2^f - \sigma_3^f, \\
\sigma_{LR}^f &= -\sigma_0^f - \sigma_1^f + \sigma_2^f + \sigma_3^f, \\
\sigma_{pol}^f &= -\sigma_0^f + \sigma_1^f + \sigma_2^f - \sigma_3^f.
\end{aligned} \tag{2.72}$$

Combining equations (2.71) and (2.68), one arrives at a model independent formula for cross sections,

$$\sigma_A^{f0}(s) \approx \frac{4\pi\alpha^2}{3} \left[\frac{r_A^{\gamma f}}{s} + \frac{sr_A^f + (s - \bar{M}_1^2)j_A^f}{|s - \bar{m}_1^2|^2} + \frac{sr_A'^f + (s - \bar{M}_2^2)j_A'^f}{|s - \bar{m}_2^2|^2} \right], \quad A = T, FB, LR, pol. \tag{2.73}$$

In formula (2.73), the functions $F^{fi}(s)$ and terms without poles are neglected for simplicity.

At the Born level, the SM coefficients are [148]

$$\begin{aligned}
r_A^{\gamma f} &= \frac{1}{4} N_f \sum_{i=0}^3 [\pm 1] |R_\gamma^f|^2, \\
r_A^f &= N_f \left\{ \frac{1}{4} \sum_{i=0}^3 [\pm 1] |R_Z^{fi}|^2 + 2 \frac{\bar{\Gamma}_1}{M_1} \Im m C_A^f \right\}, \\
j_A^f &= N_f \left\{ 2 \Re e C_A^f - 2 \frac{\bar{\Gamma}_1}{M_1} \Im m C_A^f \right\}, \\
C_A^f &= \frac{1}{4} (R_\gamma^f)^* \sum_{i=0}^3 [\pm 1] R_Z^{fi}.
\end{aligned} \tag{2.74}$$

The signs $[\pm 1]$ are the same as the cross sections σ_A^f in equation (2.72). The parameters of the Z_2 peak are

$$\begin{aligned}
r_A^{f'} &= N_f \left\{ \frac{1}{4} \sum_{i=0}^3 [\pm 1] |R_{Z'}^{fi}|^2 + 2 \frac{\bar{\Gamma}_2}{M_2} \Im m(C_A'^f - C_A''^f) \right\}, \\
j_A^{f'} &= N_f \left\{ 2 \Re e C_A'^f - 2 \frac{\bar{\Gamma}_2}{M_2} \Im m C_A'^f + 2 \left(1 - \frac{M_1^2}{M_2^2} \right) \Re e C_A''^f + 2 \frac{\bar{\Gamma}_2}{M_2} \Im m C_A''^f \right\}, \\
C_A'^f &= \frac{1}{4} (R_\gamma^f)^* \sum_{i=0}^3 [\pm 1] R_{Z'}^{fi}, \\
C_A''^f &= \frac{1}{4} \sum_{i=0}^3 [\pm 1] R_{Z'}^{fi} (R_{Z'}^{fi})^*. \tag{2.75}
\end{aligned}$$

M_1/M_2 is a small parameter because the Z_1 and Z_2 peaks are well separated. We therefore neglected terms of the order M_1^3/M_2^3 , $M_1\Gamma_1/M_2^2$ or smaller. This keeps the formulae (2.75) relatively simple.

Before the formula (2.73) can be used for fits to data, QED (and QCD) corrections must be taken into account [148]. Initial state corrections can be calculated by the convolution (2.21). Final state radiation and the interference between initial and final state radiation can be included by a different convolution [148]. However, these corrections don't change the pole structure. Therefore, they could be absorbed into effective coefficients (2.74) and (2.75).

2.1.5.2 Model dependent Z' measurements

Z_2 measurements at the Z_2 peak are precision measurements. They require radiative corrections. Unfortunately, these corrections depend on all the parameters of the whole theory. If these are poorly known, theoretical uncertainties arise. This is similar to LEP 1 and SLC where theoretical errors of the radiative corrections at the Z_1 peak arise through the unknown Higgs mass and through the experimental errors of the top- and the W mass. At a Z_2 peak, the situation is much more uncertain. Today it is not known whether a Z_2 exists at all. It is even more speculative to predict the underlying gauge group. If it is known, one would still need some idea about the breaking scheme, the particle content and particle masses to calculate radiative corrections. We have shown in the previous sections that some information can be obtained by future experiments below the Z_2 peak.

Because of the difficulties mentioned above, we have to constrain ourselves to general conclusions and estimates in the Born approximation. The cross section at the resonance peak can be expressed through branching ratios,

$$\sigma_T(e^+e^- \rightarrow f\bar{f}) \approx \sigma_T^f(M_2^2; Z_2, Z_2) = \frac{12\pi}{M_2^2} \frac{\Gamma_2^e \Gamma_2^f}{\Gamma_2 \Gamma_2} = \frac{12\pi}{M_2^2} Br_2^e Br_2^f. \tag{2.76}$$

For a Z_2 originating in usual GUT's, one expects millions of muon pairs and tens of millions of hadron pairs per year from Z_2 decays at the proposed electron or muon colliders. This is similar to the situation at LEP 1 and SLC. The systematic errors at future colliders are expected to be at the same level as at LEP 1 or SLC. Therefore, it can be expected that the Z_2 couplings to fermions could be measured with a similar precision as the Z_1 couplings.

The measurements of Z_2 couplings constrain the ZZ' mixing angle. The constraints from the Z_2 peak are expected to be stronger than those from the Z_1 peak because in a GUT the couplings of the Z_1 to fermions are in general larger than the couplings of the Z_2 to fermions. A sensitivity to $\theta_M \approx 10^{-4}$ is derived in reference [143].

The measurements of Z_2 couplings constrain parameters of the GUT. In a naive estimate, one would expect an accuracy of a measurement of $\cos\beta$ of an E_6 GUT comparable to the accuracy of the $\sin^2\theta_W$ measurement at the Z_1 peak.

The measurement of M_2 and Γ_2 is limited by the beam energy spread and by the error of the energy calibration $\Delta\sqrt{s}$; $\Delta M_2, \Delta\Gamma_2 > \Delta\sqrt{s}$.

2.1.5.3 Limit on g_2

The best limit one can put on a weakly interacting Z' is obtained for $M_2 = \sqrt{s}$. The cross section at the Z_2 peak (2.76) is independent of the ratio g_2/g_1 . The sensitivity to g_2/g_1 is limited at an e^+e^- collider because it has a finite beam energy spread $\Delta\sqrt{s}/\sqrt{s}$. Only cross sections of e^+e^- pairs with $\sqrt{s} = M_2 \pm \Gamma_2$ are enhanced. The observed number of Z_2 events can be approximated for $\Delta\sqrt{s} > \Gamma_2$,

$$N_{ff}^{Z'} \approx L \frac{\Gamma_2}{M_2} \frac{\sqrt{s}}{\Delta\sqrt{s}} \sigma_T^0(M_2^2; Z', Z') \approx \frac{g_2^2}{g_1^2} L \frac{\Gamma_1}{M_1} \frac{\sqrt{s}}{\Delta\sqrt{s}} \frac{12\pi}{M_2^2} Br_2^e Br_2^f. \quad (2.77)$$

In the last step of the approximation, we assumed

$$\frac{\Gamma_2}{M_2} \approx \frac{g_2^2 \Gamma_1}{g_1^2 M_1}. \quad (2.78)$$

A Z' produces a signal of n_σ standard deviations if

$$N_{ff}^{Z'} = n_\sigma \sqrt{N_{ff}^{SM}} = n_\sigma \sqrt{L \sigma_T^f(M_2^2)}. \quad (2.79)$$

An estimate for g_2^{lim} can now be obtained from equation (2.77),

$$g_2^{lim} \approx g_1 \sqrt{n_\sigma} \left[\frac{\Delta\sqrt{s}}{\sqrt{s}} \frac{M_1}{\Gamma_1} \frac{1}{12\pi Br_2^e Br_2^f} \right]^{1/2} \left[\frac{\sigma_T^{f0}(M_2^2) M_2^4}{L} \right]^{1/4}. \quad (2.80)$$

Assuming

$$\Delta\sqrt{s}/\sqrt{s} = 1\%, \quad Br_2^e = Br_2^\mu = 3.36\%, \quad L = 80 fb^{-1}, \quad \text{and} \quad M_2 = 1 TeV, \quad (2.81)$$

we get $g_2^{lim} \approx g_1/140$ with 95% confidence ($n_\sigma = 2$) for the reaction $e^+e^- \rightarrow \mu^+\mu^-$.

2.1.6 Z' limits at $s > M_2^2$

Above the Z_2 resonance, the sensitivity to ZZ' mixing is much lower than on the resonance. We therefore neglect the mixing identifying the Z_1 and Z_2 with the Z and Z' .

Suppose that a Z' was missed below its resonance because it has very weak couplings. The question we want to discuss here is, for which coupling strengths is it possible to detect such

a Z' above its resonance. If the couplings to all fermions are very small, the Z' eventually escapes detection. A vector boson, which couples to quarks only, can still have quite large couplings and be consistent with the present data. See reference [151] for a discussion of this point and for further references and [152] for bounds on such a Z' from different experiments.

It turns out that the error of the photon energy measurement $\Delta E_\gamma/E_\gamma$ is an important input of the bounds because they arise from events with a fermion pair and one hard photon in the final state. At a $\mu^+\mu^-$ collider, this parameter limits the constraints. However, as mentioned in the previous section, the proposed e^+e^- colliders suffer from a large beam energy spread $\Delta\sqrt{s}/\sqrt{s}$. Then, the error of the photon energy ΔE_γ in the estimates has to be replaced by $\Delta E_\gamma + \Delta\sqrt{s}$.

2.1.6.1 Model independent limits on g_2

Starting from relation (2.51), an upper bound g_2^{lim} on the coupling strength g_2 of the Z' to SM fermions can be derived,

$$g_2^{lim} \approx g_1 \sqrt{\frac{\Delta O}{O} \cdot \frac{s - M_{Z'}^2}{s}}. \quad (2.82)$$

It follows that a one percent cross section measurement of the reaction $e^+e^- \rightarrow f\bar{f}$ can exclude models with $g_2 > g_1/7$ at 95% confidence for all $M_{Z'} < \sqrt{s}$.

The sensitivity to a Z' is considerably larger than (2.82) if one considers the photon energy spectrum of the reaction $e^+e^- \rightarrow f\bar{f}\gamma$. As discussed in section 2.1.2.1 and shown in figure 2.2, the spectrum of the photons radiated from the initial state has sharp peaks for energies which set the $f\bar{f}$ subsystem back to the resonance. The energy $E_\gamma = \Delta \cdot E_{beam}$ of the photons responsible for the radiative tail is distributed in the narrow range $\Delta^+ < \Delta < \Delta^-$ with $\Delta^\pm = 1 - M_{Z'}^2/s \pm M_{Z'}\Gamma_{Z'}/s$. The number of events with these photons can be estimated from the magnitude of the radiative tail (2.27),

$$N_\gamma^{Z'} \approx L\sigma_T(s; Z', Z')\beta_e \frac{\pi M_{Z'}}{2 \Gamma_{Z'}} \approx \frac{g_2^2}{g_1^2} L\sigma_T(s; Z, Z)\beta_e \frac{\pi M_Z}{2 \Gamma_Z}. \quad (2.83)$$

In the last step of approximation (2.83), we used the estimate (2.78) and

$$\frac{\sigma_T(s; Z', Z')}{\sigma_T(s; Z, Z)} \approx \frac{g_2^4}{g_1^4}. \quad (2.84)$$

Of course, these approximations can be improved if more details of the model are known.

The SM background also contributes photons to the interval (Δ^-, Δ^+) . The number of these events can be estimated by the convolution (2.21),

$$N_\gamma^{SM} = L \left[\sigma_T^{ISR}(s) - \sigma_T^0(s) \right] = L \int_{\Delta^-}^{\Delta^+} dv \sigma_T^0 \left(s(1-v) \right) H_A^e(v) \approx L\sigma_T^0(s) \frac{\beta_e(\Delta^+ - \Delta^-)}{\Delta^*(1 - \Delta^*)}. \quad (2.85)$$

Δ^* is some value between Δ^- and Δ^+ . We assumed that $\sigma_T^0(s) \sim 1/s$ for energies between $1/s$ and $1/[s(1 - \Delta^*)]$. The estimate (2.85) can be compared with the SM result in figure 2.2. It gives a satisfactory prediction away from resonances.

The ratio of the Z' signal and the SM background for photon energies between Δ^- and Δ^+ can now be estimated as

$$\frac{N_\gamma^{Z'}}{N_\gamma^{SM}} \approx \frac{\pi M_Z^2}{4 \Gamma_Z^2} \frac{\sigma_T^0(s; Z, Z)}{\sigma_T^0(s)} \left(1 - \frac{M_{Z'}^2}{s}\right). \quad (2.86)$$

Again, the approximation (2.78) is used. Note that the ratio (2.86) is independent of g_2/g_1 . Numerically, we get $N_\gamma^{Z'}/N_\gamma^{SM} \approx 40$ for

$$\sigma_T^\mu(1 \text{ TeV}^2) \quad \text{and} \quad M_\eta = 800 \text{ GeV}. \quad (2.87)$$

This estimate is in a good agreement with figure 2.2.

To detect the Z' signal, two additional conditions must be fulfilled. The luminosity must be high enough to produce a reasonable number of events and the error of the photon energy $\Delta E_\gamma/E_\gamma$ must be small enough to detect the signal above the background.

Let us first assume an arbitrarily good photon energy resolution. Assume that the events are Poisson distributed. Then, zero observed events exclude all theories with 95% confidence, which predict $N_\gamma^{Z'} \geq 3$. This can be interpreted as a limit g_2^{lim} on g_2 ,

$$g_2^{lim} = g_1 \left[\frac{N_\gamma^{Z'}}{N_{ff}^{SM}} \frac{\sigma_T^0(s)}{\sigma_T^0(s; Z, Z)} \frac{2}{\pi \beta_e} \frac{\Gamma_Z}{M_Z} \right]^{1/2}. \quad (2.88)$$

N_{ff}^{SM} is the number of fermion pairs expected in the Born approximation as defined in equation (2.79). The estimate (2.88) gives the best bound on g_2 , which could be reached with a given luminosity in the reaction $e^+e^- \rightarrow f\bar{f}\gamma$. Numerically, we get $g_2^{lim} \approx g_1/45$ under the assumptions (2.87) and

$$L = 80 \text{ fb}^{-1} \quad \text{and} \quad N_\gamma^{Z'} = 3. \quad (2.89)$$

Unfortunately, the energy resolution $\Delta E_\gamma/E_\gamma \approx 0.1/\sqrt{E_\gamma/\text{GeV}}$ of real detectors is finite [153]. As a result, all photons with energies $\Delta = (1 - M_{Z'}^2/s)(1 \pm \Delta E_\gamma/E_\gamma)$ are observed in the experiment. For the expected luminosities at future colliders, there are photons N_γ^{SM} from the background even in the narrowest bin of the photon energy. Numerically, we get $N_\gamma^{SM} \approx 30$ from the estimate (2.85) under the assumptions (2.87), (2.89) and $\Delta E_\gamma/E_\gamma = 1\%$, which is in good agreement with figure 2.2. With such an event number, we can assume Gaussian statistics in our estimates. One expects a $n_\sigma - \sigma$ signal for theories predicting

$$N_\gamma^{Z'} = n_\sigma \sqrt{N_\gamma^{SM}}. \quad (2.90)$$

The resulting expression for g_2^{lim} can easily be derived from equations (2.90), (2.85) and (2.83),

$$g_2^{lim} = g_1 c_r \left[\frac{8}{\pi^2 \beta_e} \frac{\Gamma_Z^2}{M_Z^2} \right]^{1/4} \approx g_1 \cdot 0.266 c_r, \quad c_r = \left[\frac{\Delta E_\gamma}{E_\gamma} \frac{1}{N_{ff}^{SM}} \right]^{1/4} \left[n_\sigma \frac{\sigma_T^0(s)}{\sigma_T^0(s; Z, Z)} \frac{\sqrt{s}}{M_{Z'}} \right]^{1/2}. \quad (2.91)$$

Numerically, we get $g_2^{lim} \approx g_1/24$ with 95% confidence ($n_\sigma = 2$) under the same conditions as before and a photon energy resolution of 1% and $\sqrt{s}/M_{Z'} \approx 1$.

As we see, the consideration of fermion pair events with one additional hard photon gives a considerable improvement of g_2^{lim} obtained from off-resonance fermion pair production.

Present upper bounds on g_2 from fermion pair production without additional photons are displayed in figure 2.11. Fermion pair events accompanied with hard photons are investigated at LEP [154]. This allows to reconstruct cross sections and asymmetries of $e^+e^- \rightarrow \mu^+\mu^-$ for energies lower than \sqrt{s} .

2.1.6.2 Measurements of $M_{Z'}$

If a Z' signal with $M_{Z'}^2 < s$ is found, the Z' mass can be measured,

$$M_{Z'} = \sqrt{s \left(1 - \frac{E_\gamma^{peak}}{E_{beam}} \right)}, \quad \frac{\Delta M_{Z'}}{M_{Z'}} = \frac{\Delta E_\gamma}{2E_\gamma} \left(\frac{s}{M_{Z'}^2} - 1 \right). \quad (2.92)$$

We exploited formula (2.29) in the derivation of this estimate. E_γ^{peak} is the photon energy of the hard photons from the radiative return. Using the knowledge of $M_{Z'}$, one can tune the energy to the resonance and perform precision measurements there.

2.2 Z' search in $e^+e^- \rightarrow e^+e^-$ and $e^-e^- \rightarrow e^-e^-$

Bhabha and Møller scattering can probe the Z' couplings to electrons only. While Bhabha events serve as additional observables in e^+e^- collisions, Møller scattering requires the e^-e^- option of a linear collider.

Although the luminosity of e^-e^- collisions is expected to be smaller than that of e^+e^- collisions because of the anti-pinch effect, Møller scattering has the advantage of two polarized beams and of a cleaner environment.

Early Z' analyses can be found in references [155, 156, 157] for Bhabha scattering and in reference [157] for Møller scattering.

2.2.1 Born Approximation

2.2.1.1 Amplitude

In Bhabha (Møller) scattering, electrons and positrons (only electrons) appear in the final state. The neutral gauge bosons are exchanged in the s and t (t and u) channels. The resulting angular distributions are very singular for small scattering angles. Møller scattering has a symmetrical angular distribution. The angular distribution of Bhabha scattering is peaked in the forward direction.

Considerations similar to fermion pair production in section 2.1.1 show that these reactions can constrain only the model independent parameters a_e^N and v_e^N . As off-resonance fermion pair production, they are rather insensitive to ZZ' mixing. We therefore neglect the mixing angle putting $\theta_M = 0$.

2.2.1.2 Cross section

The Born cross section of *Bhabha scattering* including the Z' exchange is, following the notation of reference [158],

$$\frac{d\sigma}{dc} = \frac{\pi\alpha^2}{2s} \left(f_0 + (\lambda_+ - \lambda_-)f_1 + \lambda_+\lambda_-f_2 \right) \quad (2.93)$$

with

$$\begin{aligned}
f_0 &= (1+c^2) \cdot G_1(s, s) + 2c \cdot G_3(s, s) - 2 \frac{(1+c)^2}{1-c} \cdot [G_1(s, t) + G_3(s, t)] \\
&\quad + 2 \frac{(1+c)^2 + 4}{(1-c)^2} \cdot G_1(t, t) + 2 \frac{(1+c)^2 - 4}{(1-c)^2} \cdot G_3(t, t), \\
f_1 &= (1+c)^2 H(s, s) - 4 \frac{(1+c)^2}{1-c} H(s, t) + 4 \frac{(1+c)^2}{(1-c)^2} H(t, t), \\
f_2 &= -f_0 + \frac{16}{(1-c)^2} [G_1(t, t) - G_3(t, t)]
\end{aligned} \tag{2.94}$$

and

$$\begin{aligned}
G_1(s, t) &= \Re e \sum_{m,n=0}^N \chi_m(s) \chi_n^*(t) \left[v_e(m) v_e(n)^* + a_e(m) a_e(n)^* \right]^2, \\
G_3(s, t) &= \Re e \sum_{m,n=0}^N \chi_m(s) \chi_n^*(t) \left[v_e(m) a_e(n)^* + a_e(m) v_e(n)^* \right]^2, \\
H(s, t) &= \Re e \sum_{m,n=0}^N \chi_m(s) \chi_n^*(t) \left[v_e(m) v_e(n)^* + a_e(m) a_e(n)^* \right] \left[v_e(m) a_e(n)^* + a_e(m) v_e(n)^* \right] \\
&\quad \text{with } t = -\frac{s}{2}(1-c).
\end{aligned} \tag{2.95}$$

The summation runs over the exchanged gauge bosons. See section 2.1.1 for further definitions.

The Born cross section of *Møller scattering* including the Z' exchange is [121],

$$\begin{aligned}
\frac{d\sigma}{dc} &= \frac{16\pi\alpha^2}{s} \sum_{m,n=0}^N \frac{\frac{g_n^2 g_m^2}{(4\pi\alpha)^2}}{(\mu_m^2 - c^2)(\mu_n^{*2} - c^2)} \\
&\quad \left\{ 4\lambda_1 (R_m^2 R_n^{*2} + L_m^2 L_n^{*2}) \mu_m \mu_n^* + 4\lambda_2 (R_m^2 R_n^{*2} - L_m^2 L_n^{*2}) \mu_m \mu_n^* \right. \\
&\quad \left. + \lambda_3 R_m L_m R_n^* L_n^* \left[\mu_m \mu_n^* + (1 + \mu_m \mu_n^* + 2\mu_m + 2\mu_n^*) c^2 + c^4 \right] \right\}
\end{aligned} \tag{2.96}$$

with

$$\mu_n = 1 + 2 \frac{m_n^2}{s} \quad \text{and} \quad \lambda_3 = 1 + \lambda_+ \lambda_- \tag{2.97}$$

Again, the summation runs over the exchanged gauge bosons. R_m and L_m denote the left- and right handed couplings to electrons, $L_m = L_e(m)$, $R_m = R_e(m)$. Further definitions can be found in section 2.1.1.

Alternatively to formulae (2.95) and (2.96), the Z' contributions can be included by form factors as explained in section 1.4.

2.2.1.3 Observables

Consider first *Bhabha scattering*. Only contributions proportional to f_0 can be measured with unpolarized beams. With polarized electrons, one can measure the left-right asymmetry,

$$A_{LR}(c) = \frac{d\sigma_L - d\sigma_R}{d\sigma_L + d\sigma_R}. \tag{2.98}$$

It is sensitive to contributions proportional to f_1 . Two polarized beams allow a measurement of the asymmetry [155],

$$A_{2L}(c) = \frac{d\sigma_{LL} - d\sigma_{RR}}{d\sigma_{LL} + d\sigma_{RR}}. \quad (2.99)$$

It is sensitive to contributions proportional to f_2 . This is different from fermion pair production and W pair production where two polarized beams give no new information compared to electron polarization only.

LEP 2 has naturally transverse beam polarization. Then, transverse asymmetries [155] can be considered,

$$A_T^\phi(c) = \frac{d\sigma^\phi - d\sigma^{\phi+\pi/2}}{d\sigma^\phi + d\sigma^{\phi+\pi/2}} \quad \text{with} \quad \frac{d\sigma^\phi}{dc} = \int_{\phi-\pi/4}^{\phi+\pi/4} \frac{d\sigma}{d\phi dc} d\phi. \quad (2.100)$$

In contrast to Bhabha scattering, it is sure that in *Møller scattering* both electron beams can be highly polarized. With two polarized beams, one can measure several angular distributions [121],

$$\frac{1}{\sigma} \frac{d\sigma}{dc}, \quad \frac{1}{\sigma^{LL}} \frac{d\sigma^{LL}}{dc}, \quad \frac{1}{\sigma^{RR}} \frac{d\sigma^{RR}}{dc}, \quad \frac{1}{\sigma^{LR}} \frac{d\sigma^{LR}}{dc}, \quad (2.101)$$

which are all linear combinations of the three contributions (2.96) proportional to λ_1 , λ_2 and λ_3 .

In fixed target Møller scattering, the left–right asymmetry

$$A_{LR}(e^-e^- \rightarrow e^-e^-) = \frac{\sigma_L - \sigma_R}{\sigma_L + \sigma_R} = \frac{G_\mu Q^2}{\sqrt{2}\pi\alpha} \frac{1-y}{1+y^4+(1-y)^4} (1-4s_W^2) \\ \text{with } Q^2 = y(2m_e^2 + 2m_e E_{beam})_{fixed\ Target} \quad y = -\frac{(p' - p)^2}{(p' + p)^2} \quad (2.102)$$

is of special interest. It can be measured with very high precision in future experiments [159]. The last sequence in equation (2.102) is valid [160] in the limit $\sqrt{s} \ll M_Z^2$. $p(p')$ are the energy–momenta of one initial (final) electron.

2.2.2 Radiative Corrections

The generalization of the SM radiative corrections to s -channel Z' exchange is discussed in section 2.1.2. No essential new problems arise due to the Z' exchange in the t or u channel. We therefore limit ourselves to give the main references to the SM processes.

QED corrections to SM Bhabha scattering can be found, for example, in [161, 162]. QED corrections are universal allowing a generalization of the SM result to the whole process including additional Z' contributions. See references [158, 162, 163, 164] for results of weak corrections. Weak corrections together with ZZ' mixing could be taken into account as in the case of fermion pair production by the replacements (2.30) and (2.31) of the couplings. In reference [165] one finds the needed formulae. However, such a replacement is not necessary in Bhabha and Møller scattering because these reactions are as insensitive to ZZ' mixing as off–resonance fermion pair production.

QED corrections to Møller scattering are calculated in reference [166], while the electroweak corrections to A_{LR} are calculated in reference [160]. QED initial state corrections can be taken into account [167] by the structure function approach [81].

QCD corrections to both processes enter as virtual corrections at one loop as described in references [160, 164].

2.2.3 Z' Constraints

2.2.3.1 Model independent constraints on v_e^N and a_e^N

Estimate In contrast to fermion pair production, the total cross section and simple asymmetries are not very sensitive to a Z' . The best sensitivity is achieved by fits to angular distributions of polarized cross sections. For Møller scattering, the Cramer-Rao minimum variance bound [120] is given in the second reference of [121] in the limit $M_Z^2 \ll s \ll M_{Z'}^2$, $s_W = 1/4$. We have in our notation,

$$\chi_\infty^2 \approx 256\pi \frac{L}{s} \left[(R_e^N)^4 + (L_e^N)^4 \right] = 32\pi \frac{L}{s} \left[(v_e^N)^4 + 6(v_e^N a_e^N)^2 + (a_e^N)^4 \right]. \quad (2.103)$$

This bound corresponds to the sensitivity of an experiment with an infinite number of angular bins and no systematic errors. It can be compared with the constraints (2.47) and (2.48) obtained for different observables in fermion pair production.

In particular, the estimate (2.103) predicts the widths of the bands in the R'_e, L'_e plane allowed by left- and right handed electron scattering alone,

$$|R_e^N|, |L_e^N| < \left[\frac{\chi_\infty^2 s}{256\pi L} \right]^{1/4}. \quad (2.104)$$

Future Constraints Model independent Z' limits from Møller scattering are studied in [121] at the Born level. Figure 2.15 shows the regions of Z' couplings to electrons, which could be excluded. L' and R' in figure 2.15 are related to our conventions as $L' = 2R'_e g_2/e$, $R' = 2L'_e g_2/e$. R' and L' are restricted independently in experiments with both beams right handed or both beams left handed polarized. The estimate (2.104) is in good agreement with figure 2.15. For one left and one right handed beam, one is sensitive to Z' models where the combination $R'L'$ exceeds a certain value. This property can immediately be read off from the cross section (2.96). The allowed region for unpolarized beams is also shown in figure 2.15. The distributions of two left-handed or two right-handed scattered electrons contain almost all information on a Z' . In contrast to fermion pair production, polarized beams give important improvements already to the Z' exclusion limits.

The exclusion limits from Møller scattering are compared with those from Bhabha scattering and fermion pair production in figure 2.16. We have $v_{Z'} = 2v'_e g_2/e$, $a_{Z'} = 2a'_e g_2/e$ in our conventions. Under the assumptions made in [167], Møller scattering gives the best Z' constraints to the model independent Z' exclusion limits. After the inclusion of observables with electrons and τ 's in the final state, the exclusion limits of Møller scattering and fermion pair production become comparable. The exclusion limits of Bhabha scattering would improve with polarized positron beams.

The influence of systematic errors due to the polarization error, the angular resolution and the luminosity error on Z' exclusion limits are studied in reference [167].

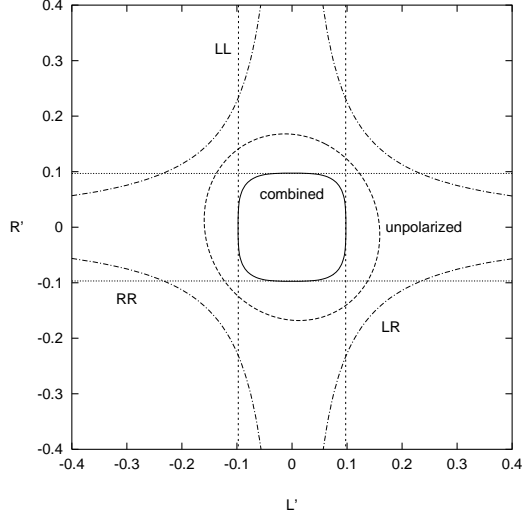


Figure 2.15 Areas of the leptonic Z' couplings L' and R' , which are excluded with 95% confidence by Møller scattering for different beam polarizations. $\sqrt{s} = 500 \text{ GeV}$, $L = 10 \text{ fb}^{-1}$ and $M_{Z'} = 2 \text{ TeV}$ were assumed. The results are obtained by collecting events with $|c| < 0.985$ in 10 equal bins. This is figure 1 from the first reference of [121].

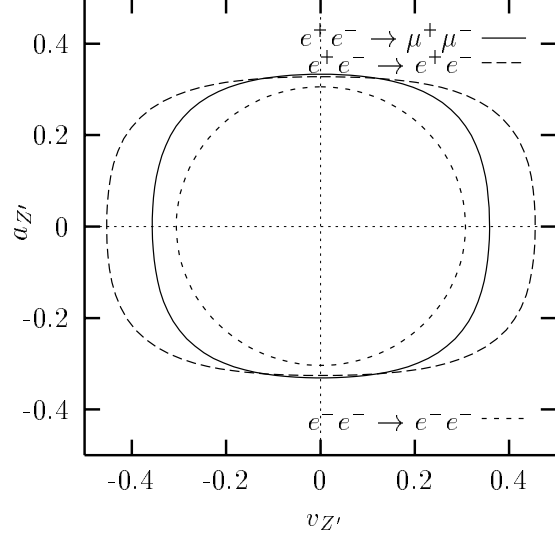


Figure 2.16 Exclusion limits (95% CL) from fermion pair production, Bhabha and Møller scattering for the couplings of the Z' to leptons including systematic errors. The numerical input is $\sqrt{s} = 500 \text{ GeV}$, $L = 50 \text{ fb}^{-1}$ ($L = 25 \text{ fb}^{-1}$) for e^+e^- (e^-e^-) scattering. The electron polarization is $P_e = 90\%$, $\Delta P_e/P_e = 1\%$, $\Delta L/L = 0.5\%$, $|\cos \theta| < 0.985$, $\Delta \theta = 10 \text{ mrad}$. Ten equal bins in $\cos \theta$ are chosen. This is figure 5 from reference [167].

Z' limits can also be obtained from $e^- \mu^-$ scattering [169]. Assuming generation universality, this reaction constrains the same parameter combination as Møller- or Bhabha scattering. The exchange of neutral gauge bosons in $e^- \mu^-$ scattering is possible only in the t channel. However, it seems to be much more difficult to create a highly polarized muon beam of high luminosity than an electron beam with the same properties.

2.2.3.2 Model dependent constraints on $M_{Z'}$

Estimate An estimate of Z' limits from Bhabha and Møller scattering can be obtained by considerations similar to those which lead to the estimate (2.51). The observable O is now the relative number of events in a certain angular bin. Comparing the shift $\Delta^{Z'} O$ due to a Z' with the SM prediction O_{SM} , one gets

$$\frac{\Delta^{Z'} O}{O_{SM}} \approx \frac{g_2^2 |\Re\{\chi_2 \chi_0\}|}{g_1^2 |\chi_0|^2} = \frac{g_2^2 t}{g_1^2 t - M_{Z'}^2}. \quad (2.105)$$

It follows that

$$M_{Z'} < M_{Z'}^{lim} = \sqrt{s \cdot \frac{1-c}{2}} \left(1 + \frac{g_1^2 O}{g_2^2 \Delta O}\right)^{1/2} = \sqrt{s \cdot \frac{1-c}{2}} \left(1 + \frac{1}{\Delta o}\right)^{1/2} \quad (2.106)$$

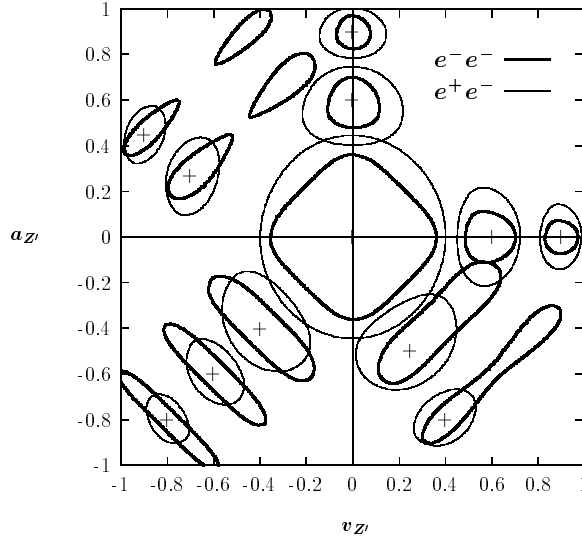


Figure 2.17 Contours of resolvability at 95% confidence of the Z' couplings around several possible true values marked with a '+'. The assumptions are $\sqrt{s} = 0.5 \text{ TeV}$, $L = 40(20) \text{ fb}^{-1}$ for e^+e^- (e^-e^-) collisions. Ten bins in the scattering angle between 10° and 170° are used. The Z' mass is 2 TeV . This is figure 5 from the third reference of [121].

produces a signal in the observable O . A similar estimate of $M_{Z'}^{lim}$ can be derived from the constraint (2.103).

Comparing the estimates (2.106) and (2.51), we conclude that the Z' mass limits from Bhabha and Møller scattering could be competitive to $e^+e^- \rightarrow f\bar{f}$ with leptons in the final state only. For completely specified models where the annihilation into quarks contributes to $M_{Z'}^{lim}$, the mass exclusion limit from fermion pair production is better.

Future Constraints Future constraints on $M_{Z'}$ can be obtained from figures 2.15 and 2.16 using the scaling (2.52). The limits from Møller scattering are better than those from $e^+e^- \rightarrow \mu^+\mu^-$ and $e^+e^- \rightarrow e^+e^-$. However, $e^+e^- \rightarrow f\bar{f}$ gives better limits on $M_{Z'}$ if observables with quarks in the final state are included.

A measurement of A_{LR} (2.102) in a fixed target experiment at SLAC is expected to have the precision $\Delta A_{LR} = 1.4 \cdot 10^{-8}$, while the SM prediction is $A_{LR} = 1.8 \cdot 10^{-7}$ [160]. A Z' from the E_6 group (1.41) would multiply A_{LR} by the factor [168]

$$1 + 7 \frac{M_Z^2}{M_{Z'}^2} \left(\cos^2 \beta + \sqrt{\frac{5}{3}} \sin \beta \cos \beta \right). \quad (2.107)$$

Therefore, the experiment is sensitive to $M_{Z'} < 870 \text{ GeV}$.

2.2.3.3 Errors of model measurements

The error of a Z' model measurement in Bhabha and Møller scattering is given by the estimates (2.62) and (2.63). Of course, these reactions can only constrain observables involving the Z' couplings to electrons.

Figure 2.17 shows the result of a corresponding analysis. Fermion pair production and Møller scattering are complementary in a model measurement. Fermion pair production removes a sign ambiguity present in the measurements of Møller scattering.

2.3 Z' search in $e^+e^- \rightarrow W^+W^-$

The symmetry eigenstate Z' does not couple to the W pair due to the $SU(2)_L$ gauge symmetry. The process $e^+e^- \rightarrow W^+W^-$ is sensitive to a Z' only in the case of a non-zero ZZ' mixing. The individual interferences of W pair production rise proportional to s in the limit of large center-of-mass energies \sqrt{s} . In the SM, the sum of all interferences scales like $\ln s/s$ in the limit of large s due to a delicate gauge cancellation. In the case of a non-zero ZZ' mixing, the couplings of the Z_1 differ from the SM predictions for the Z . Then, the gauge cancellation present in the SM is destroyed. The result is a huge magnification of new physics effects at large energies. Unitarity is restored at energies $s \gg M_2^2$ independently of details of the large gauge group.

Similar to the reaction $e^+e^- \rightarrow f\bar{f}$, it is useful to distinguish different cases,

$$\begin{aligned} \text{case 1:} & \quad s < M_2^2, \\ \text{case 2:} & \quad s \approx M_2^2, \\ \text{case 3:} & \quad s > M_2^2, \end{aligned} \tag{2.108}$$

where $s \approx M_2^2$ means $(M_2 - \Gamma_2)^2 < s < (M_2 + \Gamma_2)^2$.

Case 1 gives stringent *exclusion limits* on ZZ' mixing.

Case 2 allows the best exclusion limit or the most accurate *measurement* of the ZZ' mixing angle if a Z' exists.

Case 3 cannot add new information compared to the cases 1 and 2.

We assume here no mixing of the SM W bosons with extra charged gauge bosons. Furthermore, we neglect a possible mixing between SM fermions and exotic fermions. These effects are considered, for example, in reference [170]. A measurement of the W polarization would be very useful to separate ZZ' and lepton mixing effects [125] and for a simultaneous constraint of many anomalous couplings [171, 172].

An early analysis of Z' effects in W pair production can be found in [173].

2.3.1 Born Approximation

2.3.1.1 Amplitude

Following reference [93], we write the amplitude as $\mathcal{M} = \mathcal{M}_t + \mathcal{M}_s$, where the s and t channel contributions including a Z' are

$$\begin{aligned} \mathcal{M}_t^{\lambda_-} &= \frac{\lambda_- - 1}{4t_\nu s_W^2} \times \mathcal{T}^{\lambda_-}(s, c), \\ \mathcal{M}_s^{\lambda_-} &= \left(-\frac{g_{WW\gamma}e}{s} + \frac{g_{WWZ_1}g_1 [v_e(1) - \lambda_- a_e(1)]}{s - M_1^2} \right. \\ &\quad \left. + \frac{g_{WWZ_2}g_2 [v_e(2) - \lambda_- a_e(2)]}{s - M_2^2} \right) \times \mathcal{G}^{\lambda_-}(s, c). \end{aligned} \tag{2.109}$$

$\lambda_-(= -\lambda_+) = \pm 1$ is the electron (positron) helicity as defined in section 2.1.1, \sqrt{s} is the total center-of-mass energy of the e^+e^- pair, $c = \cos \theta$ where θ is the angle between the W^+

and the positron and the invariant t_ν is defined in equation (2.120). The extra neutral gauge boson changes only the s channel amplitude. The functions $\mathcal{T}^{\lambda-}(s, c)$ and $\mathcal{G}^{\lambda-}(s, c)$ are not important in the following discussion. They are the same as in the SM and can be found, for example, in reference [171].

The amplitude of W pair production is linear in the Z_2 couplings to the electron. This makes the W pair production sensitive to the absolute sign of these couplings. Their measurement can remove the sign ambiguity present in fermion pair production where the Z_2 couplings to fermions always appear in pairs.

The coupling constants of the interactions between three gauge bosons are

$$g_{WW\gamma} = e, \quad g_{WWZ_1} = e \frac{c_W}{s_W} c_M, \quad g_{WWZ_2} = e \frac{c_W}{s_W} s_M. \quad (2.110)$$

The contribution of the extra neutral gauge boson can be absorbed in two s -dependent anomalous couplings [174],

$$g_{WW\gamma}^* = e(1 + \delta_\gamma) \quad \text{and} \quad g_{WWZ_1}^* = e(\cot \theta_W + \delta_Z). \quad (2.111)$$

The s channel amplitude including a Z' is then

$$\mathcal{M}_s^{\lambda-} = \left(-\frac{g_{WW\gamma}^* e}{s} + \frac{g_{WWZ_1}^* g_1 [v_e - \lambda_- a_e]}{s - M_1^2} \right) \times \mathcal{G}^{\lambda-}(s, \theta), \quad (2.112)$$

where δ_γ and δ_Z contain contributions due to the Z_2 exchange and due to the ZZ' mixing in the Z_1 exchange [93],

$$\begin{aligned} \delta_\gamma &= \frac{c_W}{s_W} c_M \frac{v_e g_1}{e} \left(\frac{a_e(1)}{a_e} - \frac{v_e(1)}{v_e} \right) \hat{\chi}_1 + \frac{c_W}{s_W} s_M \frac{v_e g_2}{e} \left(\frac{a_e(2)}{a_e} - \frac{v_e(2)}{v_e} \right) \hat{\chi}_2, \\ \delta_Z &= -\frac{c_W}{s_W} + \frac{c_W}{s_W} c_M \frac{a_e(1)}{a_e} \frac{\hat{\chi}_1}{\hat{\chi}_Z} + \frac{c_W}{s_W} s_M \frac{g_2 a_e(2)}{g_1 a_e} \frac{\hat{\chi}_2}{\hat{\chi}_Z}, \end{aligned} \quad (2.113)$$

and

$$\hat{\chi}_n = \frac{s}{s - m_n^2}, \quad n = Z, 1, 2. \quad (2.114)$$

Because W pair production is studied sufficiently far away from the Z_1 peak, we can neglect the Z and Z_1 widths putting $m_Z = M_Z$ and $m_1 = M_1$. We know from present measurements [92] that $M_Z - M_1 < 150 \text{ MeV}$. This allows the approximation

$$\frac{\hat{\chi}_1}{\hat{\chi}_Z} \approx 1 - \frac{2M_Z(M_Z - M_1)}{s - M_Z^2} \approx 1. \quad (2.115)$$

The expressions for δ_γ and δ_Z can then be written as

$$\delta_\gamma = \frac{c_W}{s_W} \frac{v_e}{e} \left(\frac{a_e^M}{a_e} - \frac{v_e^M}{v_e} \right) \left(1 - \frac{\hat{\chi}_2}{\hat{\chi}_Z} \right) \hat{\chi}_Z, \quad \delta_Z = \frac{c_W}{s_W} \frac{a_e^M}{g_1 a_e} \left(1 - \frac{\hat{\chi}_2}{\hat{\chi}_Z} \right), \quad (2.116)$$

where v_e^M and a_e^M are defined in equation (2.4). The terms proportional to $\hat{\chi}_2$ dominate in the case $s \approx M_Z^2$ but can be neglected in the case $s \ll M_Z^2$. Relation (2.116) shows that

measurements of W pair production below the Z_2 peak constrain the same combinations a_e^M, v_e^M as do measurements of fermion pair production on the Z_1 resonance.

Experimental constraints on the anomalous couplings $g_{WW\gamma}^*$ and $g_{WWZ_1}^*$ bound the parameters δ_γ and δ_Z in a model independent way. Constraints on δ_γ and δ_Z can be interpreted as a constraint to the combinations of Z' parameters given in equation (2.113). Far below the Z_2 resonance, the Z_2 mass, the ZZ' mixing angle and the Z' couplings to fermions cannot be constrained separately.

2.3.1.2 Cross section

The Born cross section with N exchanged gauge bosons is, following the notation of reference [175],

$$\begin{aligned} \frac{d\sigma^{\lambda-\lambda_+}}{dc} &= \frac{\sqrt{\lambda}}{\pi s^2 s_1 s_2} \left\{ \sum_{m,n=0}^N \Re e \left\{ \frac{e^4}{s^2} \tilde{\chi}_m(s) \tilde{\chi}_n^*(s) C_T(\text{initial fermions}) \right\} G_{CC3}^{33} \right. \\ &\quad + \sum_{n=0}^N \Re e \left\{ \frac{e^2 (g_1 2c_W)^2}{8s} \tilde{\chi}_n^*(s) [v_e^*(n) + a_e^*(n)] \right\} G_{CC3}^{3f}(\lambda_1 + \lambda_2) \\ &\quad \left. + \frac{(g_1 2c_W)^4}{32} G_{CC3}^{ff}(\lambda_1 + \lambda_2) \right\} \end{aligned} \quad (2.117)$$

with

$$\lambda = (s - s_1 - s_2)^2 - 4s_1 s_2 \quad \text{and} \quad \tilde{\chi}_n(s) = \frac{g_n g_{WWZ_n}}{4\pi\alpha} \frac{s}{s - m_n^2}. \quad (2.118)$$

The definition of the propagator $\tilde{\chi}_n(s)$ is slightly different from (2.7) to absorb the coupling constants from one triple gauge boson vertex and from one gauge boson-fermion vertex. The invariant masses squared s_1 and s_2 of the two W 's are equal to M_W^2 for on-shell W production. The definitions of $C_T(\text{initial fermions})$ and of the helicity combinations λ_1, λ_2 are the same as introduced in section 2.1.1.

The kinematic G -functions are [175, 176],

$$\begin{aligned} G_{CC3}^{33}(s; s_1, s_2; c) &= \frac{1}{32} [\lambda C_1 + 12s_1 s_2 C_2], \\ G_{CC3}^{3f}(s; s_1, s_2; c) &= \frac{1}{8} \left[(s - s_1 - s_2) C_1 - \frac{4s_1 s_2 [s(s_1 + s_2) - C_2]}{t_\nu} \right], \\ G_{CC3}^{ff}(s; s_1, s_2; c) &= \frac{1}{8} \left[C_1 + \frac{4s_1 s_2 C_2}{t_\nu^2} \right] \end{aligned} \quad (2.119)$$

with

$$C_1 = 2s(s_1 + s_2) + C_2, \quad C_2 = \frac{\lambda}{4}(1 - c^2), \quad t_\nu = \frac{1}{2} (s - s_1 - s_2 - c\sqrt{\lambda}). \quad (2.120)$$

The notation used in equations (2.117)-(2.120) allows a generalization to off-shell W pair production and the inclusion of other 4-fermion background diagrams [175].

In the case where the helicities $\tau_+(\tau_-)$ of the $W^+(W^-)$ can be measured, the cross sections $\frac{d\sigma_{\tau_+\tau_-}^{\lambda-\lambda_+}}{dc}$ should be considered. A corresponding analysis for on-shell W production can be found in references [125, 172].

2.3.1.3 Observables

Our starting point for the construction of observables are the differential cross sections $\frac{d\sigma_{\tau^+\tau^-}^{\lambda_-\lambda_+}}{dc}$. They allow for the measurement of total cross sections and asymmetries [177, 178],

$$\begin{aligned}
\sigma_T^{\lambda_-\lambda_+} &= \int_{-1}^{+1} dc \frac{d\sigma^{\lambda_-\lambda_+}}{dc}, \\
\sigma_T^{\lambda_-\lambda_+} A_{FB}^{\lambda_-\lambda_+} &= \int_0^1 dc \frac{d\sigma^{\lambda_-\lambda_+}}{dc} - \int_{-1}^0 dc \frac{d\sigma^{\lambda_-\lambda_+}}{dc}, \\
\sigma_T A_{LR} &= \sigma_T^{\lambda_-= -1} - \sigma_T^{\lambda_-= 1} \equiv \sigma_T^- - \sigma_T^+, \\
\sigma_T A_{LR,FB} &= \int_0^1 dc \frac{d\sigma^-}{dc} - \int_{-1}^0 dc \frac{d\sigma^-}{dc} - \int_0^1 dc \frac{d\sigma^+}{dc} + \int_{-1}^0 dc \frac{d\sigma^+}{dc}, \\
\sigma_T^{\lambda_-\lambda_+} A_{CE}^{\lambda_-\lambda_+}(z) &= \int_{-z}^z dc \frac{d\sigma^{\lambda_-\lambda_+}}{dc} - \int_z^1 dc \frac{d\sigma^{\lambda_-\lambda_+}}{dc} - \int_{-1}^{-z} dc \frac{d\sigma^{\lambda_-\lambda_+}}{dc}. \tag{2.121}
\end{aligned}$$

We omit the indices numbering the polarizations of the W 's to simplify the notation. The observables defined above can be understood as summed over the W polarizations or as written for fixed W polarizations. As in the reaction $e^+e^- \rightarrow f\bar{f}$, the helicities $\lambda_{\pm} = -(+)1$ stand for a left (right) handed electron or positron. Missing polarization indices of the electrons or positrons mean the average over initial polarizations.

A real detector cannot measure from $c = -1$ to $c = 1$. The correction for this effect can be trivially taken into account in the observables (2.121). Furthermore, an integration over only a part of the range of c is sometimes recommended to obtain maximum sensitivity to new physics as pointed out in the second reference of [143].

The unpolarized cross section is dominated by the scattering of left-handed electrons, $\sigma_T \approx \frac{1}{4}\sigma_T^{-+}$. The cross section of right handed electrons excludes the neutrino exchange giving a cross section, which is symmetric in the scattering angle. This induces a relation [177] between two observables, $A_{LR,FB} = A_{FB}$. Cross sections with two left handed or two right handed beams are zero.

In the LEP 2 storage ring, the electrons and positrons have naturally transverse polarization. The azimuthal asymmetry A_T is then an interesting alternative observable [172],

$$\frac{d(\sigma_T A_T)}{dc} = 2 \int_0^{2\pi} d\phi_W \frac{d^2\sigma}{dc d\phi_W} \cos(2\phi_W). \tag{2.122}$$

The W is an unstable particle, which can only be identified through its decay products. A hadronic W decay allows a measurement of the W 's energy-momentum but not an identification of its charge. A leptonic W decay allows a charge identification but not a measurement of the energy-momentum because a part of it is carried away by the neutrino. If one W decays leptonically and one W decays hadronically, the most complete information about both W 's can be extracted. Only a part of the produced W 's can be reconstructed in the detector leading to an effective reduction of the luminosity.

If the W polarization can be measured, a more detailed analysis is possible. For details, we refer to [39] and [179].

For the definition of optimal observables [64] in $e^+e^- \rightarrow W^+W^-$, see reference [65].

2.3.2 Background and Radiative Corrections

The expected accuracy of the measurement of the total W^+W^- cross section at future e^+e^- colliders is about 1%. It has to be met by the theoretical prediction. Therefore, radiative corrections have to be considered. A short overview can be found in [180], for details and extensive original references see [39].

All present Z' analyses of W pair production are done in the Born approximation. An analysis including all radiative corrections relevant to LEP 2 could in principle be done with any of the codes described in reference [39] if the code allows a setting of the anomalous couplings $g_{WWZ_1}^*$ and $g_{WW\gamma}^*$.

2.3.2.1 Background

W bosons are unstable particles, which can be detected only through their decay products,

$$e^+e^- \rightarrow (W^+W^-) \rightarrow f_1f_2f_3f_4. \quad (2.123)$$

We have also non-resonant (background) processes to the same order of perturbation theory,

$$e^+e^- \rightarrow f_1f_2f_3f_4, \quad (2.124)$$

which go directly to the same final state. Their contribution has to be added coherently to the process (2.123) with off-shell W 's to get a gauge invariant result. Different FORTRAN codes calculating the complete process (2.124) are compared in reference [39].

2.3.2.2 QED corrections

QED corrections to the amplitude with Z' exchange can be deduced from the SM results. We therefore give here only a short description of the related SM corrections.

Initial state radiation The QED corrections to on-shell W pair production are calculated in reference [181]. One would like to separate initial state corrections from final state corrections and the interference between them in the calculation for off-shell W pair production because it is much more involved. Unfortunately, this cannot be done in a gauge invariant way. The reason is a charge flow from the initial state to the final state in W pair production. This problem can be treated by the current splitting technique [182], in which the chargeless neutrino exchanged in the t channel is divided into two charge flows of opposite sign. Now the charge flows of the initial and the final state are separated, and the gauge invariance of initial state QED corrections is ensured as it is in the case of Z pair production.

Initial state QED corrections to off-shell W pair production are calculated in [182]. They reach several % near the WW threshold. The corrections can be split into universal contributions, which are described by the flux function (2.21) or structure function (2.20) approaches with the same functions $H_A^c(v)$ or $D(x, s)$ derived for fermion pair production, and into non-universal contributions depending on the particular process. The non-universal contributions to off-shell W and Z production are numerically suppressed by a factor s_1s_2/s^2 [182]. The initial state QED corrections to off-shell W pair production calculated in the flux function

(2.21) or structure function (2.20) approach are therefore a good approximation within the expected accuracy of the data. The generalization of these SM results to cross sections including Z_2 exchange is straight forward.

The radiative corrections to the background (2.124) are a small correction to a small contribution. QED corrections to the background are usually taken into account by the convolutions (2.20) or (2.21).

Coulomb singularity The Coulomb singularity [183] arises from long range electromagnetic interactions between the produced massive charged particles. We get the correction

$$\sigma^{Coul} = \sigma_T \left(1 + \frac{\alpha\pi}{2\lambda} \right) \quad (2.125)$$

for W pair production, which diverges near threshold where the velocity λ of the W 's approaches zero. It indicates that perturbation theory is not applicable in this region. Fortunately, the non-zero width Γ_W and a slight off-shell production of the W 's regularize [184] the Coulomb singularity. Nevertheless, the numerical effect can exceed 6% for the total cross section near threshold [184].

Coulomb singularities also arise in QED and QCD corrections to pair production of massive fermions [87]. There, the singularity can be avoided by a calculation in the limit of massless fermions or by a cut on the invariant mass of the massive fermion pairs. Such a cut is desirable for quark pairs in any case to avoid non-perturbative bound state regions.

2.3.2.3 Weak corrections

The SM one-loop correction to on-shell W^+W^- production is calculated in reference [185]. The calculation of the complete SM one-loop correction to the process (2.124) is very complex [186] and not done. If it is known in the future, the weak corrections in the presence of ZZ' mixing can be treated as described in section 2.1.2.

2.3.2.4 QCD corrections

QCD corrections give sizeable contributions to distributions and cross sections. They enter the width of the W , where they can reach several %, see [187]. QCD corrections can be naively implemented multiplying the cross section by the factor $1 + \frac{\alpha_s}{\pi}$ for every gauge boson decaying into a quark pair. Such a procedure is only a rough guess for background diagrams and for cross sections with kinematic cuts.

QCD corrections are calculated to $O(\alpha_s)$ for on-shell W pair production including the final W polarizations and kinematic cuts in references [188]. The calculation for the complete process $e^+e^- \rightarrow \mu\bar{\nu}_\mu u\bar{d}$ can be found in reference [189]. The results of $O(\alpha_s)$ corrections to $e^+e^- \rightarrow q_1\bar{q}_2q_3\bar{q}_4$, the CC10, CC11 and CC20 processes, can be found in reference [190]. See also reference [191] for further references.

No new problems arise in QCD corrections to processes with Z_2 exchange.

2.3.3 Z' constraints at $s < M_2^2$

To order θ_M , a Z' would modify the cross section due to changes in the $Z_1 e^+ e^-$ couplings and due to the Z_2 exchange contribution. Modifications due to the mass shift $\Delta M = M_Z - M_1$ in the Z_1 propagator are small, see discussions above equation (2.115), and of the order θ_M^2 . Far below the Z_2 resonance, the contribution of the Z_2 exchange can also be neglected because it has the additional suppression factor s/M_2^2 . Therefore, the Z' signal considered here arises due to the modification of the $Z_1 e^+ e^-$ coupling.

All Z' effects can be absorbed in the anomalous couplings δ_γ and δ_Z defined in equation (2.113). A search for a Z' in $W^+ W^-$ production is therefore a special case of a search for anomalous couplings [171, 174, 192, 193]. Far below the Z_2 peak, one has to take special care to separate Z' models from other theories predicting anomalous couplings. One hint for a Z' would be a non-zero δ_γ , which is usually absent in other theories due to the $U(1)_{em}$ gauge invariance. In a general data analysis, one should try to constrain many anomalous couplings simultaneously and show that all combinations perpendicular to δ_Z are zero. If at least one of these perpendicular combinations is not zero, this will indicate that there is other new physics in addition to a Z' . See reference [194] for a corresponding analysis.

An additional check of the Z' hypothesis would be a comparison with deviations in $e^+ e^- \rightarrow f \bar{f}$ below the Z_2 peak. The final proof of the hypothesis would be a measurement at the Z_2 peak.

We assume in the following that all deviations from the SM are due to a Z' and ignore the possible confusion with other physics.

2.3.3.1 Model independent constraints on $g_{\gamma WW}^*$, $g_{Z' WW}^*$ or v_e^M , a_e^M

Estimate Consider the cross section $e_R^- e^+ \rightarrow W^+ W^-$. Only the s -channel contributes to the scattering of right-handed electrons. Expanding the total cross section σ_T^+ in the limit of large s , we get

$$\sigma_T^+ \approx \frac{\alpha^2 \pi c_W^4}{12s} \left[1 - \frac{2s}{M_Z^2} \left(\delta_\gamma - \delta_Z \frac{s_W}{c_W} \right) \right]. \quad (2.126)$$

The first term is the leading SM contribution, the second and third terms are the leading contributions in the parameters δ_γ and δ_Z . The *two* leading powers in s have canceled in the SM term, while only the leading power in s has canceled in the contributions proportional to δ_γ and δ_Z . It follows that the observable σ_T^+ will see a signal if

$$\frac{\Delta \sigma_T^+}{\sigma_T^+} < \frac{\Delta^{Z'} \sigma_T^+}{\sigma_T^+} \approx \frac{2s}{M_Z^2} \left| \delta_\gamma - \delta_Z \frac{s_W}{c_W} \right|, \quad (2.127)$$

where $\Delta \sigma_T^+ / \sigma_T^+$ is the relative experimental error and $\Delta^{Z'} \sigma_T^+$ is the deviation due to a Z' .

Similar considerations can be used for the scattering of left-handed electrons. Unfortunately, the region of forward scattering $c \approx 1$ gives a much reduced sensitivity to a Z' . In this region most of the SM events are produced (making the cross section proportional to $\ln s/s$), while the leading contributions in δ_γ and δ_Z are not logarithmically enhanced. One can avoid this pollution effect by fits to angular distributions. Alternatively, the forward region can be excluded from the integration. The sensitivity to a Z' depends on details of this procedure as

shown in figure 2 of the second reference of [143]. We estimate the sensitivity of the observable σ_T^- to Z' effects doing an expansion of $d\sigma_T^-(c)/dc$ around the point $c = 0$,

$$\frac{d\sigma^-(c=0)}{dc} \sim \frac{1}{s} \left(\frac{1}{4} + 2c_W^4 \right) - \frac{s_W^2}{M_Z^2} \left[\delta_\gamma + \delta_Z \frac{\frac{1}{2} - s_W^2}{s_W c_W} \right]. \quad (2.128)$$

It follows that the observable σ_T^- will see a signal, if

$$\frac{\Delta\sigma_T^-}{\sigma_T^-} < \frac{\Delta^{Z'}\sigma_T^-}{\sigma_T^-} \approx \frac{s}{M_Z^2} \frac{s_W^2}{\left(\frac{1}{4} + 2c_W^4\right)} \left| \delta_\gamma + \delta_Z \frac{\frac{1}{2} - s_W^2}{s_W c_W} \right|. \quad (2.129)$$

As expected from an inspection of the amplitude (2.112), the scattering of left- and right-handed electrons constrains different combinations of δ_γ and δ_Z ,

$$\frac{\Delta^{Z'}\sigma_T^\pm}{\sigma_T^\pm} \sim \left| \delta_\gamma - \delta_Z \frac{g_1}{e} \left(v_e \mp a_e \right) \right|. \quad (2.130)$$

The scattering of unpolarized electrons gives constraints similar to those from e_L^- scattering. Any single observable selected from σ_T , σ_T^+ or σ_T^- is blind to an infinite band in the δ_γ, δ_Z plane. Combining the results from different cross sections, one is insensitive only to a closed region in this plane. For later use, it is instructive to give a rough estimate of the size of this region using (2.129),

$$|\delta_\gamma|, |\delta_Z| < \delta_\gamma^{lim}, \delta_Z^{lim} \approx \frac{\frac{1}{4} + 2c_W^4}{s_W^2} \cdot \frac{\Delta\sigma_T}{\sigma_T} \frac{M_Z^2}{s} \approx 6.2 \cdot \frac{\Delta\sigma_T}{\sigma_T} \frac{M_Z^2}{s}. \quad (2.131)$$

Assuming that the experimental error consisting of statistical and systematic errors scales like the statistical error, $\Delta\sigma/\sigma \approx 1/\sqrt{N} \approx \sqrt{s/L}$, we get a scaling [143] of these constraints with the center-of-mass energy and the integrated luminosity,

$$\delta_\gamma^{lim}, \delta_Z^{lim}, |v_e^M|, |a_e^M| \sim \sqrt{\frac{1+r^2}{sL}}. \quad (2.132)$$

It is the same as derived for anomalous couplings [195]. As before, r is the ratio of the systematic and statistical errors. At the proposed colliders, the statistical errors dominate the error of the observable σ_T^+ , while the error of σ_T^- is usually dominated by systematic errors depending on the cut on c .

Let us make a remark regarding the comparison with $e^+e^- \rightarrow f\bar{f}$. A Z' signal will arise there, if the Z' interferences give deviations larger than the experimental error. Consider the deviation due to the $\gamma Z'$ interference,

$$\Delta^{Z'}\sigma_T \approx \frac{1}{s} \cdot \chi_\gamma(s)\chi_2(s) \approx \frac{1}{s} \cdot 1 \cdot \frac{s}{s - M_2^2} \approx \frac{1}{M_2^2}. \text{ It follows } \frac{\Delta^{Z'}\sigma_T}{\sigma_T} \approx \frac{s}{M_2^2}. \quad (2.133)$$

The constraint has the *same* dependence on s as the constraints (2.127) and (2.129). However, the important difference is that the constraint from fermion pair production is normalized to M_2^2 , while the constraint from W pair production is normalized to M_Z^2 . The ratio s/M_2^2 is small far below the Z_2 peak, while s/M_Z^2 is large at future colliders independently of M_2^2 . This difference is responsible for the enhanced sensitivity of W pair production to the ZZ' mixing angle.

Present Constraints Present constraints on anomalous couplings from LEP data are given in reference [196]. Unfortunately, the constraints given there don't allow a derivation of an excluded region of δ_γ and δ_Z .

Future Constraints Future constraints on δ_γ and δ_Z are given in reference [93]. This analysis is done at the born level and based on $\sqrt{s} = 0.5 TeV$ and $L = 50 fb^{-1}$ assuming 90% polarization of the electrons, 30% detection efficiency of the W bosons and 2% systematic errors. The differential cross section is considered in 10 equal bins in c for $|c| < 0.98$. The resulting constraints are shown in figure 2.18. As expected from the estimates, the cross sections σ_T^+ and σ_T^- or σ_T alone are insensitive to bands in the δ_γ, δ_Z plane. The quantitative agreement with the estimates (2.127) and (2.129) is good.

The model independent limit on δ_γ and δ_Z can be easily converted into limits on the ZZ' mixing angle for any fixed Z' model. For a fixed θ_M , every model is represented by a dot in the δ_γ, δ_Z plane. We show the region of the E_6 and LR models for $\theta_M = 0.002$ in figure 2.18. The ratio of δ_γ and δ_Z is determined by the couplings of the Z' to fermions only, independent of the ZZ' mixing angle and the Z_2 mass,

$$\frac{\delta_Z}{\delta_\gamma} = \frac{e}{g_1 v_e} \frac{1}{\chi_Z} \left(1 - \frac{v'_e a_e}{a'_e v_e} \right)^{-1}. \quad (2.134)$$

If one varies the mixing angle θ_M for a fixed model, one moves on a straight line in the δ_γ, δ_Z plane. The corresponding line is shown in figure 2.18 for $Z' = \chi$. Those values of θ_M , for which one hits the model independent bound, define the constraint on θ_M for that specific model. The limits on θ_M obtained directly from a one-parameter fit for a previously fixed model are expected to be stronger.

In the case of a deviation of δ_γ and δ_Z from zero, the relation (2.134) between the Z' couplings to electrons, can be tested in fermion pair production. Such a cross check [194] would help to verify that the deviation is due to a Z' . In the case of a disagreement, the deviation cannot be due to a Z' alone.

The model independent constraints on δ_γ and δ_Z can be converted into model independent constraints on v_e^M and a_e^M using the relations (2.116). The mass dependence introduced by the propagator $\hat{\chi}_2$ can be neglected far below the Z_2 resonance. Applying this procedure to the limits presented in figure 2.18, one gets the constraints on v_e^M, a_e^M shown in figure 2.3.

In contrast to measurements of fermion pair production, W pair production cannot constrain Z' couplings to fermions $f \neq e$. Therefore, the sensitivity of W pair production to ZZ' mixing is reduced for models where the Z' has small couplings to electrons.

2.3.3.2 Constraints on θ_M

Estimate Combining the definition (2.116) of δ_γ and δ_Z and the estimate (2.131), we derive an estimate for θ_M . Assuming $v'_e \approx v_e$ and $a'_e \approx a_e$, we get from δ_Z

$$|\theta_M| < \theta_M^{lim} \approx 3.4 \cdot \frac{\Delta\sigma_T}{\sigma_T} \cdot \frac{M_Z^2 g_1}{s g_2} \left(1 - \frac{\hat{\chi}_2}{\hat{\chi}_Z} \right)^{-1}. \quad (2.135)$$

We have $\hat{\chi}_2/\hat{\chi}_Z \approx 0$ far below the Z_2 resonance. The scaling with s , L and r is the same as for δ_γ and δ_Z .

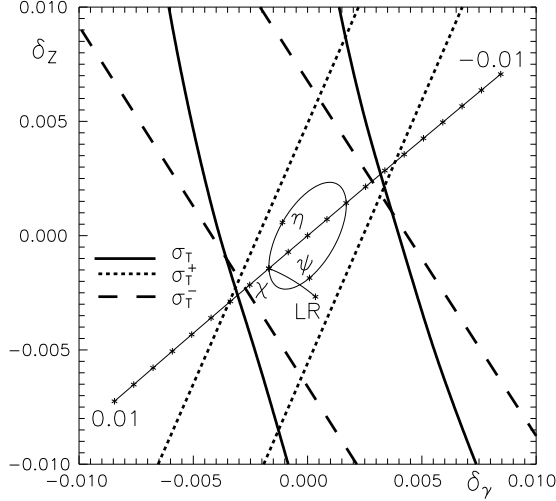


Figure 2.18 Upper bounds (95% CL) on non-standard couplings $(\delta_\gamma, \delta_Z)$ from σ_T^+, σ_T^- and σ_T in $e^+e^- \rightarrow W^+W^-$. See the text for the numerical input. The bands containing $(\delta_\gamma, \delta_Z) = (0, 0)$ cannot be excluded by the observables. The thin lines (the ellipse and the line from the χ to the LR model) are the regions of the E_6 and LR models for $\theta_M = 0.002$. The straight thin line is the region for $Z' = \chi$ for different values for θ_M varied in steps of 0.001. This an update of figure 1 of reference [93].

The estimate (2.135) can be compared with the estimate (2.43) derived for fermion pair production at the Z_1 peak. We see that the sensitivity of W pair production to θ_M becomes eventually better for large energies.

Future Constraints Limits on θ_M at future colliders are presented in reference [93]. It is an update of the older analyses [125, 143].

Figure 2.19 shows the future limit on θ_M as a function of M_2 for $Z' = \psi$. Remembering that the estimate (2.135) ignores details of the Z' model and is based on a crude approximation of the excluded region, it gives a reasonable prediction of the constraint on θ_M in the limit $M_2 \rightarrow \infty$. The present limit on M_ψ and the expected improvement from fermion pair production at the same collider are also indicated. The limit $M_{Z'}^{lim}$ from $e^+e^- \rightarrow f\bar{f}$ is obtained from table 2.4. We took the entry of analysis [126] for $20 fb^{-1}$ with systematic errors but scaled from $L = 20 fb^{-1}$ to $L = 50 fb^{-1}$ by relation (2.53). Also shown are the relations between θ_M and M_2 from the mass and the (model dependent) Higgs constraint.

If s approaches M_2 , the influence of $\hat{\chi}_2/\hat{\chi}_Z$ on δ_γ and δ_Z , in equation (2.135) becomes dominant leading to an additional enhancement to be discussed in the next section.

The limit on θ_M can be compared with the present constraint $-0.0022 < \theta_M < 0.0026$ for the ψ model taken from table 2.1. We see from figure 2.18 that the reaction $e^+e^- \rightarrow W^+W^-$ at a $500 GeV$ collider can add only little to the limits on the ψ from $e^+e^- \rightarrow f\bar{f}$. However, the estimate (2.135) predicts a considerable improvement of the sensitivity for higher energies.

The analysis of figure 2.19 can be repeated for different Z' models. The constraint on $\theta_M(M_2 \rightarrow \infty)$ for different E_6 models is plotted as function of $\cos \beta$ in figure 4 of reference [125].

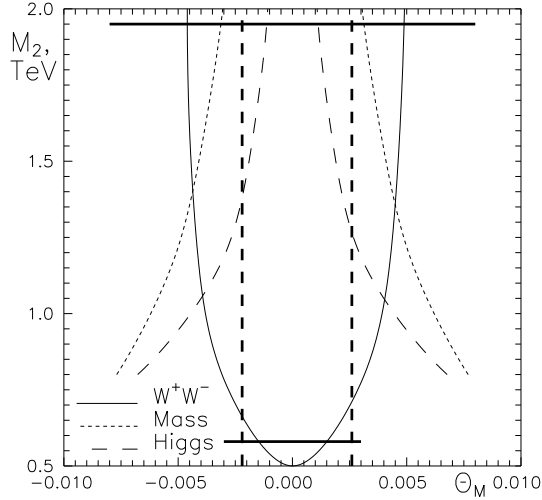


Figure 2.19 Allowed domains (95% CL) of θ_M, M_2 for the ψ model. The region below the solid curve can be excluded with $e^+e^- \rightarrow W^+W^-$ at $\sqrt{s} = 0.5 \text{ TeV}$ and $L = 50 \text{ pb}^{-1}$. See the text for further inputs of the analysis. The current limit on M_2 (θ_M) and the expected exclusion limit on M_2 from $e^+e^- \rightarrow f\bar{f}$ are indicated by the thick solid (dashed) lines. The thin dotted (dashed) lines correspond to the mass constraint (1.16) with $\Delta M = 0.2 \text{ GeV}$ (the Higgs constraint (1.17)). This is an update of figure 2 from reference [93].

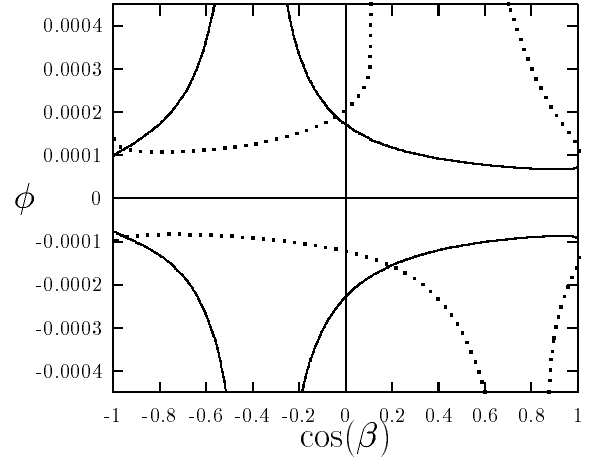


Figure 2.20 Upper limits (95% CL) for $\Phi = \theta_M$ as function of the E_6 model parameter $\cos \beta$ at $\sqrt{s} = M_2 \pm \Gamma_2/2$ for 90% left (right) handed polarized electrons solid (dotted) solid line. Positrons are unpolarized. The input is $M_2 = 1 \text{ TeV}$, $L = 50 \text{ fb}^{-1}$ and a systematic error of 2%. I thank A.A. Pankov for providing this figure.

2.3.3.3 Constraints on M_2

The interference of the Z_2 exchange with the SM contributions is sensitive to the Z_2 mass. Consider the change in the observable O due to the $Z_1 Z_2$ interference ignoring details of the Z' model ($a'_e \approx a_e, v'_e \approx v_e$),

$$\frac{\Delta^{Z'} O}{O_{SM}} \approx \frac{g_2 g_{WWZ_2}}{g_1 g_{WWZ_1}} \frac{s - M_1^2}{s - M_2^2} \approx \frac{g_2}{g_1} \theta_M \frac{s}{s - M_2^2}. \quad (2.136)$$

We took into account that $\theta_M \ll 1$ and that $s \gg M_1^2$ at future colliders in the last step of the approximation. It follows that

$$M_2 < M_{Z'}^{lim} = \sqrt{s} \left(1 + \theta_M \frac{g_2}{g_1} \frac{O}{\Delta O} \right)^{1/2} \quad (2.137)$$

would give a signal in the observable O . Compared to the estimate (2.51) derived for fermion pair production, the sensitivity to M_2 from W pair production is suppressed by the ZZ' mixing angle. Remembering the discussion in section 2.1.3.2, θ_M is constrained to be small by measurements at the Z_1 peak independently of the model. Therefore, the Z' mass bound from W pair production cannot compete with that from fermion pair production.

The resulting indirect bounds on $M_{Z'}$, which one obtains combining the constraint on θ_M with the Higgs constraint depend on the extended Higgs sector. They are worse than the constraints from fermion pair production, compare figure 2.19. Figures similar to figure 2.19 are shown for other E_6 models and $\sqrt{s} = 0.5 TeV$ and $\sqrt{s} = 1 TeV$ in reference [93].

2.3.3.4 Model measurements

Assume that there are non-zero anomalous couplings δ_γ and δ_Z . Then, these couplings can be measured in future experiments. The errors of such measurements can be estimated taking into account that the deviations of cross sections are linear in δ_γ and δ_Z . One gets

$$\Delta\delta_\gamma, \Delta\delta_Z \approx \delta_\gamma^{lim}, \delta_Z^{lim}. \quad (2.138)$$

The estimate for the error of a θ_M measurement is

$$\Delta\theta_M \approx \theta_M^{lim}. \quad (2.139)$$

2.3.4 Z' measurements at $s \approx M_2^2$

The production of W pairs near the Z_2 peak is essentially different from the production far below the resonance. At $s \approx M_2^2$ we definitely know that there exists a Z' . We also know its mass, its width and its couplings to fermions. This information is provided best by fermion pair production on the resonance due to the large statistics of this reaction.

Unfortunately, a description of WW production has the same problem as the description of $f\bar{f}$ production on the Z_2 resonance. The needed radiative corrections within the GUT depend on many unknown parameters.

2.3.4.1 Constraints on θ_M

The production of W^+W^- pairs on the Z_2 resonance is suppressed because it is proportional to θ_M^2 . For $\sqrt{s} \approx M_2 \pm \Gamma_2/2$, the Z_1Z_2 interference, being proportional to θ_M , is most sensitive to ZZ' mixing because it is enhanced by the Z_2 propagator.

An estimate of the sensitivity to θ_M is given by (2.135) as in the case $s < M_2^2$ with the important difference that the ratio $\hat{\chi}_2/\hat{\chi}_Z$, where the width of the Z_2 must now be taken into account, gives the dominant contribution [93],

$$|\theta_M| < \theta_M^{lim} \approx 3.4 \cdot \frac{\Delta\sigma_T}{\sigma_T} \cdot \frac{M_Z^2}{s} \frac{g_1}{g_2} \left| \Re e \frac{\chi_Z}{\chi_2} \right|. \quad (2.140)$$

Compared to the off-resonance case, we have the additional enhancement factor $|\Re\chi_Z/\chi_2| \approx 2\Gamma_2/M_2$ with $2\Gamma_2/M_2 \approx (1/20-1/50)$ depending on the particular Z' model and on the number of the exotic fermion generations to which the Z' can decay. The gain in the sensitivity due to all factors in equation (2.140) is so large that it overcompensates the loss in the sensitivity due to the poor statistics. This is the reason why W pair production near the Z_2 resonance is much more sensitive to θ_M than fermion pair production. See references [143] for a further discussion of this effect.

The increase in the sensitivity for \sqrt{s} approaching M_2 can be seen in figure 2.19. Repeating the procedure for different E_6 models, one arrives at figure 2.20. The constraint on θ_M given there agrees with the estimate (2.140) derived for E_6 models with $2\Gamma_2/M_2 = 1/20$. Figure 2.20 again demonstrates the essential role of beam polarization for exclusion limits in $e^+e^- \rightarrow W^+W^-$. The sensitivity to θ_M becomes stronger for higher energies according to the scaling (2.132).

2.3.4.2 Measurements of θ_M

In the previous section, we assumed that there is a Z' but that the ZZ' mixing angle is so small that only an upper bound can be set in the experiment. We now assume θ_M is large enough to give a signal. Then, the error of a θ_M -measurement is given by equation (2.139) where now θ_M^{lim} must be taken from the estimate (2.140).

2.3.5 Z' Constraints at $s > M_2^2$

Consider the constraint on θ_M (2.135), which transforms to

$$|\theta_M| < 3.4 \cdot \frac{\Delta\sigma_T}{\sigma_T} \cdot \frac{M_Z^2 g_1}{s g_2 M_2^2} = 3.4 \cdot \frac{\Delta\sigma_T}{\sigma_T} \cdot \frac{M_Z^2 g_1}{M_2^2 g_2} \quad (2.141)$$

in the limit of high energies, $s \gg M_2^2$. We see that there is no further enhancement of the sensitivity with rising s . All contributions to the cross sections (2.126) and (2.128) are proportional to $1/s$. Unitarity is restored independently of the details of the large gauge group. This can be understood treating the Z_1 and Z_2 as massless particles in the limit $s \gg M_2^2$. Then, one can consider the unmixed states Z and Z' instead of Z_1 and Z_2 and remember that the Z' does not couple to W 's. The resulting cross section for $e^+e^- \rightarrow W^+W^-$ obviously behaves like the SM for large s .

The estimate (2.141) of the sensitivity to θ_M is always much worse than case 2 where additional enhancement factors were present.

Possible Z' signals from the radiative return to the Z_2 resonance cannot compete with fermion pair production due to lower statistics.

2.4 Z' search in other reactions

The only SM processes in e^+e^- and e^-e^- collisions with two particles in the final state not yet considered are $e^+e^- \rightarrow ZZ$ and $e^+e^- \rightarrow ZH$. They are similar to W pair production. However, they don't have the enhancement factors of new physics. Therefore, these reactions are much less sensitive to a Z' than W pair production.

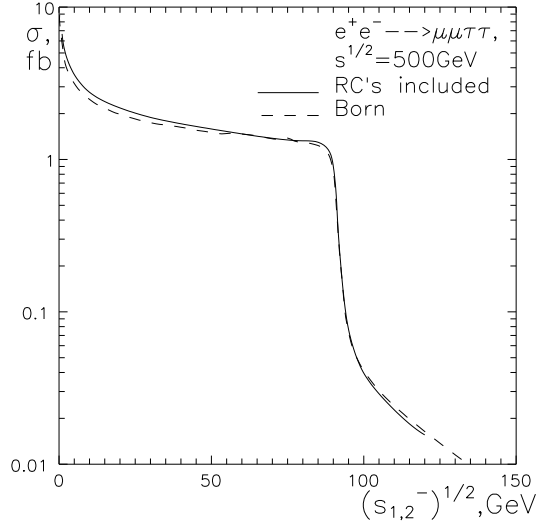


Figure 2.21 $\sigma(e^+e^- \rightarrow \mu^+\mu^-\tau^+\tau^-)$ for $\sqrt{s} = 500 \text{ GeV}$ as function of the lower cut $s_{1,2}^-$ on the invariant energies s_1 and s_2 of the final muon and tau pairs. The solid (dotted) curves show total cross sections with (without) initial state QED corrections.

Higher order processes cannot compete in setting Z' limits due to statistics [197]. Some higher order processes have cross sections comparable to those of two particle final states. Resonating gauge bosons or collinear radiation of light particles can be responsible for this enhancement. However, these enhancement mechanisms do not enhance the Z' contributions. Therefore, they “pollute” a potential Z' signal and should be removed by appropriate kinematic cuts. With these cuts, the resulting cross sections are too small to compete with two particle final states.

The effect is demonstrated [198] in figure 2.21. A cut $s_{1,2}^-$ on the invariant masses s_1 and s_2 of the $\mu^+\mu^-$ and $\tau^+\tau^-$ pairs suppresses first the photon exchange ($s_{1,2}^-$ are small). For $s_{1,2}^- > M_Z^2$, the Z exchange is suppressed too. The resulting cross section is approximately a factor α^2 smaller than cross sections of particle pair production. As expected, the effect is not altered by radiative corrections.

The reactions $e^+e^- \rightarrow Z'Z'$ and $e^+e^- \rightarrow e^+e^-Z'$ are considered in references [200, 201]. The second process is difficult to observe above the background [201]. The first process needs very high energies. It was proposed [200] to use this process to resolve ambiguities in the experimental determination of the E_6 breaking parameter θ . However, this ambiguity can already be resolved by measurements below the Z' peak [130].

The individual interferences of WW scattering ($e^+e^- \rightarrow e^+e^-W^+W^-$) scale like s^2 while the total cross section scales in the SM like $1/s$ for very high energies. As in $e^+e^- \rightarrow W^+W^-$, a non-zero ZZ' mixing angle would destroy this gauge cancellation. Therefore, it could be interesting to investigate the potential of WW scattering for a Z' search at TeV colliders.

Chapter 3

Z' search at pp and $p\bar{p}$ colliders

The Z' signal at hadron colliders comes from *direct* production. This is a principle difference compared to e^+e^- and ep collisions. Therefore, the mass of a detectable Z' must be smaller than the center-of-mass energy of the colliding protons. In practice, the Z' must be at least two times lighter because it is produced in collisions of partons. The Z' is detected through its decay products, which must be separated from the SM background. Unfortunately, the background in a hadronic environment makes it difficult or sometimes impossible to measure potential interesting observables.

The decay of a Z' to a *fermion pair* would probably give the first Z' signal in hadron collisions. The invariant mass of the final state fermion pair is centered around the Z' mass. This allows for a good separation of the signal from the background and for a measurement of the Z' mass. The signature was exploited in the past to measure the properties of the SM Z boson at the UA1 and UA2 experiments [202]. Different fermions in the final state can be tagged providing various cross sections and asymmetries as observables. See references [49, 203, 204, 205] for some old analyses.

Rare Z' decays, $Z' \rightarrow f_1\bar{f}_2V$ (with $V = W, Z$ and f_1, f_2 are higher order processes. However, they are enhanced by large logarithms due to collinear and soft radiation. They give interesting complementary information in a Z' model measurement.

The Z' decay to W pairs is possible only in the case of ZZ' mixing. Unfortunately, this decay mode suffers from the SM background of the associated production of a W and two jets [206].

Associated production of a Z' together with another gauge boson, $pp \rightarrow Z'V$, $V = Z, W, \gamma$ is of higher order compared to the production of a single Z' . However, for $s \gg M_Z^2$ these processes are logarithmically enhanced similar to soft photon radiation. They add independent information about Z' models.

There are no other processes known in hadron collisions, which are useful to add further information on a Z' .

3.1 Born cross section of $pp(p\bar{p}) \rightarrow Z' \rightarrow f\bar{f}$

The considered reaction is much less sensitive to ZZ' mixing than e^+e^- experiments at the Z_1 peak. Therefore, any ZZ' mixing effects can be neglected putting $\theta_M = 0$ and identifying the Z_1 with the Z and the Z_2 with the Z' .

The Born cross section of the production of a Z' , which decays to a fermion pair is

$$\begin{aligned}
\sigma_A \left(pp(p\bar{p}) \rightarrow (\gamma, Z, Z')X \rightarrow f\bar{f}X \right) &\equiv \sigma_A^f \\
&= \sum_q \int_0^1 dx_1 \int_0^1 dx_2 \sigma_A(sx_1x_2; q\bar{q} \rightarrow f\bar{f}) G_A^q(x_1, x_2, M_{Z'}^2) \theta(x_1x_2s - M_\Sigma^2) \\
&= \sum_q \frac{M}{s} \int_{M_\Sigma^2}^s dQ^2 \int_{-y^{max}}^{y^{max}} dy \sigma_A(sx_1x_2; q\bar{q} \rightarrow f\bar{f}) G_A^q(x_1, x_2, M_{Z'}^2) \theta(x_1x_2s - M_\Sigma^2),
\end{aligned} \tag{3.1}$$

where M_Σ is the sum of the masses of the final particles, $x_{1,2} = \sqrt{\frac{Q^2}{s}} e^{\pm y}$ and y is the rapidity. The functions $G_A^q(x_1, x_2, M_{Z'}^2)$, $A = T, FB$ depend on the structure functions of the quarks,

$$\begin{aligned}
G_T^q(x_1, x_2, M_{Z'}^2) &= q(x_1, M_{Z'}^2) \bar{q}(x_2, M_{Z'}^2) + \bar{q}(x_1, M_{Z'}^2) q(x_2, M_{Z'}^2), \\
G_{FB}^q(x_1, x_2, M_{Z'}^2) &= q(x_1, M_{Z'}^2) \bar{q}(x_2, M_{Z'}^2) - \bar{q}(x_1, M_{Z'}^2) q(x_2, M_{Z'}^2).
\end{aligned} \tag{3.2}$$

The expressions for $\sigma_A(sx_1x_2; q\bar{q} \rightarrow f\bar{f})$, $A = T, FB$ can be easily derived from equations (2.6)-(2.9). These formulae also contain the dependence on the helicity of the initial and final fermions.

If the polarization of the final fermion is measurable, one can observe

$$\sigma_{pol}^f = \sigma_T^{f\uparrow} - \sigma_T^{f\downarrow}. \tag{3.3}$$

If polarized proton beams are available [207], the ‘‘left–right’’ cross section is of interest [208],

$$\begin{aligned}
\sigma_{LR}^f &= \sigma_L^f - \sigma_R^f, \\
G_{LR}^q(x_1, x_2, M_{Z'}^2) &= \left[q^\uparrow(x_1, M_{Z'}^2) - q^\downarrow(x_1, M_{Z'}^2) \right] \bar{q}(x_2, M_{Z'}^2) + \left[\bar{q}^\uparrow(x_1, M_{Z'}^2) - \bar{q}^\downarrow(x_1, M_{Z'}^2) \right] q(x_2, M_{Z'}^2).
\end{aligned} \tag{3.4}$$

$\sigma_{L,R}$ are the total production cross sections with one left or right handed initial quark. As in the case of e^+e^- collisions, the difference of σ_{FB} for a left and right handed quark in the initial state can be considered [208],

$$\begin{aligned}
\sigma_{LR,FB}^f &= \sigma_{L,FB}^f - \sigma_{R,FB}^f, \\
G_{LR,FB}^q(x_1, x_2, M_{Z'}^2) &= \left[q^\uparrow(x_1, M_{Z'}^2) - q^\downarrow(x_1, M_{Z'}^2) \right] \bar{q}(x_2, M_{Z'}^2) - \left[\bar{q}^\uparrow(x_1, M_{Z'}^2) - \bar{q}^\downarrow(x_1, M_{Z'}^2) \right] q(x_2, M_{Z'}^2).
\end{aligned} \tag{3.5}$$

More complicated cross sections can be measured if both proton beams are polarized.

3.2 Higher order processes and background

3.2.1 Rare Z' decays

The decay modes $Z' \rightarrow f_1\bar{f}_2V$ (with $V = W, Z$ and f_1, f_2 ordinary fermions) [209] are enhanced by logarithms due to collinear and soft radiation, compare equation (1.32). The decays $Z' \rightarrow$

$Zl^+l^- \rightarrow l_2^+l_2^-l^+l^-$ and $Z' \rightarrow Wl\nu_l$ can be separated from the background [210, 211]. The first process shows only a weak dependence on the Z' couplings serving as a consistency check of the experiment, while the second “gold-plated” decay mode yields useful and complementary information about the Z' couplings [211, 212, 213]. The rare decays where f_1 and f_2 are quarks can also be measured, although with a larger systematic error [211].

3.2.2 Associated Z' production

The production of a Z' in association with another gauge boson, $pp \rightarrow Z'V$, $V = Z, W, \gamma$ is logarithmically enhanced for high energies similar to soft photon radiation from the initial state. The total cross section of the partonic subprocess is [44]

$$\sigma_T(q\bar{q} \rightarrow Z'V) = \frac{g_1^2 g_2^2}{4\pi s} [L_q^2 L_q'^2 + R_q^2 R_q'^2] \left\{ \frac{1 + m_+^2}{1 - m_+^2} \ln \frac{1 - m_+ + \lambda}{1 - m_+ - \lambda} - 2\lambda \right\},$$

with $m_+ = M_{Z'}^2/s + M_V^2/s$ and $\lambda = \lambda(1, M_{Z'}^2/s, M_V^2/s)$, (3.6)

where λ is the kinematic function (2.118). The cross section (3.6) is known from electron positron collisions [214].

Associated Z' production gives complementary information and is free of SM backgrounds [44, 215]. It can compete with other processes in the determination of the parameters of a Z' model [211].

3.2.3 Radiative Corrections

In a first approximation, the tree level Z' contributions can be added to the SM cross section. This approach neglects radiative corrections to the new physics treating them as a small correction to a small effect. This approximation is probably true for a first Z' discovery but has to be checked in a Z' model measurement. In the following we briefly mention the main Standard Model corrections.

3.2.3.1 QCD corrections

QCD corrections are numerically most important. They increase the lowest order cross section of vector boson production at the Tevatron by 20 – 30%. These corrections are often called K factors.

Corrections to the unpolarized Drell–Yan process are known to order $O(\alpha_s^2)$ for the invariant mass distribution [216]. For rapidity– and x –distributions, they are calculated to order $O(\alpha_s)$ [217] and partly to order $O(\alpha_s^2)$ [218]. Soft gluon contributions can be treated to all orders by exponentiation [219]. QCD corrections to polarized hadron scattering are known to order $O(\alpha_s)$ [220].

3.2.3.2 QED and weak corrections

QED corrections are model independent. As in e^+e^- collisions, initial state corrections, final state corrections and the interference between them are separately gauge invariant for neutral current processes. Numerically, the dominant corrections come from final state radiation [221].

The corrections from initial state radiation and the interference between initial and final state radiation are small after factorizing the collinear singularities into the parton distribution functions [221]. As in e^+e^- collisions, final state corrections do not feel the neutral gauge boson exchanged before.

Pure weak corrections are expected to already be very small for the Standard Model Z production [221]. The corrections to Z' production are expected to be even smaller.

3.2.4 Background

The fermions coming from Z' decay have an invariant mass, which is peaked around $M_{Z'}$. Fermion pairs with the same invariant mass could also be produced by gluon, photon or Z exchange.

The experience of existing hadron colliders shows that b -quarks [222] and dijets [223] can be detected [224]. However, the sensitivity to new gauge bosons from quark pairs is reduced compared to muon and electron pairs due to the QCD background.

The background to τ pairs is considered in [225] and found to be manageable for a Z' originating in an E_6 GUT. It is shown there that the signal can be distinguished from the background of W^+W^- production and from the background coming from misidentified jets, which could be accidentally recognized as τ decay products. Furthermore, the background from top pairs decaying to τ pairs can be managed. Even the background from Drell-Yan production of τ 's can be removed although this is harder [225] than in the case of muon pairs.

3.3 Observables

Similar to the case of e^+e^- collisions, the total cross sections σ_T^f and different asymmetries serve as observables,

$$\sigma_T^f, \quad A_{FB}^f = \frac{\sigma_{FB}^f}{\sigma_T^f}, \quad A_{pol}^f = \frac{\sigma_{pol}^f}{\sigma_T^f}, \quad A_{LR}^f = \frac{\sigma_{LR}^f}{\sigma_T^f}, \quad A_{LR,FB}^f = \frac{\sigma_{LR,FB}^f}{\sigma_T^f}. \quad (3.7)$$

Note that $A_{LR,FB}$ in our notation is A_{FB}^{pol} in reference [208], while we reserve A_{pol} for final state polarization asymmetries following the notation of reference [225].

Not all observables (3.7) can be measured in a real experiment. In addition to the constraints mentioned in section 2.1.1.4, complications arise because the signal has to be detected above the background of the hadronic environment.

As in e^+e^- collisions, A_{pol}^f is independent of the couplings to initial fermions. In hadron collisions, all dependence on the quark structure functions also drops out [225].

For lepton pairs in the final state, rapidity ratios can be defined [211],

$$r_{y1} = \frac{\int_{-y_1}^{y_1} \frac{d\sigma_T^l}{dy} dy}{\left(\int_{-y_{max}}^{-y_1} + \int_{y_1}^{y_{max}} \right) \frac{d\sigma_T^l}{dy} dy}, \quad A_{FB y1} = \frac{\left(\int_{-y_1}^0 - \int_0^{y_1} \right) \frac{d\sigma_{FB}^l}{dy} dy}{\left(\int_{-y_{max}}^{-y_1} - \int_{y_1}^{y_{max}} \right) \frac{d\sigma_{FB}^l}{dy} dy}. \quad (3.8)$$

The observable r_{y1} is useful in distinguishing between different Z' models, while $A_{FB y1}$ being ‘‘a refinement of a refinement’’ is less sensitive to different Z' models [211].

Rare Z' decays $Z' \rightarrow f_1 f_2 V$ allow for the definition of the ratios,

$$r_{uZ} \equiv \frac{Br(Z' \rightarrow l^+ l^- Z)}{Br(Z' \rightarrow l^+ l^-)}, \quad r_{\nu\nu Z} \equiv \frac{Br(Z' \rightarrow \nu \bar{\nu} Z)}{Br(Z' \rightarrow l^+ l^-)}, \quad r_{l\nu W} \equiv \frac{Br(Z' \rightarrow l^\pm \nu W)}{Br(Z' \rightarrow l^+ l^-)}. \quad (3.9)$$

The index l refers to a summation over e and μ and the index ν in $r_{\nu\nu Z}$ to the summation over ν_e, ν_μ and ν_τ . The ratios r_{hadZ} and r_{hadW} , where the fermions f_1 and f_2 are quarks can be defined analogously. $r_{l\nu W}$ depends only on the Z' couplings to leptons.

The cross sections of associated Z' production enter the ratios

$$R_{Z'V} = \frac{\sigma(pp \rightarrow Z'V) Br_2^l}{\sigma(pp \rightarrow Z') Br_2^l}, \quad V = Z, W, \gamma. \quad (3.10)$$

3.4 Z' constraints

3.4.1 Model independent constraints on σ_T^f

3.4.1.1 Estimate

The signal of extra neutral gauge bosons in hadron collisions is a number $N_{Z'}$ of excessive fermion pairs with an invariant mass around $M_{Z'}$. In the case of absence of a signal, the observable σ_T^f is constrained independently of the Z' model.

We give here an approximation of σ_T^f to make the dependence of Z' exclusion limits and Z' model measurements on the center-of-mass energy, the integrated luminosity and model parameters transparent [226]. Such an estimate is useful to extrapolate from Z' limits known for *one* collider and Z' model to other colliders and Z' models.

Consider σ_T^μ neglecting the background. Equation (3.1) can be approximated treating the resonating Z' propagator of $\sigma_T^\mu(Q^2; q\bar{q} \rightarrow f\bar{f})$ in the narrow width approximation,

$$\frac{Q^4}{|Q^2 - M^2 + iM\Gamma|^2} \longrightarrow \delta(Q^2 - M^2) \frac{\pi M^4}{M\Gamma}. \quad (3.11)$$

We obtain

$$\sigma_T^\mu = \frac{4\pi^2}{3s} \frac{\Gamma_{Z'}}{M_{Z'}} Br_2^\mu \sum_q Br_2^q f^q \left(\frac{\sqrt{s}}{M_{Z'}}, M_{Z'}^2 \right) \quad (3.12)$$

$$\text{with} \quad f^q(r_z, M_{Z'}^2) = \int_{1/r_z^2}^1 \frac{dx}{x} G_T^q \left(x, \frac{1}{x r_z^2}, M_{Z'}^2 \right) \quad \text{and} \quad r_z = \frac{\sqrt{s}}{M_{Z'}}. \quad (3.13)$$

The function $f^q(r_z, M_{Z'}^2)$ has only a very weak dependence on $M_{Z'}^2$, in the region we are interested in. We therefore can drop the second argument approximating $f^q(r_z, M_{Z'}^2) \approx f^q(r_z)$.

The inspection of Z' limits at the proposed colliders shows [133] that the functions $f^q(r_z)$ are needed only in a narrow interval of r_z , i.e. $3 < r_z < 5$ for pp collisions and $2 < r_z < 3.5$ for $p\bar{p}$ collisions. Under these conditions, the functions for different quarks $q = u, d$ differ mainly by a constant factor. Hence, we can make the following replacement in equation (3.12),

$$\sum_q Br_2^q f^q \left(\frac{\sqrt{s}}{M_{Z'}}, M_{Z'}^2 \right) \approx f^u \left(\frac{\sqrt{s}}{M_{Z'}} \right) \left[Br_2^u + \frac{1}{C_{ud}} Br_2^d \right] \quad (3.14)$$

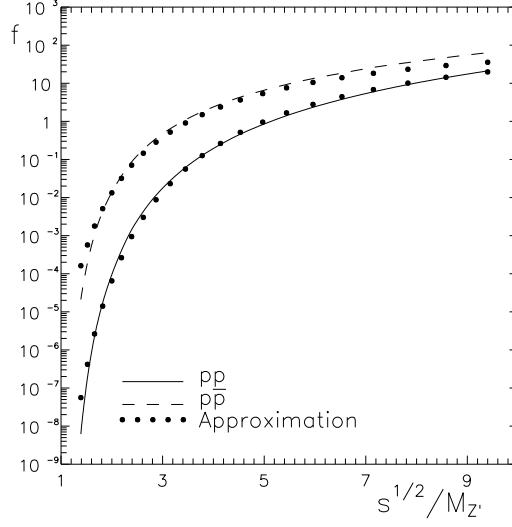


Figure 3.1 The function $f^u(\sqrt{s}/M_{Z'}, 25 \text{ TeV}^2)$ and the approximation (3.15). The curves of $f^u(\sqrt{s}/M_{Z'}, Q^2)$ for $Q^2 = 1 \text{ TeV}^2$ could not be distinguished from $Q^2 = 25 \text{ TeV}^2$. This is figure 1 from reference [226].

with $C_{ud} = f^u(r_z)/f^d(r_z) \approx 2$ (≈ 25) at pp ($p\bar{p}$) colliders. We see that σ_T^μ has a reduced sensitivity to $Z'd\bar{d}$ couplings.

The integral defining the function $f^u(r_z)$ could be approximated by the function $r_z^a(r_z - 1)^b$, which takes into account the parametrization of the structure functions. However, we prefer an approximation by an exponential function because it can be inverted analytically. We get

$$f^u(r_z) \approx C e^{-A/r_z}, \quad C = 600 \text{ (300)}, \quad A = 32 \text{ (20)} \text{ for } pp \text{ (} p\bar{p}\text{) collisions.} \quad (3.15)$$

The approximation (3.15) and the exact calculation (3.13) of $f^u(r_z)$ are shown in figure 3.1. We use the structure functions [227]. The dependence of our results on this choice is negligible. Note that the fit works satisfactorily up to $r_z = 10$. It cannot describe SM Z production at the Tevatron where we have $r_Z \approx 20$.

Collecting all approximations, σ_T^μ can be written as

$$\sigma_T^\mu \equiv \frac{N_{Z'}}{L} \approx \frac{1}{s} c_{Z'} C \exp \left\{ -A \frac{M_{Z'}}{\sqrt{s}} \right\}, \quad (3.16)$$

$$\text{with} \quad c_{Z'} = \frac{4\pi^2}{3} \frac{\Gamma_{Z'}}{M_{Z'}} Br_2^\mu \left[Br_2^u + \frac{1}{C_{ud}} Br_2^d \right].$$

All details of the Z' model are collected in the constant $c_{Z'}$. For convenience, we list the value of $c_{Z'}$ for some Z' models:

| Model: | χ | ψ | η | LR | SSM |
|---------------------------------|--------|--------|--------|------|-------|
| $1000 \cdot c_{Z'}(pp)$: | 1.17 | 0.572 | 0.712 | 1.35 | 2.27 |
| $1000 \cdot c_{Z'}(p\bar{p})$: | 0.40 | 0.437 | 0.556 | 0.77 | 1.41 |

(3.17)

The approximate exponential dependence of σ_T^μ (and of $N_{Z'}$) on $M_{Z'}$ can be recognized, for instance, in figures 1 to 5 of reference [49]. It even holds in associated Z' production, $pp \rightarrow Z'W, pp \rightarrow Z'Z$, as can be seen from figure 3 of reference [44]. The reason is that associated production happens for very constrained values of $Q^2 \approx (M_{Z'} + M_V)^2$ only; for smaller Q^2 , the process is forbidden by kinematics, for larger Q^2 we have an exponential suppression due to structure functions.

Equation (3.16) is the starting point for several useful estimates regarding Z' constraints in hadron collisions.

3.4.1.2 Present constraints

The best present constraints on σ_T^f come from the Tevatron experiments. They give a constraint on $\sigma_T^f \equiv \sigma_T^f(pp \rightarrow Z') \cdot Br_2^f$ as a function of the invariant mass of the final fermion pair ff in the final state.

The constraint from CDF [63] for electrons and muons in the final state ($L = 110 pb^{-1}$ and $\sqrt{s} = 1.8 TeV$) is shown in figure 3.2. The corresponding constraints from D0 can be found in [228]. The CDF data constrain $\sigma_T^l < 0.04 pb$ for large invariant masses. The deviation of the experimental curves from this number for smaller Z' masses are due to the SM background. The total detection efficiencies [63] for electron and muon pairs are $\epsilon_e \approx 47\%$ and $\epsilon_\mu \approx 20\%$. The K factor from QCD corrections is $K \approx 1.3$.

The experimental results can be confronted with the estimate (3.16). The exponential dependence of σ_T^l on $M_{Z'}$ predicted by the estimate can clearly be seen in the figure. Taking into account the detection efficiencies and the K factor, the estimate (3.16) predicts $(\sigma_T^f)^{lim} \approx 0.031 pb$. This is in reasonable agreement with the exact result.

The SM background for *dijets* is much larger due to QCD effects. In reference [229], events with dijets didn't allow constraints on extra neutral gauge bosons from the E_6 GUT.

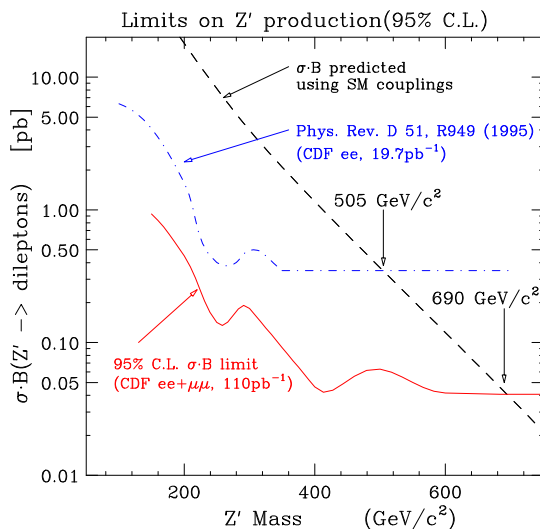


Figure 3.2 The limit on σ_T^l as a function of the dilepton mass, as well as the expectation for $Z' = SSM$. This is figure 3 from reference [63].

3.4.2 Model dependent constraint on $M_{Z'}$

3.4.2.1 Estimate

Inverting the approximation (3.16), we get a constraint on $M_{Z'}$,

$$M_{Z'} > M_{Z'}^{lim} \approx \frac{\sqrt{s}}{A} \ln \left(\frac{L c_{Z'} C}{s N_{Z'}} \right) \approx \sqrt{s} \begin{cases} 0.386 + \frac{1}{32} \ln \left(\frac{L \cdot fb}{N_{Z'} \cdot s / TeV^2} \cdot 1000 c_{Z'} \right) & pp \\ 0.583 + \frac{1}{20} \ln \left(\frac{L \cdot fb}{N_{Z'} \cdot s / TeV^2} \cdot 1000 c_{Z'} \right) & p\bar{p} \end{cases} . \quad (3.18)$$

For $M_{Z'} < M_{Z'}^{lim}$ more than $N_{Z'}$ additional events are expected.

A formula similar to (3.18) was quoted in reference [230] some time ago. However, there the dependence of $M_{Z'}^{lim}$ on Z' couplings and collider parameters is given only numerically.

Relation (3.18) describes the scaling of $M_{Z'}^{lim}$ with the center-of-mass energy and the integrated luminosity. $M_{Z'}^{lim}$ depends on L only logarithmically. Therefore, the dependence of $M_{Z'}^{lim}$ on detector efficiencies or event losses due to background suppression is only marginal.

The logarithmic dependence of $M_{Z'}^{lim}$ on L can be recognized in figure 3 of reference [131] or in figure 2.33 in reference [63]. The reduction of $M_{Z'}^{lim}$ due to a decrease of the event rate by a factor of two is predicted by relation (3.18) to be 9% (7%) for the proposed pp ($p\bar{p}$) colliders. These numbers, which do not discriminate between Z' models, s , and L , are in agreement with the last line of table 1 in reference [131].

The model dependent constant $c_{Z'}$ enters (3.18) only under the logarithm leading to the weak model dependence of Z' exclusion limits in pp and $p\bar{p}$ collisions. The physical origin of this effect is hidden in the properties of the structure functions defining (3.13) the function $f(r_z)$. Therefore, relation (3.18) obtained for σ_T^μ is qualitatively true for other observables too.

Radiative corrections lead to deviations of $N_{Z'}$ from the Born prediction. The effect on $M_{Z'}^{lim}$ is moderate because $N_{Z'}$ enters this limit only under the logarithm.

The scaling (3.18) is the complement of relation (2.53) derived for $e^+e^- \rightarrow f\bar{f}$. The strong model dependence of Z' exclusion limits from e^+e^- collisions is due to their direct dependence on the square of the coupling constants of the Z' to fermions, see (2.47).

In the last step, equation (3.18) is written in a form, which makes the logarithm nearly zero for GUT's at the proposed colliders. We see that the numerical influence of the logarithm is suppressed by a small prefactor. The constant terms 0.386 and 0.583 give an estimate for the average sensitivity of $pp(p\bar{p})$ collisions to a Z' in units of \sqrt{s} .

For practical purposes, it is useful to rewrite equation (3.18) as

$$\frac{M_{Z'}^{lim}(s, L)}{M_{Z'}^{lim}(s_0, L_0)} \approx \frac{\sqrt{s}}{\sqrt{s_0}} \left(1 + \xi \ln \frac{s_0 L}{s L_0} \right) \quad \text{with} \quad \xi = \left[\ln \frac{L_0 c_{Z'} C}{s_0 N_{Z'}} \right]^{-1}, \quad (3.19)$$

where now all model dependence is hidden in the constant ξ . Normalizing at one collider, equation (3.19) predicts the limits at another collider. All Z' exclusion limits published in figure 1 of reference [133] can be reproduced by the estimate (3.19) with an accuracy of 10% for $\xi = 0.13$ (0.10) for pp ($p\bar{p}$) collisions.

3.4.2.2 Present constraints

No Z' signal is found in present experiments. This negative search result can be interpreted as exclusion limits $M_{Z'}^{lim}$ in different models.

The limits quoted in reference [63] are in a good agreement with the prediction (3.18).

| Model: | χ | ψ | η | LR | SSM |
|---------------------------------|--------|--------|--------|------|-------|
| $M_{Z'}^{lim}/GeV$ from [63]: | 595 | 590 | 620 | 630 | 690 |
| $M_{Z'}^{lim}/GeV$ from (3.18): | 552 | 560 | 582 | 611 | 665 |

Table 3.1 The lower bounds (95% CL) on the Z' mass from the analysis [63] compared to the estimate (3.18). The finite detection efficiencies ϵ_e, ϵ_μ and the K -factor as given in section 3.4.1.2 are taken into account in the estimates.

3.4.2.3 Future constraints

The minimal input of the different analyses are the integrated luminosity L and the center-of-mass energy \sqrt{s} of the colliding particles (pp or $p\bar{p}$), a list of observables entering the fit and the number of Z' events $N_{Z'}$ demanded for a signal. If applied, kinematic cuts and radiative corrections must be specified. It follows a list of different analyses.

Reference [133] GODFREY95: This is a theoretical analysis for different future colliders based on σ_T^e and σ_T^μ with $N_{Z'} = 10$. No Z' decays to exotic fermions are assumed. 1-loop QCD corrections are included in the Z' production. The Z' decay is calculated including 2-loop QCD, 1-loop QED corrections and top-quark decays. We selected two scenarios to present them in table 3.2. The numbers are taken from table 2 of reference [8] and from figure 1 of [133].

Reference [131] RIZZO96: This is a theoretical analysis for different future colliders based on σ_T^e and σ_T^μ with $N_{Z'} = 10$. No Z' decays to exotic fermions are assumed. No radiative corrections are included. We selected two scenarios for our table 3.2. The numbers are taken from table 1 of [131].

The results of the different analyses are compared with the estimate (3.18). We see that the prediction (3.18) agrees with the exact results within 10% in a wide range of L and s .

3.4.3 Model independent constraint on g_2/g_1

Figure 3.2 gives constraints on g_2/g_1 . According to the estimate (3.16), σ_T^μ scales as $\Gamma_{Z'}/M_{Z'} \sim g_2^2$. The missing factor depends on the Z' model. It is given in (2.78) for $Z' = SSM$ if no decays to exotic fermions are allowed. The resulting constraint $g_2 < g_2^{lim}$ can be obtained graphically from figure 3.2 by an appropriate shift of the signal cross section. We get $g_2^{lim} \approx g_1/4.5$ for $Z' = SSM$ and $M_{Z'} < 400 GeV$.

3.4.4 Errors of Model measurements

| Analysis | $\frac{\sqrt{s}}{\text{TeV}}$ | $L \cdot \text{fb}$ | χ | ψ | η | LR | SSM | estimate (3.18) |
|----------|-------------------------------|---------------------|--------|--------|--------|------|-------|-----------------|
| [133] | 2($p\bar{p}$) | 10 | 1.04 | 1.05 | 1.07 | 1.10 | 1.15 | 1.06 |
| [133] | 14(pp) | 100 | 4.38 | 4.19 | 4.29 | 4.53 | 4.80 | 4.47 |
| [131] | 60(pp) | 100 | 13.3 | 12.0 | 12.3 | 13.5 | 14.4 | 13.7 |
| [131] | 200(pp) | 1000 | 43.6 | 39.2 | 40.1 | 43.2 | 44.9 | 49.3 |

Table 3.2 The lower bound on the Z' mass $M_{Z'}^{lim}$ in TeV excluded by the different analyses described in the text. The estimate (3.18) is added for $Z' = SSM$. This is table 1 from reference [226].

3.4.4.1 Estimate

Model parameters can be measured if some of the observables O introduced in section 3.3 give a signal. A reasonable model measurement requires enough events to assume that they have a normal distribution. The one- σ statistical error can then be estimated using equation (3.16),

$$\Delta A_{FB}^l \approx \frac{1}{\sqrt{N_{Z'}}} \approx \sqrt{\frac{s}{L} \frac{1}{c_{Z'} C}} \exp \left\{ \frac{AM_{Z'}}{2\sqrt{s}} \right\}. \quad (3.20)$$

Relation (3.20) relies on the approximation (3.15), which becomes inaccurate for too large $\sqrt{s}/M_{Z'}$. The error of other observables also scales as (3.20) with s and L , however, the prefactors differ.

Compared to the exclusion limit $M_{Z'}^{lim}$, the error of a model measurement is much more model dependent because the influence of the constant $c_{Z'}$ is no longer logarithmically suppressed. The dependence on the integrated luminosity is the same as in equation (2.65). Therefore, the dependence of model measurements on systematic errors in hadron collisions is as pronounced as in e^+e^- collisions.

Combining equations (3.18) and (3.20), we can predict ΔO for a given $M_{Z'} < M_{Z'}^{lim}$ if we know $M_{Z'}^{lim}$ from the observable O alone for the same collider,

$$\Delta O \approx (N_{Z'})^{-f_m/2} \cdot \left(\frac{s}{L} \frac{1}{c_{Z'} C} \right)^{\frac{1}{2}(1-f_m)}, \quad f_m = M_{Z'}/M_{Z'}^{lim}. \quad (3.21)$$

It is the complement to the estimates (2.62) and (2.63) derived for e^+e^- collisions, which relate exclusion limits and measurements of the same confidence level. Relation (3.21) relates exclusion limits from $N_{Z'}$ expected Z' events to one- σ errors of model measurements. To relate exclusion limits of 95% confidence ($N_{Z'} = 3$) to measurements of 95% confidence, equation (3.21) modifies to

$$\Delta O \approx 2 \cdot 3^{-f_m/2} \cdot \left(\frac{s}{L} \frac{1}{c_{Z'} C} \right)^{\frac{1}{2}(1-f_m)}. \quad (3.22)$$

Both estimates (3.22) and (2.63) are shown in figure (3.3). The estimate (3.22) depends on collider parameters, while the estimate (2.63) is universal for e^+e^- collisions. Note that both estimates do not work for too small f_m .

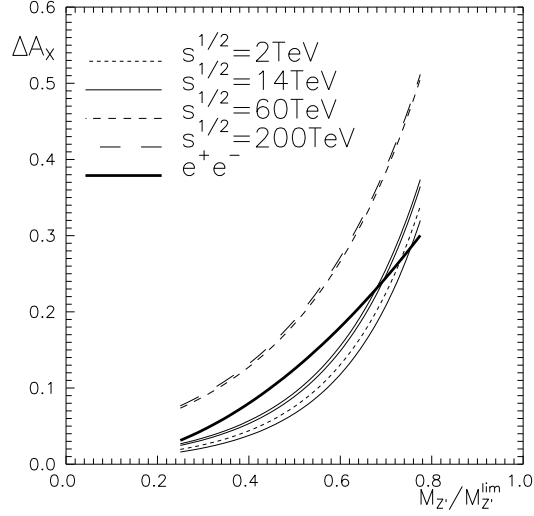


Figure 3.3 The estimate of ΔO (95% CL) as a function of $M_{Z'}/M_{Z'}^{lim}$ as given in equation (3.22). $M_{Z'}^{lim}$ is the Z' exclusion limit obtained from the same observable O alone. Shown are the predictions for the scenarios listed in table 3.2 for $Z' = \eta$. For $\sqrt{s} = 14 \text{ TeV}$, the dependence is shown for $Z' = \psi, \eta, SSM$ (from top to down). The thick solid line is obtained from relation (2.63).

3.4.4.2 Future measurements

The estimate (3.20) can be confronted with results of the theoretical analysis [44], which assumes $\sqrt{s} = 14 \text{ TeV} L = 100 \text{ fb}^{-1}$ and $M_{Z'} = 1 \text{ TeV}$. The measurement of $O = A_{FB}^e$ is investigated there. Having in mind the crude approximations, which lead to the estimate (3.20), the agreement is reasonable.

| Analysis | χ | ψ | η | LR | SSM |
|------------------------------|--------|--------|--------|-------|-------|
| ΔA_{FB}^e from [44]: | 0.007 | 0.016 | 0.014 | 0.006 | - |
| ΔO from (3.20): | 0.008 | 0.012 | 0.011 | 0.008 | 0.006 |

Table 3.3 Expected errors of measurements of ΔA_{FB}^e from reference [44] and from estimate (3.20).

As mentioned in section 3.3, the polarization asymmetry of τ 's in the final state depends on the couplings of the Z' to the τ only,

$$A_{pol}^\tau = v'_\tau a'_\tau / (v'^2_\tau + a'^2_\tau). \quad (3.23)$$

Therefore, it allows a model independent measurement of this combination of coupling constants. The structure functions and branching ratios of the Z' influence only the event rate

and therefore the error of A_{pol}^τ . For E_6 GUT's, it is estimated [225] as $\Delta A_{pol}^\tau \approx 1.5/\sqrt{N_{Z'}}$.

A measurement of the observables

$$r_{y1}, A_{FB}, A_{FB y1}, r_{l\nu W}, R_{Z'Z}, R_{Z'W} \text{ and } R_{Z'\gamma} \quad (3.24)$$

would give model independent information on the Z' parameters γ_L^l , γ_L^q , \tilde{U} and \tilde{D} defined in equation (1.37). For $M_{Z'} = 1 \text{ TeV}$, the expected accuracy of such an measurement at LHC is 5% for γ_L^l and between 20% and 30% for γ_L^q, \tilde{U} and \tilde{D} [211]. The estimate (3.20) predicts errors of about 1%. The estimate is considerably smaller because it relies on A_{FB}^μ . The measurements of γ_L^l , γ_L^q , \tilde{U} and \tilde{D} are based on all observables (3.24). Unfortunately, the measurements of the observables involving associated Z' production or rare Z' decays suffer from smaller statistics. See table II of reference [211] for details. This explains the difference between the results in table 3.4 and the estimate.

| | χ | ψ | η | LR |
|--------------|-----------------|----------------|-----------------|------------------|
| γ_L^l | 0.9 ± 0.016 | 0.5 ± 0.02 | 0.2 ± 0.012 | 0.36 ± 0.007 |
| γ_L^q | 0.1 | 0.5 | 0.8 | 0.04 |
| \tilde{U} | 1 ± 0.16 | 1 ± 0.14 | 1 ± 0.08 | 37 ± 6.6 |
| \tilde{D} | 9 ± 0.057 | 1 ± 0.22 | 0.25 ± 0.16 | 65 ± 11 |

Table 3.4 Values of the parameters (1.37) and its statistical error-bars for typical models determined from probes at the LHC ($\sqrt{s} = 14 \text{ TeV}$, $L = 100 \text{ fb}^{-1}$). $M_{Z'} = 1 \text{ TeV}$. This is table 3 of reference [8].

The measurements of $\gamma_L^l, \gamma_L^q, \tilde{U}$ and \tilde{D} can be used to get information on the symmetry breaking sector [45]. Similar to a model measurement in e^+e^- collisions described in section 2.1.4.4, a verification of the relations (1.39) allows to check, whether the Z' comes from the breaking of the E_6 or $SO(10)$ groups. In any case, the breaking parameters can be determined. Under the assumptions of reference [45], the statistical errors of such a measurement are around 10%. The breaking parameters $\gamma_L^l, \gamma_L^q, \tilde{U}$ define the Z' couplings to SM fermions with a 16-fold sign ambiguity. This ambiguity can be removed by measurements at e^+e^- colliders. Hadron colliders alone can reduce the sign ambiguity by collisions of polarized beams or by a measurement of observables, which are sensitive to the polarization in the final state as A_{pol}^τ .

The measurement of g_R/g_L in left-right symmetric models is considered in reference [52]. For $M_{Z'} = 1 \text{ TeV}$, this ratio could be measured at the LHC with a statistical error of about 1%.

If a Z' signal is found in hadron collisions, $M_{Z'}$ and $\Gamma_{Z'}$ can be defined by a fit to the invariant mass distribution of the final fermion pairs from the Z' decay. $M_{Z'}$ can be measured with an accuracy of $\Gamma_{Z'}$ detecting only a few Z' events. This is proven by the early measurements of the SM W - and Z -masses by the UA1 and UA2 experiments at CERN [202]. For larger event numbers, the systematic errors become important. See reference [231] for details.

Chapter 4

Z' search in other experiments

There are other experiments not yet mentioned, which can give bounds on extra neutral gauge bosons. For completeness, we briefly comment on some of them in the next sections.

4.1 ep collisions

Neutral current electron–proton scattering occurs through photon, Z or Z' exchange in the t channel. The Z' is detected by indirect effects similar to e^+e^- collisions. The additional contributions due to Z' exchange lead to deviations of observables from their SM predictions. Compared to e^+e^- collisions, ep collisions suffer from the hadronic background, in which these deviations must be detected. ep collisions are as insensitive to ZZ' mixing as off–resonance fermion pair production. Therefore, we put the ZZ' mixing angle θ_M to zero in this section and identify Z_1 and Z_2 with Z and Z' .

Some early Z' analyses can be found in the references [204, 232, 233, 234].

4.1.1 Born cross section

The **amplitude** of ep scattering depends only on the ratio of the Z' couplings and the Z' mass. The six couplings a'_f, v'_f with $f = e, u, d$ are always involved simultaneously because the Z' must couple to the initial state.

The **cross section** of the reaction $e_{L,R}^- p \rightarrow e_{L,R}^- X$ including extra neutral gauge bosons is

$$\frac{d\sigma(e_{L,R}^-)}{dxdy} = 2\pi\alpha^2 \frac{s}{Q^4} \sum_{m,n} \sigma(m, n) \quad (4.1)$$

with

$$\begin{aligned} \sigma(m, n) &= \chi_m(Q^2)\chi_n^*(Q^2) \left[[1 + (1 - y)]^2 F_2^{L,R}(x, Q^2) + [1 - (1 - y)]^2 x F_3^{L,R}(x, Q^2) \right], \\ F_2^{L,R}(x, Q^2) &= x [C_V(e) \pm C_A(e)] \sum_q [C_V(q)(q(x, Q^2) + \bar{q}(x, Q^2))], \\ x F_3^{L,R}(x, Q^2) &= \pm x [C_A(e) \pm C_V(e)] \sum_q [C_A(q)(q(x, Q^2) - \bar{q}(x, Q^2))], \\ C_V(f) &= v_f(m)v_f^*(n) + a_f(m)a_f^*(n), \quad C_A(f) = v_f(m)a_f^*(n) + a_f(m)v_f^*(n). \end{aligned} \quad (4.2)$$

The propagator $\chi_n(Q^2)$ is given in equation (2.7) and the couplings $v_f(n)$ and $a_f(n)$ are defined in equation (1.23) and (1.28). $q(x, Q^2)$ and $\bar{q}(x, Q^2)$ are structure functions of the proton. The cross section for $e_{L,R}^+$ scattering is given by equation (4.1) with the replacements $F_2^{L,R} \rightarrow F_2^{R,L}$, $F_3^{L,R} \rightarrow -F_3^{R,L}$ in equation (4.2). The kinematic variables Bjorken- x and y are defined as

$$x \equiv \frac{Q^2}{2P \cdot q}, \quad y \equiv \frac{P \cdot q}{P \cdot p_e} = \frac{Q^2}{xs} \quad \text{with} \quad Q^2 = -q^2 = -(p_e - p_l)^2, \quad \text{and} \quad s \equiv (p_e + P)^2. \quad (4.3)$$

$p_e(p_l, P)$ are the energy-momenta of the incoming electron (scattered electron, proton). s is the center-of-mass energy squared and Q^2 is the momentum transfer squared. We treat all initial and final particles as massless.

Among the different **observables**, the total cross sections are rather insensitive to a Z' because the contributions from photon exchange are very large. Charge (A_{LL}^{-+} , A_{RR}^{-+}), polarization (A_{LR}^{++} , A_{LR}^{--}) and mixed (A_{LR}^{-+} , A_{RL}^{-+}) asymmetries can be defined [233, 234],

$$A_{XY}^{mn} = \frac{d\sigma(e_X^m) - d\sigma(e_Y^n)}{d\sigma(e_X^m) + d\sigma(e_Y^n)}, \quad X, Y = L, R; \quad m, n = +, -. \quad (4.4)$$

Most of the systematic errors drop out in these asymmetries.

4.1.2 Radiative Corrections

Presently there are no hints for a Z' at HERA. We expect that possible new Z' contributions to the cross section are very small. It is therefore sufficient to take into account only the **QED corrections** in the leading log approximation (LLA) [235] to these contributions. For the other contributions, one has to take into account the SM corrections. See reference [236, 237] for an overview of SM corrections to ep collisions and for further references. QED corrections can be taken into account in a model independent way in the LLA. They consist of initial and final state radiation [238] and the Compton peak [239].

The full $O(\alpha)$ QED and **weak corrections** can be found in references [37, 240]. See also section 2.1.2.2 for further references to weak corrections. They can be taken into account [235] by form factors [85] as described in section 2.1.2.2. As discussed in reference [235], the electroweak corrections are of the same size as the Z' effects. Therefore, they must be taken into account in a Z' analysis at ep colliders. The M_t - and M_H -dependence of weak corrections in presence of Z' production is discussed in reference [241].

The **QCD corrections** to Z' production are the same as in the SM. See references [242] for a short review and for further references.

4.1.3 Z' constraints

A **model independent** Z' analysis in ep collisions always involves the six Z' couplings a'_f, v'_f , $f = e, u, d$. If the condition (1.26) is assumed, the model independent analysis can constrain the five combinations (1.36). ep collisions are sensitive to the relative sign of the Z' couplings. A model independent analysis for HERA is carried out in reference [243]. Unfortunately, HERA cannot compete with hadron colliders [244, 248] in setting Z' bounds for usual GUT's.

Model dependent Z' limits at electron proton colliders can be obtained by considerations similar to those explained for e^+e^- collisions. We get the following scaling of $M_{Z'}^{lim}$ with L and s ,

$$M_{Z'}^{lim} \approx \sqrt{Q^2} \left(1 + \frac{1}{\Delta o}\right)^{1/2} \sim \left[\frac{sL}{1+r^2}\right]^{1/4}. \quad (4.5)$$

The scaling is the same as in e^+e^- collisions. Therefore, the dependence on systematic errors is the same. The difference is that the error Δo depends on the kinematic variable Q^2 . Reasonable statistics are obtained for Q^2 well below s . As a result, ep collisions are sensitive to extra neutral gauge bosons with masses comparable to the center-of-mass energy \sqrt{s} . The model dependence of these bounds is large as in e^+e^- collisions.

See reference [245] for a first analysis of **future exclusion limits** including radiative corrections. A recent analyses can be found in reference [246]. A comparison of the numbers in table 4.1 with those of table 3.2 demonstrates that HERA cannot compete in setting mass limits to a Z' predicted in typical extended gauge theories. The scaling (4.5) describes nicely the changes with the luminosity.

| $M_{Z'}/GeV$ | χ | ψ | η | LR |
|-------------------|--------|--------|--------|------|
| $L = 0.5 fb^{-1}$ | 390 | 210 | 240 | 420 |
| $L = 1.0 fb^{-1}$ | 470 | 260 | 290 | 500 |
| ratio | 1.21 | 1.24 | 1.21 | 1.19 |

Table 4.1 The 95% CL predictions for $M_{Z'}^{lim}$ from HERA with $\sqrt{s} = 314 GeV$ and the integrated luminosities quoted in the table. The first two rows are taken from table 3 of reference [246].

Recently, the anomalous high Q^2 events observed at HERA [247] received much attention. As pointed out in reference [248], these deviations from the SM cannot be explained by a Z' coming from typical extended gauge theories, which is compatible with the present LEP and Tevatron data. Two models, the excited weak boson model [249] and the BESS model [19] are not ruled out by the present data.

4.2 Atomic parity violation

The measurement of parity-nonconserving transitions in atoms has reached a precision [250, 251], which allows constraints to extra neutral gauge bosons competitive [109, 110, 252, 253] to those from collider experiments.

Parity violating transitions occur due to the exchange of vector bosons with axial couplings. The experimental results are usually given in terms of the weak charge,

$$Q_W = -2C_{1u}(2Z + N) - 2C_{1d}(Z + 2N), \quad C_{1q} = 2a_e(1)v_q(1), \quad q = u, d. \quad (4.6)$$

It arises due to the coherent interaction of the electron with all $Z(N)$ protons (neutrons) in the nucleus of the considered atom.

To calculate the SM prediction of Q_W , radiative corrections [254] must be applied,

$$C_{1u} = -\rho'_{PV} \left(\frac{1}{2} - \frac{4}{3} s_W^2(0)_{eff} \right), \quad C_{1d} = -\rho'_{PV} \left(-\frac{1}{2} + \frac{2}{3} s_W^2(0)_{eff} \right). \quad (4.7)$$

For $^{133}_{55}\text{Cs}$, we have $Q_W = -376C_{1u} - 422C_{1d}$. The resulting SM prediction [255] for $M_t = 175 \text{ GeV}$ and $m_H = 100 \text{ GeV}$ is $Q_W^{SM} = -73.04$.

This can be compared with the present experimental value [250],

$$Q_W = -72.11(27)_{exp}(89)_{theory}. \quad (4.8)$$

The agreement with the SM prediction is used to constrain possible new physics.

The exchange of extra neutral gauge bosons would give additional contributions to parity violating transitions in atoms. For $^{133}_{55}\text{Cs}$, the predicted change in the weak charge is [109]

$$\Delta Q_W = \left(\frac{M_Z^2}{M_1^2} - 1 \right) (Q_W^{SM} + 73.8) - \theta_M \frac{g_2}{g_1} (Q_W^{(2)} + 2a_e(2)Q_W^{SM}) + 2 \frac{M_1^2 g_2^2}{M_2^2 g_1^2} a_e(2) Q_W^{(2)} \quad (4.9)$$

with $Q_W^{(2)} = -376v_u(2) - 422v_d(2)$. The first contribution is numerically negligible [109] due to an accidental cancellation between the two contributions and due to the present experimental constraint on $M_Z^2/M_1^2 - 1 = \rho_{mix} - 1 < 0.003$ already mentioned in section 2.1.3.1. The constraint (4.9) can therefore be parametrized as [109]

$$\Delta Q_W \approx \gamma_1 \theta_M + \gamma_2 \frac{M_1^2}{M_2^2}. \quad (4.10)$$

The coefficients γ_1 and γ_2 are given for some models in table 4.2.

The present constraints on the ZZ' mixing angle θ_M from measurements at the Z_1 peak are stronger than those, which would result from atomic parity violation. As a result, measurements of atomic parity violation constrain mainly M_1/M_2 .

| | χ | ψ | η | LR |
|------------|--------|--------|--------|-------|
| γ_1 | -138.0 | 37.2 | -114.0 | -46.9 |
| γ_2 | 65.6 | 0.0 | -16.4 | 74.7 |

Table 4.2 Values of the parameters γ_1 and γ_2 computed for $s_W^2 = 0.2334$ for different Z' models. The numbers are taken from table IX of reference [109].

Note however, that the weak charge Q_W can receive compensating contributions from more than one new physics source, which would relax the Z' limits. Such cancellation effects are explicitly demonstrated in reference [256].

4.3 Neutrino scattering

High energy neutrino scattering experiments provided interesting limits on Z' parameters in the past. Today, they cannot compete with the limits from collider experiments. See references [6, 7] for a review and references to older experiments. Recent results of neutrino scattering experiments can be found in references [257, 258], a recent review is given in reference [259].

Neutrino–electron and neutrino–nucleon scattering experiments measure the couplings of the neutrino to the Z boson [259],

$$v_\nu = -0.035 \pm 0.012 \pm 0.012, \quad a_\nu = -0.503 \pm 0.006 \pm 0.016. \quad (4.11)$$

These measurements are complementary to experiments at the Z_1 peak because they measure the couplings at much lower center-of-mass energies. The weak- and QED corrections to neutrino scattering are given in the first reference of [238] and in references [260].

As e^+e^- collisions at the Z_1 peak, the agreement of these measurements with the SM prediction constrains physics beyond the SM. The constraints on extra neutral gauge bosons obtained by the CHARM II Collaboration [258] are given in table 4.3. Comparisons of the excluded ranges in the $\theta_M - M_{Z'}$ plane with L3 measurements can be found in figure 46 of reference [259].

The CHARM, CCFR and CDHS collaborations quote model independent results on neutrino–nucleon scattering [259]. These results can be converted into constraints on different extra neutral gauge bosons using the formalism of reference [7]. The resulting numbers for an unconstrained Higgs sector are given in table 4.3.

| | χ | ψ | η | LR |
|------------------------------|--------|--------|--------|------|
| reference [258] | 262 | 135 | 100 | 253 |
| table XI of reference [259] | 215 | 54 | 87 | |
| figures 2 of reference [261] | 500 | 155 | 190 | 220 |

Table 4.3 Present 95% CL limits on $M_{Z'}$ in GeV in different Z' models from neutrino scattering experiments.

Recently, **low energy neutrino scattering** experiments ($\nu_e e \rightarrow \nu_e e$) are proposed [261]. The proposal foresees to place a strong neutrino source in the center of a neutrino detector. Such a neutrino source with an activity of $1.67 \pm 0.03 MCi$ based on ^{51}Cr was already used to calibrate the GALLEX neutrino experiment. A $\bar{\nu}_e$ source based on ^{147}Pm is proposed to have an activity of $5 - 15 MCi$ [261]. All these sources emit neutrinos with energies well below $1 MeV$. New detectors are proposed to measure the small recoil energy of the scattered electrons with high precision [261].

The experiment measures the neutrino couplings. This information can be used to set limits on extra neutral gauge bosons. The possible constraints on the ZZ' mixing angle

cannot compete with the present LEP measurements, while the possible bounds on $M_{Z'}$ are interesting. They are shown in figures 1 and 2 of reference [261]. We produce mass limits from figure 2 of that reference neglecting systematic errors and present them in table 4.3.

4.4 Cosmology

The number of light neutrinos interacting with the SM Z boson is known from experiments at the Z_1 -resonance to be $N_\nu = 2.989 \pm 0.012$ [91].

GUT's containing extra neutral gauge bosons also predict the existence of additional (right handed) neutrinos. The number of these neutrinos, which do not interact with the SM Z boson, is not constrained by the experiments at LEP and SLAC.

The big bang nucleosynthesis of neutrons and the related **abundance of ${}^4\text{He}$** in the universe is sensitive to any particles with a mass lighter or about 1 MeV [262], the mass difference between the proton and the neutron. Assuming a primeval ${}^4\text{He}$ abundance $Y_P = 0.242 \pm 0.003$, one gets [262] a 95% CL interval $N_\nu = 3.0 - 3.7$ assuming the $\text{D}+{}^3\text{He}$ lower bound to the baryon density, and $N_\nu = 3.0 - 3.2$ assuming $(\text{D}/\text{H})_P = (2.5 \pm 0.75) \cdot 10^{-5}$ [263].

This measurement of N_ν can be interpreted as a constraint on theories predicting light neutrinos and light Z' s [264]. The resulting bounds on $M_{Z'}$ are stronger than those from collider experiments but they contain more assumptions on the model.

Constraints on extra neutral gauge bosons from the **supernova SN 1987A** are considered in references [265, 266, 267, 268]. Models of stellar collapse predict an energy release of $4 \cdot 10^{46}W$. The measured neutrino events suggest an energy release exceeding $2 \cdot 10^{46}W$ within 10 seconds. Therefore, at most $2 \cdot 10^{46}W$ could be emitted by other particles. In particular, additional neutrinos lighter than about 50 MeV , the core temperature, would carry away a part of the energy. They can be produced through nucleon-nucleon bremsstrahlung ($NN \rightarrow NN\nu_R\bar{\nu}_R$) in presence of a light Z' .

The agreement between the models of stellar collapse and the neutrino observation puts constraints on extra neutral gauge bosons if there are additional light neutrinos present in the model. These constraints are considerably stronger than present collider limits except for models where the Z' coupling to right-handed neutrinos vanishes [265]. Of course, these limits are based on more model assumptions than the collider constraints. A non-zero ZZ' mixing would only strengthen the limits [266]. The influence of radiative corrections on the limits is small [266].

Chapter 5

Summary and conclusions

In this review, we have investigated the phenomenology of extra neutral gauge bosons. We have considered in detail the Z' constraints, which can be obtained at e^+e^- , e^-e^- and $\mu^+\mu^-$ colliders. At these machines, fermion pair production, Bhabha scattering, Møller scattering and W pair production can contribute to a Z' analysis. The constraints from lepton colliders are compared with those from pp and $p\bar{p}$ colliders.

In the case of the absence of a Z' signal, lepton and hadron colliders give complementary Z' constraints. Lepton colliders give the best constraints on the ZZ' mixing angle and on weakly interacting Z' s. The exclusion limits from lepton colliders are almost insensitive to Γ_2/M_2 but they are rather model dependent. Hadron colliders give the best present constraints on the Z' mass for Z' s predicted in popular GUT's. These constraints are rather insensitive to the Z' model. They become worse for an enlarged Z_2 width, which can arise if decays to exotic fermions are kinematically allowed. The complementary role of lepton and hadron colliders is demonstrated in table 5.1.

| | χ | ψ | η | LR | SSM |
|--|--------|--------|--------|------|-------|
| Tevatron 1997 [63] | 595 | 590 | 620 | 630 | 690 |
| LEP 1997 [102] | 300 | 220 | 230 | 310 | 520 |
| end of LEP (190 GeV, 0.5 fb ⁻¹) [126] | 990 | 560 | 620 | 1100 | 1500 |
| Tevatron after run II (2 TeV, 2 fb ⁻¹) | 940 | 930 | 970 | 970 | 1040 |

Table 5.1 Present and future limits on $M_{Z'}$ (95% CL) for different E_6 models and the SSM in GeV. The last line is obtained from the present Tevatron bounds using relation (3.19).

In the case of a Z' signal, lepton and hadron colliders are complementary in a Z' model measurement. The proposed hadron colliders with unpolarized beams measure the couplings of the Z' to SM fermions with smaller errors than the proposed lepton colliders but with a 16-fold sign ambiguity. Lepton colliders with polarized electron beams measure the same couplings with a 2-fold sign ambiguity only.

The Z' limits from electron-proton colliders cannot compete with those from lepton and hadron colliders.

We emphasized the importance of model independent and model dependent Z' analyses. Both analyses are complementary. Model independent constraints are useful to restrict any

present and future Z' model. For this universality, one has to pay the price that not always all observables are useful for a model independent analysis and that model independent constraints from different reactions are not always comparable. On the other hand, additional model assumptions bias the limits. However, as far as they are consistent with the data, they help to tighten the exclusion limit or to reduce the error of the measurement of the remaining model parameters.

We reviewed the status of the radiative corrections, discussed the importance of the different radiative corrections in detail, and described how they can be included in theories including a Z' . QED corrections can be calculated in a model independent way. QCD corrections to Z' processes are the same as in the SM. Weak corrections to the new Z' contributions cannot be calculated independently of the model. We assume that the Z' effects arise first at the tree level and not in loops. Then, the higher-order corrections including new GUT particles are a small correction to a small effect and can be neglected. However, they cannot be neglected in precision measurements at the Z_2 peak.

Computer programs with these corrections are required for Z' analyses. We listed officially released FORTRAN programs relevant for a Z' search and indicated where these programs have already been used in an analysis of experimental data.

In contrast to Z' model measurements, Z' exclusion limits are rather robust against details of systematic errors.

For different reactions, we discussed kinematic cuts, which enhance the sensitivity to extra neutral gauge bosons.

We now comment on the Z' limits from different processes in more detail. They are collected in table 5.2, which summarizes the main results of the different sections of this review in a telegraphic style.

The first column refers to the considered reaction. If necessary, different cases of the center-of-mass energy are distinguished. In the next three columns, the status of the Z' search is indicated. The simplest analysis could be done at the Born level. The next step would be the investigation of radiative corrections needed to meet the accuracy of future data. We put a + there if the radiative corrections are known with an accuracy comparable or better than the expected experimental errors. This column is more subjective because neither the future experimental errors nor the magnitude of the radiative corrections are precisely known in advance. The existence of officially released computer programs containing all radiative corrections needed for a direct fit to data is indicated in the fourth column.

The last column of the table contains typical bounds on different model parameters or combinations of them and a scaling of these bounds with the integrated luminosity and the center-of-mass energy. Of course, the input of this column is only representative depending on the assumptions and limitations not given in the table but described in the corresponding sections of this review. The scaling with the luminosity assumes that the systematic error decreases proportional to the statistical error.

It follows a short comment on every row: Z' effects in fermion pair production at the Z_1 peak arise mainly through deviations in the couplings of the mass eigenstate Z_1 to fermions compared to the SM prediction for the Z boson. On-resonance Z_1 production gives the best present limits on the ZZ' mixing angle θ_M . The number in the table is a typical experimental bound for GUT's. It is almost independent of the Z' mass. Without assumptions on the Z' model, only v_f^M and a_f^M , which are the product of the ZZ' mixing angle and the Z' couplings,

can be constrained. The present constraints on v_f^M and a_f^M with $f = u, d$ could only be improved by fermion pair production at the Z_2 resonance. The strongest improvements on the present limits on v_e^M and a_e^M will come from W pair production at e^+e^- or $\mu^+\mu^-$ colliders at TeV energies.

| Reaction, c.m. energy | Born Analysis exists | Main RC's known | Program with RC's exists | Typical 95% CL constraint and scaling with c.m. energy s and integrated luminosity L |
|--|----------------------------|-----------------------|--------------------------------|--|
| $e^+e^- \rightarrow f\bar{f}$ | | | | |
| $s \approx M_1^2$ | + | + | + | $ a_e^M < 0.0005, v_e^M < 0.001 \sim L^{-1/2}$ $ a_q^M , v_q^M < 0.02, q = c, b \sim L^{-1/2}$ $ \theta_M < 0.003 \sim L^{-1/2}$ |
| $M_1^2 < s < M_2^2$ | + | + | + | $ a_l^N , v_l^N < 0.01 \sim (sL)^{-1/4}$ $M_2 > M_{Z'}^{lim} = (3 \text{ to } 8)\sqrt{s} \sim (sL)^{1/4}$ $g_2 < g_1/7$ for $M_2 < \sqrt{2s} \sim (sL)^{-1/4}$ $\frac{\Delta g_2}{g_2}, \frac{\Delta M_2}{M_2} \approx \frac{1}{2} \left(M_2/M_{Z'}^{lim} \right)^2 \sim (sL)^{-1/2}$ |
| $s \approx M_2^2$ | + | - | - | $g_2 < g_1/140 \sim L^{-1/4}$ $\Delta\Gamma_2, \Delta M_2 \approx \Delta E_{beam}$ $\Delta a_f(2)/a_f(2), \Delta v_f(2)/v_f(2) \sim L^{-1/2}$ |
| $s > M_2^2$ | + | - | - | $g_2 < g_1/24$ for $M_{Z'} \approx \sqrt{s} \sim \left(\frac{\Delta E_\gamma}{E_\gamma} \frac{s}{M_{Z'}^2} \right)^{1/4}$ |
| $e^\pm e^- \rightarrow e^\pm e^-$ | + | + | - | see $e^+e^- \rightarrow f\bar{f}$, $M_1^2 < s < M_2^2$ |
| $e^+e^- \rightarrow W^+W^-$ | | | | |
| $s < M_2^2$ | + | + | + | $ a_e^M , v_e^M < 0.00025 TeV/\sqrt{s} \sim (sL)^{-1/2}$ $ \theta_M < 0.001 TeV/\sqrt{s} \sim (sL)^{-1/2}$ |
| $s \approx M_2^2$ | + | - | - | $ \theta_M < 0.0001 TeV/\sqrt{s} \sim L^{-1/2}$ |
| $pp, p\bar{p} \rightarrow Z'X$ | | | | |
| $Z' \rightarrow l\bar{l}, b\bar{b}$ | + | + | + | $\sigma_T^\mu < 3/L \sim L^{-1}$ $M_2 > M_{Z'}^{lim} \approx \sqrt{s} \left(0.4 + \frac{1}{32} \ln \frac{L \cdot fb \cdot 1000 c_{Z'}}{3s/TeV^2} \right)$ (pp) $M_2 > M_{Z'}^{lim} \approx \sqrt{s} \left(0.6 + \frac{1}{20} \ln \frac{L \cdot fb \cdot 1000 c_{Z'}}{3s/TeV^2} \right)$ ($p\bar{p}$) |
| $pe^\pm, \bar{p}e^\pm \rightarrow e^\pm X$ | + | + | + | $M_2 > (0.7 \text{ to } 1.6)\sqrt{s} \sim (sL)^{-1/4}$ |

Table 5.2 Summary table of the Z' limits.

The Z' effects in off-resonance fermion pair production arise mainly through interferences of the Z' amplitude with the SM amplitudes. Off-resonance fermion pair production is sensitive to Z' masses considerably larger than the center-of-mass energy. The limits have a strong dependence on the Z' couplings to fermions. They are insensitive to ZZ' mixing. The exclusion limits in the table are given for typical GUT's and for colliders with $L = 80 \text{ fb}^{-1} \text{ s}/\text{TeV}^2$. If no information on the Z' model is available, one can only constrain the parameters v_f^N and a_f^N , which are proportional to ratios of the Z' couplings and the Z' mass. If the Z' couplings to all SM fermions are very small, the Z' could escape detection even for energies not far below its mass. However, it is hard to obtain such Z' s in a GUT. The errors of Z' *model measurement* and of Z' *exclusion* limits scale differently with the integrated luminosity and center-of-mass energy.

Experiments on top of the Z_2 resonance would certainly allow the most accurate measurements of the Z_2 mass, of the Z_2 width and of the Z_2 couplings to SM fermions. In such measurements, muon colliders are clearly favored against electron positron colliders because they have a much smaller beam energy spread. The accuracy of the measurements of the Z_2 couplings to fermions is expected to be comparable to the precision presently achieved at the Z_1 resonance.

As mentioned before, a weakly coupled Z' can be missed in experiments below its resonance. If its couplings are not too small, such a Z' can be observed in experiments above its resonance. In those experiments, the Z' signal arises through the hard photons, which come from the radiative return to the Z_2 resonance. These photons appear by the same mechanism, which is responsible for the hard photons from the radiative return to the Z_1 resonance at LEP 2 energies. The Z' limit from experiments above the Z_2 resonance is sensitive to the photon energy resolution.

Bhabha and Møller scattering set bounds on the model independent parameters v_e^N and a_e^N , which are comparable to off-resonance fermion pair production. Of course, Bhabha and Møller scattering can only constrain the Z' couplings to electrons. Model assumptions link Z' couplings to leptons and quarks. In model dependent analyses, fermion pair production profits from its additional observables with quarks in the final state. Therefore, the model dependent Z' limits from fermion pair production are better than those from Bhabha and Møller scattering.

W pair production is very sensitive to changes of the Z_1 couplings to fermions. Such changes destroy the gauge cancellation present in the SM. The result are large factors, which amplify the Z' effects. W pair production can give the best model independent constraints on the parameters v_e^M, a_e^M . For models where the Z' couplings to electrons are not zero, the resulting bounds on θ_M are better than those from fermion pair production. The best limits can be obtained in measurements near the Z_2 peak where the $Z_2\gamma$ and Z_2Z_1 interferences dominate. At energies above the Z_2 resonance, unitarity is restored and Z' effects are no longer enhanced by large factors.

Proton colliders can see a Z' if it is directly produced by a quark-anti-quark pair. Therefore, these colliders can detect only Z' s with masses considerably smaller than the center-of-mass energy of the colliding protons. The Z' mass exclusion limits are rather insensitive to details of the model as far as the signal can be separated from the background. This becomes harder for Z' s with small couplings or for Z' s with small branching ratios to SM fermions. The Z' exclusion limits scale non-symmetrically with the center-of-mass energy and with the inte-

grated luminosity. To improve the limits, an increase of the center-of-mass energy is favored against an increase of the luminosity. For a first Z' discovery, Z' decays to muon pairs are the favored process. In the case of a Z' signal, there are many other useful observables, which can help to measure the model parameters. The errors of Z' model measurements at hadron colliders scale with the integrated luminosity as in e^+e^- collisions but have an enhanced sensitivity to the center-of-mass energy.

Some other experiments can provide Z' limits. We could only briefly comment on ep collisions, atomic parity violation, neutrino scattering and cosmology.

Many different bounds on extra neutral gauge bosons can be obtained from various experiments. In the foreseeable future, we shall learn from the new experiments whether the Z boson has one or several massive partners as predicted by most unified theories. Let's hope for surprises.

Acknowledgments

It is a pleasure to thank Tord Riemann for many years of fruitful collaboration. With him, I started to work on extra neutral gauge bosons. He encouraged me to write this review. I had innumerable discussions with him. Many of his ideas entered this review. I'm happy to thank Sabine Riemann for several years of pleasant collaboration, during which I learned a lot of details on experiments. I'm grateful to Wolfgang Hollik, who always had time to discuss with me questions on extra neutral gauge bosons and on radiative corrections. Further, I would like to thank Francesco del Aguila and Claudio Verzegnassi for many discussions and continuous encouragement. I'm grateful to G. Altarelli, K. Ellis, S. Godfrey, P. Langacker, P. Minkovski, T.G. Rizzo and P. Zerwas, for discussions of parts of this paper, valuable hints and warm hospitality and F. Berends, M. Cvetič, W.T. Giele, N. Lockyer, K. Maeshima, A.A. Pankov, M. Peskin, M. Zralek for interesting discussions. I thank S. Riemann for providing the figures 2.5 and 2.9 and A.A. Pankov for providing figure 2.20. I benefited greatly from H. Fritzsch and R. Rückl due to their continuous support, many discussions and due to the stimulating working conditions at their institute. I thank S. Godfrey for the careful reading of the manuscript and for his many useful comments.

Finally, I would like to thank my wife Ines for her patience while this paper was written and for hints concerning the manuscript.

This work was partially supported by the German Federal Ministry of Research and Technology under contract No. 05 GMU93P, the Deutsche Forschungsgemeinschaft, and the EC contracts CHRX-CT-92-0004 and CHRX-CT940579.

Bibliography

- [1] For a review see P. Langacker, Phys. Rep. **72** (1981) 185.
- [2] R. Slansky, Phys. Rep. **79** (1981) 1.
- [3] M. Cvetič, P. Langacker, Phys. Rev. **D54** (1996) 3570; Int. J. Mod. Phys. **A11** (1996) 1246; hep-ph/9707451, Univ. of Pennsylvania preprint UPR-0761-T, To appear in G.L. Kane (ed.), “Perspectives in Supersymmetry”, World Scientific; J.D. Lykken, hep-ph/9610218.
- [4] M. Cvetič, P. Langacker, Phys. Rev. **D54** (1996) 3570; M. Cvetič, P. Langacker, Mod. Phys. Lett. **A11** (1996) 1247; J. R. Espinosa, Nucl. Phys. Proc. Suppl. **62** (1998) 187, hep-ph/9707541.
- [5] F. Zwirner, Int. J. Mod. Phys. **A3** (1989) 49.
- [6] For a review see e.g. J.L. Hewett, T.G. Rizzo, Phys. Rep. **183** (1989) 193.
- [7] P. Langacker, M. Luo, A.K. Mann, Rev. Mod. Phys. **64** (1992) 87.
- [8] M. Cvetič, S. Godfrey, in T. Barklow, S. Dawson, H. Haber, J. Siegrist (eds.), “Electroweak Symmetry Breaking and Beyond the SM”, World Scientific 1995.
- [9] see, e.g. [193] and [269]; T.G. Rizzo et al., SLAC-PUB-7365, hep-ph/9612440, to appear in Proc. of the 1996 DPF/DPB Summer Study on New Directions for High Energy Physics-Snowmass96; S. Godfrey et al., SLAC-PUB-7440, hep-ph/9704291, to appear in Proc. of the 1996 DPF/DPB Summer Study on New Directions for High Energy Physics-Snowmass96; E. Accomando et al., DESY 97-100, subm. to Phys. Rep., and references therein.
- [10] see, e.g. D. Amidei, R. Brock (eds.), “Future Electro Weak Physics at the Fermilab Tevatron”, Report of the tev_200 Study Group, FERMILAB-Pub-96/082, p. 182 and references therein.
- [11] see, e.g. R. Rückl, in G. Jarlskog, D. Rein (eds.), Proc. of the Large Hadron Collider Workshop, Aachen, Oct. 1990, CERN 90-133 (1990), vol. I, p. 229; see also [243, 245] and references therein.
- [12] A.A. Andrianov, P. Osland, A.A. Pankov, N.V. Romanenko, J. Sirkka, hep-ph/9804389.

- [13] J.L. Rosner, Phys. Lett. **B387** (1996) 113;
H. Georgy, S. L. Glashow, Phys. Lett. **B387** (1996) 341.
- [14] P. Langacker, D. London, Phys. Rev. **D38** (1988) 886;
E. Nardi, Phys. Rev. **D48** (1993) 1240;
D. London, p. 951 of reference [99].
- [15] U. Cotti, A. Zepeda, Phys. Rev. **D55** (1997) 2998.
- [16] T. Gherghetta, T.A. Kaeding, G.L. Kane, Phys. Rev. **D57** (1998) 3178, hep-ph/9701343.
- [17] P. Chiappetta, J. Layssac, F.M. Renard, C. Verzegnassi, Phys. Rev. **D54** (1996) 789;
G. Altarelli, N. di Bartolomeo, F. Feruglio, R. Gatto, M.L. Mangano, Phys. Lett. **B375**
(1996) 292;
K. Agashe, M. Graesser, I. Hinchliffe, M. Suzuki, Phys. Lett. **B385** (1996) 218.
- [18] V. Barger, K. Cheung, P. Langacker, Phys. Lett. **B381** (1996) 226.
- [19] R. Casalbuoni, S. de Curtis, D. Dominici, R. Gatto, Phys. Lett. **B155** (1985) 95; Nucl.
Phys. **B282** (1987) 235.
- [20] R. Casalbuoni et al., Nucl. Phys. **B310** (1988) 181.
- [21] R. Casalbuoni et al., Phys. Lett. **B249** (1990) 130;
R. Casalbouni et al., Phys. Lett. **B279** (1992) 397;
R. Casalbuoni et al., Phys. Rev. **D56** (1997) 2812.
- [22] R. Casalbuoni et al., Z. Phys. **C60** (1993) 315.
- [23] G. Altarelli, R. Casalbuoni, D. Dominici, F. Feruglio, R. Gatto, Nucl. Phys. **B342** (1990)
15.
- [24] B. Holdom, Phys. Lett. **B166** (1986) 196.
- [25] F. del Aguila, G.D. Coughlan, M. Quiros, Nucl. Phys. **B283** (1987) 50;
F. del Aguila, M. Quiros, F. Zwirner, Nucl. Phys. **B287** (1987) 419;
F. del Aguila, G.D. Coughlan, M. Quirós, Nucl. Phys. **B307** (1988) 633; E. **B312** (1989)
751;
F. del Aguila, M. Masip, M. Pérez-Victoria, Nucl. Phys. **B456** (1995) 531.
- [26] K.S. Babu, C. Kolda, J. March-Russel, Phys. Rev. **D54** (1996) 4635.
- [27] K.R. Dines, C. Kolda, J. March-Russel, Nucl. Phys. **B492** (1997) 104.
- [28] J.C. Pati, A. Salam, Phys. Rev. **D10** (1974) 275;
R.N. Mohapatra, J.C. Pati, Phys. Rev. **D11** (1975) 566;
G. Senjanović, R.N. Mohapatra, Phys. Rev. **D12** (1975) 1502;
Q. Shafi, C. Wetterich, Phys. Lett. **B73** (1978) 65;
G. Senjanović, Nucl. Phys. **B153** (1979) 334;
R.N. Mohapatra, in H. Fritzsch (ed.) “Quarks, Leptons, and Beyond”, (Plenum Press,

New York, (1985), p.217. R.N. Mohapatra, *Unification and Supersymmetry* (Springer, New York, (1986).

- [29] J. Polak, M. Zralek, Nucl. Phys. **B363** (1991) 385;
J. Polak, M. Zralek, Phys. Rev. **D46** (1992) 3871.
- [30] A. Leike, S. Riemann, T. Riemann, Phys. Lett. **B291** (1992) 187;
A. Leike, S. Riemann, Nucl. Phys. **B** (Proc. Suppl.) **29A** (1992) 270.
- [31] V. Barger, K. Whisnant, Phys. Rev. **D36** (1987) 3429.
- [32] R.W. Robinett, J.L. Rosner, Phys. Rev. **D25** (1982) 3036.
- [33] D. Albert, W. Marciano, D. Wyler, Z. Parsa, Nucl. Phys. **B166** (1980) 460.
- [34] S. Gorishny, A. Kataev, S. Larin, Phys. Lett. **B259** (1991) 144.
- [35] K. Chetyrkin, J. Kühn, S. Larin, Phys. Lett. **B248** (1990) 359.
- [36] A. Djouadi, C. Verzegnassi, Phys. Lett. **B195** (1987) 265;
A. Djouadi, Nuovo Cim. **A100** (1988) 357.
- [37] A.Akhundov, D. Bardin, T. Riemann, Nucl. Phys. **B276** (1980) 1.
- [38] W. Beenakker, F.A. Berends (conv.), Proc. of the LEP 2 workshop, CERN yellow report CERN 96-01, vol. 1, p. 79.
- [39] G. Altarelli, T. Sjöstrand, F. Zwirner (eds.), Proc. of the Workshop *Physics at LEP 2*, CERN 96-01, and references therein.
- [40] F.A. Berends, G.B. West, Phys. Rev. **D1** (1970) 122.
- [41] W. Beenakker, A. Denner, Int. J. Mod. Phys. **A9** (1994) 4837;
R.G. Stuart, UM-TH-96-05, hep-ph/9603351;
U. Baur, D. Zeppenfeld, Phys. Rev. Lett. **75** (1995) 1002;
E.N. Argyres et al., Phys. Lett. **B358** (1995) 339.
- [42] D.Y. Bardin, A. Leike, T. Riemann, M. Sachwitz, Phys. Lett. **B206** (1988) 539.
- [43] F. del Aguila, M. Cvetič, Phys. Rev. **D50** (1994) 3158.
- [44] M. Cvetič, P. Langacker, Phys. Rev. **D46** (1992) 4943; E: **D48** (1993) 4484.
- [45] F. del Aguila, M. Cvetič, P. Langacker, Phys. Rev. **D52** (1995) 37.
- [46] R.W. Robinett, Phys. Rev. **D26** (1982) 2388.
- [47] R.W. Robinett, J.L Rosner, Phys. Rev. **D26** (1982) 2396.
- [48] H. Fritzsch, P. Minkowski, Ann. Phys. (NY) **93** (1975) 193;
C.N. Leung, J.L. Rosner, Phys. Rev. **D29** (1982) 2132.

- [49] P. Langacker, R.W. Robinett, J.L. Rosner, Phys. Rev. **D30** (1984) 1470.
- [50] H. Georgi, S.L. Glashow, Phys. Rev. Lett. **32** (1974) 438.
- [51] L.S. Durkin, P. Langacker, Phys. Lett. **B166** (1986) 436.
- [52] M. Cvetič, P. Langacker, Phys. Rev. Lett. **68** (1992) 2871.
- [53] V. Barger, J.L. Hewett, T.G. Rizzo, Phys. Rev. **D42** (1990) 152.
- [54] N.G. Deshpande, J.A. Grifols, A. Méndez, Phys. Lett. **208** (1988) 141.
- [55] E.J. Eichten, K.D. Lane, M.E. Peskin, Phys. Rev. Lett. **50** (1983) 811;
R. Rückl, Phys. Lett. **B129** (1983) 363; Nucl. Phys. **B234** (1984) 91.
- [56] T. Riemann 1991, unpublished.
- [57] A. Leike, Acta Phys. Polon. **28** (1997) 2495, hep-ph/9710481.
- [58] D. Bardin et al., CERN-TH.6443/92, hep-ph/9412201.
- [59] J. Layssac, F.M. Renard and C. Verzegnassi, Z. Phys. **C53** (1992) 97.
- [60] J. Layssac, F.M. Renard and C. Verzegnassi, Phys. Lett. **B287** (1992) 267.
- [61] A. Leike, Phys. Lett. **B396** 1997 245.
- [62] S. Riemann, L3 Note 1961 (June 1996).
- [63] CDF Collab., F. Abe et al., Phys. Rev. Lett. **79** (1997) 2192.
- [64] D. Atwood, A. Soni, Phys. Rev. **D45** (1992) 2405.
- [65] M. Diehl, O. Nachtmann, Z. Phys. **C62** (1994) 397.
- [66] *Review of Particle Properties*, Phys. Rev. **D54** (1996) 1.
- [67] Proc. “ $\mu^+\mu^-$ Collider, A Feasibility Study”, BNL-52503, Fermilab-Conf.-96/092, LBNL-38946.
- [68] A. Leike, Z. Phys. **C62** (1994) 265.
- [69] Y.S. Tsai, Phys. Rev. **D4** (1971) 2821;
S. Kawasaki, T. Shirafuri, Y.S. Tsai, Prog. Theor. Phys. **49** (1973) 1656.
- [70] R. Alemany et al., Nucl. Phys. **B379** (1992) 3.
- [71] F. del Aguila, F. Bernabéu, N. Rius, Phys. Lett. **B280** (1992) 319.
- [72] G. Passarino, M. Veltman, Nucl. Phys. **B160** (1979) 151.
- [73] G. Bonneau, F. Martin, Nucl. Phys. **B27** (1971) 381;
F.A. Berends, G. Burgers, W.L. van Neerven, Nucl. Phys. **B297** (1988) 429.

- [74] F.A. Berends, R. Kleiss, Nucl. Phys. **B177** (1981) 237; **B260** (1985) 32;
 F.A. Berends, R. Kleiss, S. Jadach, Nucl. Phys. **B202** (1982) 63; Comput. Phys. Commun.
B29 (1983) 185;
 M. Greco, G. Pancherivi, Y. Srivastava, Nucl. Phys. **B171** (1980) 118; E: **B197** (1982)
 543.
- [75] W. Hollik, Fortsch. Phys. **38** (1990) 165.
- [76] D. Bardin et al., Nucl. Phys. **B351** (1991) 1.
- [77] F.A. Berends et al., in reference [84], Vol. 1, p.89.
- [78] A. Leike, T. Riemann, M. Sachwitz, Phys. Lett. **B241** (1990) 267.
- [79] A. Leike, T. Riemann, Z. Phys. **C51** (1991) 321.
- [80] A.A. Akhundov, D.Yu. Bardin, A. Leike, Phys. Lett. **B261** (1991) 321.
- [81] E.A. Kuraev, V.S. Fadin, Sov. J. Nucl. Phys. **41** (1985) 466;
 G. Altarelli, G. Martinelli, in J. Ellis, R. Peccei (eds.) “Physics at LEP”, CERN-86-02,
 vol. 1, p. 47.
- [82] D. Bardin et al., Phys. Lett. **B229** (1989) 405.
- [83] S.C. van der Marck, “Higher order QED corrections in Z physics”, thesis, Univ. Leiden,
 Phys. Dept. (1991).
- [84] G. Altarelli, R. Kleiss, C. Verzegnassi (eds.), “ Z physics at LEP 1”, CERN 89-08 (1989),
 and references quoted therein.
- [85] D. Bardin et al., Z. Phys. **C44** (1989) 493.
- [86] G. Degrassi, A. Sirlin, Phys. Rev. **D40** (1989) 3066.
- [87] J. Jersak, E.L. Laermann, P.M. Zerwas, Phys. Rev. **D25** (1981) 1218, E: **D36** (1987) 310;
 Phys. Lett. **B98** (1981) 363;
 A.B. Arbuzov, D.Yu. Bardin, A. Leike, Int. J. Mod. Phys. Lett. **A7** (1992) 2029, E: **A9**
 (1994) 1515.
- [88] S. Grote, J.G. Körner, Z. Phys. **C72** (1996) 255.
- [89] T.D. Lee, M. Nauenberg, Phys. Rev. **133** (1964) 1549;
 A.V. Smilga, Commun. Nucl. Part. Phys. **20** (1991) 69;
 B. Falk, L.M. Sehgal, Phys. Lett. **B325** (1994) 509;
 J.G. Körner, A. Pilaftsis, M.M. Tung, Z. Phys. **C63** (1994) 575;
 S. Groote, J.G. Körner, Z. Phys. **C74** (1997) 615.
- [90] E. Nardi, E. Roulet, D. Tommasini, Phys. Rev. **D46** (1992) 3040.
- [91] A. Blondel, Plenary talk at 28th Int. Conf. on High Energy Physics, Warsaw, July 1996;
 LEP Electroweak Working Group, CERN-preprint LEPEWWG/96-02.

- [92] W. Hollik, Acta Phys. Polon. **B27** (1996) 3685.
- [93] A.A. Pankov, N. Paver, Phys. Lett. **B393** (1997) 437.
- [94] F. del Aguila, W. Hollik, J.M. Moreno, M. Quirós, Nucl. Phys. **B372** (1992) 1.
- [95] C. Paus for the LEP experiments and the LEP Electroweak Working group, Talk given at Rencontre de la vallée d'Aoste, La Thuile, March 1997.
- [96] G. Altarelli et al., Phys. Lett. **B318** (1993) 139.
- [97] M.C. Gonzalez-Garcia, J.W.F. Valle, Phys. Rev. **D41** (1990) 2355;
M.C. Gonzalez-Garcia, J.W.F. Valle, Phys. Lett. **B236** (1990) 236;
M.C. Gonzalez-Garcia, J.W.F. Valle, Phys. Lett. **B259** (1991) 365.
- [98] P.B. Renton, Z. Phys. **C56** (1992) 355.
- [99] P. Langacker, in P. Langacker (ed.) Precision tests of the standard electroweak model, (World Scientific 1995), p. 883.
- [100] L3 Collab., Phys. Lett. **B306** (1993) 187.
- [101] DELPHI Collab., Z. Phys. **C65** (1995) 603.
- [102] S. Riemann for the L3 Collab., talk at the Conference “Beyond the Standard Model V”, Balholm, Norway, April 1997.
- [103] S. Riemann, contribution to the Proceedings of the Conference “Beyond the Standard Model V”, Balholm, Norway, April 1997.
- [104] G.J. Bobbink, in XXV Rencontres de Moriond, Les Arcs, France, March 1991;
V. Dzuba, in XXV Rencontres de Moriond, Les Arcs, France, March 1991.
- [105] Particle Data Group, Review of Particle Properties, Phys. Lett. **B239** (1990) 1.
- [106] M.C. Noecker, B.P. Masterson, E.E. Wiemann, Phys. Rev. Lett. **61** (1988) 310;
S.A. Blundell, W.R. Johnson, J. Sapirstein, Phys. Rev. Lett. **65** (1990) 1411;
V. Dzuba, V. Flambaum, O. Sushkov, Phys. Lett. **A141** (1988) 147.
- [107] CDF Collab., F. Abe et al., Phys. Rev. Lett. **65** (1990) 1;
UA2 Collab., J. Alitti et al., Phys. Lett. **B241** (1990) 150.
- [108] The LEP Collaborations: ALEPH,DELPHI,L3 and OPAL, Phys. Lett. **B276** (1992) 247.
- [109] P. Langacker, M. Luo, Phys. Rev. **D45** (1992) 278.
- [110] G. Altarelli et al., Phys. Lett. **B261** (1991) 146; **B263** (1991) 459.
- [111] The LEP Collaborations, CERN/PPE/93-157.
- [112] G. Altarelli, R. Barbieri, S. Jadach, Nucl. Phys. **B369** (1992) 3; E: **B376** (1992) 444.

- [113] Joint report of the LEP Collaborations, LEP Electroweak Working Group, and SLD Heavy Flavor Group, CERN-PPE/96-183.
- [114] E. Torrence, ICHEP96.
- [115] L3 Collab., Phys. Lett. **B370** (1996) 126; L3 notes # 2057 and # 2065.
- [116] LEP: Electroweak working group, LEPEWWG 97-01.
- [117] G. Altarelli, in XXVII Rencontres de Moriond, Les Arcs, France, March 1992;
 B. Brandl, in XXVII Rencontres de Moriond, Les Arcs, France, March 1992;
 F.L. Linde, in XXVII Rencontres de Moriond, Les Arcs, France, March 1992;
 K. Maeshima, in XXVII Rencontres de Moriond, Les Arcs, France, March 1992;
 J. Nash, in XXVII Rencontres de Moriond, Les Arcs, France, March 1992;
- [118] W. Hollik, Z. Phys. **C8** (1981) 149;
 M. Boehm, W. Hollik, Z. Phys. **C23** (1984) 31.
- [119] D.P. Sidhu, Phys. Rev. **D22** (1980) 1158.
- [120] W.T. Eadie et al., *Statistical Methods in Experimental Physics*, North Holland, 1971.
- [121] D. Choudhury, F. Cuypers, A. Leike, Phys. Lett. **B333** (1994) 531;
 F. Cuypers, Int. J. Mod. Phys. **A11** (1996) 1571, hep-ph/9602426;
 F. Cuypers, Nucl. Phys. **B474** (1996) 72.
- [122] C.H. Llewellyn Smith, D.V. Nanopoulos, Nucl. Phys. **B78** (1974) 205.
- [123] P. Osland, A.A. Pankov, Phys. Lett. **B403** (1997) 93.
- [124] K. Miyabayashi, talk presented at “Moriond-95”.
- [125] A.A. Babich, A.A. Pankov, N. Paver, Phys. Lett. **B346** (1995) 303.
- [126] A. Leike, S. Riemann, Z. Phys. **C75** (1997) 341.
- [127] G. Montagna, F. Piccinini, J. Layssac, F.M. Renard, C. Verzegnassi, Z. Phys. **C75** (1997) 641.
- [128] B. Schrempp, F. Schrempp, N. Wermes, D. Zeppenfeld, Nucl. Phys. **B296** (1988) 1.
- [129] J.L. Hewett, T.G. Rizzo, in R. Orava (ed.), Proc. of the “Workshop on Physics and Experiments with Linear Colliders”, Sept. 1991, Saariselkä, Finland, Vol. II, p. 489; J.L. Hewett, T.G. Rizzo, Vol. II, p. 501.
- [130] A. Djouadi, A. Leike, T. Riemann, D. Schaile, C. Verzegnassi, in R. Orava (ed.) Proc. of the “Workshop on Physics and Experiments with Linear Colliders”, Sept. 1991, Saariselkä, Finland, Vol. II, p. 515; Z. Phys. **C56** (1992) 289.

- [131] T.G. Rizzo, SLAC-PUB-7279, contribution to “High Energy Physics-Snowmass96”, hep-ph/9609248.
- [132] S. Godfrey, OCIP/C-96-6, hep-ph/9612384, to appear in Proc. of the 1996 DPF/DPB Summer Study on New Directions for “High Energy Physics-Snowmass96”.
- [133] S. Godfrey, Phys. Rev. **D51** (1995) 1402.
- [134] G. Montagna, O. Nicosini, F. Piccinini, F.M. Renard, C. Verzegnassi, Phys. Lett. **B371** (1996) 277;
J. Layssac et al., in P.M. Zerwas (ed.), Proc. of the Workshop on “ e^+e^- collisions at TeV energies: The physics potential”, DESY 96-123D, p. 335, hep-ph/9602327.
- [135] A. Leike, hep-ph/9708436, to appear in the proceedings of the workshop on “ e^+e^- collisions at TeV energies: The physics potential”, DESY 97-123E.
- [136] MARK II Collab., M.E. Levi et al., Phys. Rev. Lett. **51** (1983) 1941;
HRS Collab., M. Derrick et al., Phys. Rev. **D31** (1985) 2352;
MAC Collab., W.W. Ash et al., Phys. Rev. Lett. **55** (1985) 1831.
- [137] Pluto Collab., C. Berger et al., Z. Phys. **C21** (1983) 53;
Jade Collab., W. Bartel et al., Z. Phys. **C26** (1985) 507;
CELLO Collab., H-J. Behrend et al., Phys. Lett. **B191** (1987) 209;
Mark J Collab., B. Adeva et al., Phys. Rev. **D38** (1988) 2665;
TASSO Collab., W. Braunschweig et al., Z. Phys. **C40** (1988) 163.
- [138] VENUS Collab., K. Abe et al., Z. Phys. **C48** (1990) 13;
TOPAZ Collab., B. Howell et al., Phys. Lett. **B291** (1992) 206;
AMY Collab., C. Velissaris et al., Phys. Lett. **B331** (1994) 227.
- [139] S. Riemann, DESY-ZEUTHEN 96-07, hep-ph/9610513, to appear in Proc. of the 1996 DPF/DPB Summer Study on New Directions for “High Energy Physics-Snowmass96”.
- [140] T.G. Rizzo, in ICHEP 96 (QCD161:H51:1996) 1421, hep-ph/9604420.
- [141] T.G. Rizzo, Phys. Rev. **D55** (1997) 5483.
- [142] C. Dib, F.J. Gilman, Phys. Rev. **D36** (1987) 1337.
- [143] A.A. Pankov, N. Paver, Phys. Lett. **B272** (1991) 425;
A.A. Pankov, N. Paver, Phys. Lett. **B274** (1992) 483;
A.A. Pankov, N. Paver, Phys. Rev. **D48** (1993) 63.
- [144] T.G. Rizzo, hep-ph/9710229, to appear in the proceedings of 2nd International Workshop on Electron-Electron Interactions at TeV Energies (e- e- 97), Santa Cruz, CA, September 1997.
- [145] T. Barklow, P. Chen, W. Kozanecki, in P.M. Zerwas (ed.), Proc. of the “Workshop on e^+e^- collisions at 500 GeV : The physics potential”, DESY 93-123B, p. 845.

- [146] D. Schulte, R. Settles, in P.M. Zerwas (ed.), Proc. of the Workshop on “ e^+e^- collisions at TeV energies: The physics potential”, DESY 96-123D, p. 527.
- [147] W. Beenakker, F.A. Berends, S.C. van der Marck, Z. Phys. **C46** (1990) 687;
 A. Borrelli, M. Consoli, L. Maiani, R. Sisto, Nucl. Phys. **B333** (1990) 357;
 F. Jegerlehner, in A. Faessler (ed.), Prog. Part. Nucl. Phys., vol. 27, p.1 (Pergamon Press, Oxford, U.K., 1991);
 R. Stuart, Phys. Lett. **B262** (1991) 113;
 T. Riemann, Phys. Lett. **B293** (1992) 451.
- [148] A. Leike, T. Riemann, J. Rose, Phys. Lett. **B273** (1991) 513.
- [149] T. Riemann, talk given at 21st International Colloquium on Group Theoretical Methods in Physics (ICGTMP 96), Goslar, Germany, 15-20 Jul 1996, hep-ph/9709208.
- [150] L3 Collab., O. Adriani et al., Phys. Lett. **B315** (1993) 494; Phys. Rep. **236** (1993) 1;
 M. Consoli, M. Piccolo, hep-ph/9505261, unpublished;
 M. Martinez, in J.W.F. Valle, A. Ferrer (eds.) Proc. of the Int. Workshop on El. Part. Phys.: Present and Future (World Scientific, River Edge, N.J., 1996), p. 32;
 The S -Matrix Subgroup of the LEP Electroweak Working Group, A. Blondel et al., LEPEWWG/LS/96-01 (1996), unpublished;
 Opal Collab., G. Alexander et al., Phys. Lett. **B376** (1996) 232;
 S. Dutta, S. Ganguli, M. Grünwald, A. Gurtu, C. Paus, L3 note # 1914 (1996), unpublished;
 The L3 Line Shape Group, G. Bobbink et al., L3 note # 1980 (1996), unpublished.
- [151] C.D. Carone, H. Murayama, Phys. Rev. **74** (1995) 3122.
- [152] A.E. Nelson, N. Tetradis, Phys. Lett. **B221** (1989) 80.
- [153] R. Settles, in P.M. Zerwas (ed.), Proc. of the “Workshop on e^+e^- collisions at 500 GeV : The physics potential”, DESY 93-123C, p. 591.
- [154] OPAL Collab., Phys. Lett. **B273** (1991) 338;
 L3 Collab., Phys. Lett. **B374** (1996) 334;
 DELPHI Collab., Z. Phys. **C75** (1997) 581.
- [155] W. Hollik, A. Zepeda, Z. Phys. **C12** (1982) 67.
- [156] G. Bélanger, S. Godfrey, Phys. Rev. **D34** (1986) 1309.
- [157] H.A. Olsen, P. Osland, Phys. Rev. **D25** (1982) 2895;
 J.L. Hewett, T.G. Rizzo, Z. Phys. **C36** (1987) 209.
- [158] D. Bardin, W. Hollik, T. Riemann, Z. Phys. **C49** (1991) 485.
- [159] T. Averett et al., SLAC Proposal-E-15X;
 K.S. Kumar, E.W. Hughes, R. Holmes, P.A. Sounder, Mod. Phys. Lett. **A10** (1995) 2979.
- [160] A. Czarnecki, W.J. Marciano, Phys. Rev. **D53** (1996) 1066.

- [161] F.A. Berends, K.J.F. Gaemers, R. Gastmans, Nucl. Phys. **B68** (1974) 541;
M. Consoli, M. Lo Presti, M. Greco, Phys. Lett. **133B** (1982) 415;
M. Greco, Phys. Lett. **177B** (1983) 97; Riv. Nuovo Cim. **11** (1988) 1;
F.A. Berends, R. Kleiss, Nucl. Phys. **B228** (1983) 357;
M. Caffo, R. Gatto, E. Remiddi, Nucl. Phys. **B252** (1985) 378;
F.A. Berends, R. Kleiss, W. Hollik, Nucl. Phys. **B304** (1988) 712;
W. Beenakker, F.A. Berends, S.C. van der Mark, Nucl. Phys. **B349** (1991) 323;
M. Caffo, H. Czyz, E. Remiddi, Il Nuovo Cim., Vol**105A** No 2 (1992) 277; J. Mod. Phys.
C4 (1993) 591.
- [162] K. Tobimatsu, Y. Shimizu, Progr. Theor. Phys. **75** (1986) 905; Comput. Phys. Commun.
48 (1988) 335.
- [163] M. Böhm, A. Denner, W. Hollik, R. Sommer, Phys. Lett. **144B** (1984) 414.
- [164] M. Böhm, A. Denner, W. Hollik, Nucl. Phys. **B304** (1988) 687.
- [165] J. H. Field, T. Riemann, Comput. Phys. Commun. **94** (1996) 53.
- [166] R. Gastmans, Y. Van Ham, Phys. Rev. **D10** (1974) 3629.
- [167] F. Cuyper, PSI-PR-96-32, hep-ph/9611336, to appear in Proc. of the 1996 DPF/DPB
Summer Study on New Directions for “High Energy Physics-Snowmass96”.
- [168] W.J. Marciano, in L. De Porcel and C. Dunwoodie (eds.), “Spin Structure in High
Energy Processes”, Proc. of the 21st SLAC Summer Institute, Stanford, California, 1993,
(SLAC Report No. 444, Stanford, 1994).
- [169] J.C. Montero, V. Pleitez, M.C. Rodriguez, hep-ph/9803450.
- [170] A.A. Babich, A.A. Pankov, N. Paver, Phys. Lett. **B299** (1993) 351.
- [171] G.Gounaris, J.L. Kneur, J. Layssac, G. Moulataka, F.M. Renard, D. Schildknecht, in
P.M. Zerwas (ed.), Proc. of the “Workshop on e^+e^- collisions at 500 GeV: The physics
potential”, DESY 93-123B, p. 735.
- [172] V.V. Andreev, A.A. Pankov, N. Paver, Phys. Rev. **D53** (1996) 2390.
- [173] R. Najima, S. Wakaizumi, Phys. Lett. **B184** (1987) 410;
P. Kalyniak, M.K. Sundaresan, Phys. Rev. **D35** (1987) 75.
- [174] J.-M. Frère, M. Tytgat, J.M. Moreno, J. Orloff, Nucl. Phys. **B429** (1994) 3.
- [175] D. Bardin, T. Riemann, Nucl. Phys. **B462** (1996) 3.
- [176] T. Muta, R. Najima, S. Wakaizumi, Mod. Phys. Lett. **A1** (1986) 203.
- [177] P. Comas, A. Méndez, Phys. Lett. **B260** (1991) 211.
- [178] G. Gounaris, J. Layssac, G. Moulataka, F.M. Renard, Int. J. Mod. Phys. **A8** (1993) 3285.

- [179] M. Frank, P. Mättig, R. Settles, W. Zeuner, in Proc. of the “Workshop on e^+e^- collisions at 500 GeV: The physics potential”, DESY 93-123A, p. 235.
- [180] A. Leike, Nucl. Phys. B (Proc. Suppl.) **51C** (1996) 71.
- [181] K. Kołodziej, M. Zrałek, Phys. Rev. **D43** (1991) 3619;
W. Beenakker, F.A. Berends, T. Sack, Nucl. Phys. **B367** (1991) 287;
W. Beenakker, K. Kołodziej, T. Sack, Phys. Lett. **B258** (1991) 469.
- [182] D. Bardin, M. Bilenky, A. Olchevski, T. Riemann, Phys. Lett. **B308** (1993) 403; E: Phys. Lett. **B357** (1995) 725; complete revised version: hep-ph/9507277.
- [183] A. Sommerfeld, Atombau und Spektrallinien (Vieweg, Braunschweig, 1939) Bd. 2; A.D. Sakharov, Sov. Phys. JETP **18** (1948) 631.
- [184] V.S. Fadin, V.A. Khoze, A.D. Martin, Phys. Lett. **B311** (1993) 311; **B320** (1994) 141; D. Bardin, W. Beenakker, A. Denner, Phys. Lett. **B317** (1993) 213.
- [185] M. Lemonine, M. Veltman, Nucl. Phys. **B164** (1980) 445;
R. Phillippe, Phys. Rev. **D26** (1982) 1588;
M. Böhm et al., Nucl. Phys. **B304** (1988) 463;
J. Fleischer, F. Jegerlehner, M. Zrałek, Z. Phys. **C42** (1989) 409;
W. Beenakker, K. Kołodziej, T. Sack, Phys. Lett. **B262** (1991) 125;
J. Fleischer, K. Kołodziej, F. Jegerlehner, Phys. Rev. **D47** (1993) 830.
- [186] A. Aeppli, G.J. van Oldenborgh, D. Wyler Nucl. Phys. **B428** (1994) 126.
- [187] D. Bardin, R. Kleiss (conv) et al., in Ref. [39], v. 2, p. 3.
- [188] E. Maina, M. Pizzo, Phys. Lett. **B369** (1996) 341;
K.J. Abraham, B. Lampe Nucl. Phys. **B478** (1996) 507.
- [189] E. Maina, R. Pittau, M. Pizzio, Phys. Lett. **B393** (1997) 445.
- [190] E. Maina, R. Pittau, M. Pizzio, hep-ph/9709454;
E. Maina, R. Pittau, M. Pizzio, hep-ph/9710375.
- [191] A. Signer, SLAC-PUB-7490; hep-ph/9705218.
- [192] G. Gounaris, J-L.Kneur, D. Zeppenfeld, in reference [39], p. 525.
- [193] See the corresponding contributions to reference DESY-96-123D.
- [194] A.A. Pankov, N. Paver, C. Verzegnassi, hep-ph/9701359, to appear in Int. J. Mod. Phys. **A**.
- [195] M. Bilenky, J.L. Kneur, F.M. Renard, D. Schildknecht, Nucl. Phys. **B419** (1994) 240.
- [196] OPAL Collab., K. Ackerstaff et al., CERN-PPE/97-125.

- [197] F. Berends, M. Dubinin, in In “St. Petersburg 1996, High energy physics and quantum field theory” p. 151, hep-ph/9702344.
- [198] D. Bardin, A. Leike, T. Riemann, Phys. Lett. **B344** (1995) 383.
- [199] D. Bardin, J. Biebel, D. Lehner, A. Leike, A. Olchevski, T. Riemann, Comput. Phys. Commun. **104** (1997) 161.
- [200] T.G. Rizzo, Ames Lab Report IS-J-3092 (1988).
- [201] T.G. Rizzo, Ames Lab Report IS-J-3091 (1988).
- [202] UA1 Collab., G. Arnison et al., Phys. Lett. **126B** (1983) 398;
UA2 Collab., P. Bagnaia et al., Phys. Lett. **B129** (1983) 130.
- [203] V. Barger, N.G. Desphane, J.L. Rosner, K. Whisnant, Phys. Rev. **D35** (1987) 2893.
- [204] S. Capstick, S. Godfrey, Phys. Rev. **D37** (1988) 2466.
- [205] F. del Aguila, M. Quirós, F. Zwirner, Nucl. Phys. **B284** (1987) 530;
P. Chiappetta, M. Greco (conv.), in G. Jarlskog, D. Rein (eds.), Proc. of the Large Hadron Collider workshop, CERN 90-10 (1990) p. 685.
- [206] F. del Aguila, L. Ametller, R.D. Field, L. Garrido, Phys. Lett. **B221** (1989) 408.
- [207] S.Y. Lee, F.D. Courant, Phys. Rev. **D41** (1990) 292, and references therein;
RHIC–SPIN Collab., proposal, 1992.
- [208] A. Fiandrino, P. Taxil, Phys. Rev. **D44** (1991) 3490.
- [209] T. Rizzo, Phys. Lett. **B192** (1987) 125.
- [210] F. del Aguila, B. Allés, Ll. Ametller, A. Grau, Phys. Rev. **D48** (1993) 425.
- [211] F. del Aguila, M. Cvetič, P. Langacker, Phys. Rev. **D48** (1993) 969.
- [212] M. Cvetič, P. Langacker, Phys. Rev. **D46** (1991) R14.
- [213] J.L. Hewett, T.G. Rizzo, Phys. Rev. **D47** (1993) 4981.
- [214] V. Baier, V. Fadin, V. Khoze, Sov. Phys. JETP **23** (1966) 104.
- [215] T. Rizzo, Phys. Rev. **D47** (1993) 956.
- [216] G. Altarelli, R.K. Ellis, G. Martinelli, Nucl. Phys. **B143** (1978) 521, E: **B146** (1978) 544;
J. Abad, B. Humpert, Phys. Lett. **80B** (1979) 286;
J. Kubar-André, F.E. Paige, Phys. Rev. **D19** (1979) 221;
B. Humpert, W.L. van Neerven, Phys. Lett. **84B** (1979) 327, E: **85B** (1979) 471; **89B** (1979) 69; Nucl. Phys. **B184** (1981) 225;
A.P. Contogouris, J. Kripfganz, Phys. Rev. **D20** (1979) 2295;

- A.N. Schellekens, W.L. van Neerven, Phys. Rev. **D21** (1980) 2619; **D22** (1980) 1623;
 K. Hikasa, Phys. Rev. **D29** (1984) 1939;
 D.A. Dicus, S.S.D. Willenbrock, Phys. Rev. **D34** (1986) 148;
 T. Matsuura, W.L. van Neerven, Z. Phys. **C38** (1988) 623;
 T. Matsuura, S.C. van der Marck, W.L. van Neerven, Phys. Lett. **B211** (1988) 171; Nucl. Phys. **B319** (1989) 570;
 R. Hamberg, T. Matsuura, W.L. van Neerven, Nucl. Phys. **B345** (1990) 331; **B359** (1991) 343;
 W.L. van Neerven, E.B. Zijlstra, Nucl. Phys. **B382** (1992) 11.
- [217] G. Altarelli, R.K. Ellis, G. Martinelli, Nucl. Phys. **B157** (1979) 461;
 J. Kubar, M. le Bellac, J.L. Meunier, G. Plaut, Nucl. Phys. **B175** (1980) 251.
- [218] P.J. Rijken, W.L. van Neerven, Phys. Rev. **D51** (1995) 44.
- [219] C.T.H. Davies, W.J. Stirling, Nucl. Phys. **B244** (1984) 377;
 C.T.H. Davies, W.J. Stirling, B.R. Webber, Nucl. Phys. **B256** (1985) 413;
 G. Altarelli, R.K. Ellis, M. Greco, G. Martinelli, Nucl. Phys. **B246** (1984) 12;
 G. Altarelli, R.K. Ellis, G. Martinelli, Z. Phys. **C27** (1985) 617.
- [220] P. Ratcliffe, Nucl. Phys. **B223** (1982) 45;
 A. Weber, Nucl. Phys. **B382** (1992) 63;
 B. Kamal, Phys. Rev. **D53** (1996) 1142;
 W. Vogelsang, A. Weber, Phys. Rev. **D48** (1993) 2073;
 A.P. Contogouris, B. Kamal, Z. Merebashvili, Phys. Lett. **B337** (1994) 169;
 T. Gehrmann, Nucl. Phys. **B498** (1997) 245; hep-ph/9710508;
 S.Chang, C. Corianò, R.D. Field, Phys. Lett. **B403** (1997) 344, hep-ph/9702252.
- [221] U. Baur, S. Keller, W. Sakumoto, D. Wackerroth, hep-ph/9609315, to be published in Proc. of 1996 Annual Divisional Meeting (DPF 96) of the Division of Particles and Fields of the American Physical Society, Minneapolis, MN, 10-15 Aug 1996;
 U. Baur, S. Keller, W. Sakumoto, Phys. Rev. **D57** (1998) 199, hep-ph/9707301.
- [222] CDF Collab., F. Abe et al., Phys. Rev. Lett. **77** (1996) 5176;
 CDF Collab., F.Abe et al., Phys. Rev. **D55** (1997) 2546.
- [223] CDF Collab., F. Abe et al., Phys. Rev. Lett. **77** (1996) 5336.
- [224] CDF Collab., F. Abe et al., CDF/PUB/ELECTROWEAK/CDFR/3493 (1993) 2542 and Phys. Rev. Lett. **74** (1995) 3538,
 CDF Collab., F. Abe et al., Phys. Rev. Lett. **77** (1996) 5336;
 D0 Collab., S. Abachi et al., FERMILAB-CONF-96-168-E, 1996, to appear in Proc. of the “28th International Conference on High-energy Physics”, (ICHEP 96), Warsaw, Poland, 25-31 Jul 1996;
 T.G. Rizzo, Phys. Rev. **D48** (1993) 4236.
- [225] J.D. Anderson, M.H. Austern, Phys. Rev. **D46** (1992) 290; Phys. Rev. Lett. **69** (1992) 25.

- [226] A. Leike, Phys. Lett. **B402** (1997) 374.
- [227] A.D. Martin, W.J. Stirling, R.G. Roberts, Phys. Lett. **B354** (1995) 155.
- [228] D0 Collab., S. Abachi et al., Phys. Lett. **B385** (1996) 471;
 D0 Collab., S. Abott et al., Contribution to the *XVIII Int. Symposium on Lepton Photon Interactions*, Hamburg, Germany, August 1997;
 G. Gómez, talk at the APS Conference, Washington, April 1997.
- [229] The CDF II dedector: Technical Design Report, November 1996, FERMILAB-Pub-96/390-E.
- [230] F. del Aguila, J.M. Moreno, M. Quirós, Phys. Rev. **D40** (1988) 2481;
 F. del Aguila, J.M. Moreno, M. Quirós, Phys. Rev. **D41** (1989) 134.
- [231] J.L Hewett, T.G. Rizzo, Phys. Rev. **D45** (1992) 161.
- [232] V.D. Angelopoulos, J. Ellis, D.V. Nanopoulos, N.D. Tracas, Phys. Lett. **B176** (1986) 203.
- [233] F. Cornet, R. Rückl, Phys. Lett. **B184** (1987) 263; in: Proc. of the workshop on Physics at future Accelerators, La Thuile, Italy 1987, CERN 87-07, vol. II, p. 190.
- [234] S. Capstick, S. Godfrey, Phys. Rev. **D35** (1987) 3351.
- [235] J. Blümlein, A. Leike, T. Riemann, in G. Jarlskog, D. Rein (eds.), Proc. of the Large Hadron Collider Workshop, Aachen, Oct 1990, CERN 90-133 (1990), vol. II, p. 1010.
- [236] A. Akhundov, D. Bardin, L. Kalinovskaya, T. Riemann, Fortsch. Phys. **44** (1996) 373.
- [237] A. Arbuzov, D. Bardin, J. Blümlein, L. Kalinovskaya, T. Riemann, DESY-95-185, hep-ph/9511434;
 D. Bardin, J. Blümlein, P. Christova, L. Kalinivskaya, T. Riemann, Acta Phys. Polon. **B28** (1997) 511.
- [238] A. De Rujula, R. Petronzio, A. Savoy-Navarro, Nucl. Phys. **B154** (1979) 394;
 M. Consoli, M. Greco, Nucl. Phys. **B186** (1981) 519;
 E. Kuraev, N. Merenkov, V. Fadin, Sov. J. Nucl. Phys. **47** (1988) 1009;
 J. Blümlein, Z. Phys. **C47** (1990); Phys. Lett. **B271** (1991) 267;
 I. Akushevich, T. Kukhto, Yad. Fiz. **52** (1990) 1442; Acta Phys. Polon. **B22** (1991) 771.
- [239] L.W. Mo, Y.S. Tsai, Rev. Mod. Phys. **41** (1969) 205;
 I. Akushevich, T. Kukhto, F. Pacheco, J. Phys. **G18** (1992) 1737;
 J. Blümlein, G. Levman, H. Spiesberger, in E. Berger (ed.), Proc. of the Workshop on Research Directions of the Decade, Snowmass 1990) (World Scientific, Singapore, 1992), p. 554; J. Phys. **G19** (1993) 1695;
 J. Kripfganz, H. Möhring, H. Spiesberger, Z. Phys. **C49** (1991) 501;
 J. Blümlein, Z. Phys. **C65** (1995) 293.

- [240] D. Bardin, C. Burdik, P. Christova, T. Riemann, Z. Phys. **C42** (1989) 679; Z. Phys. **C44** (1989) 149;
D. Bardin, P. Christova, L. Kalinovskaya, T. Riemann, Phys. Lett. **B357** (1995) 456.
- [241] T.G. Rizzo, Contribution to the Snowmass Summer Study 1990, p. 560.
- [242] J. Blümlein, Talk given at 25th International Symposium on Multiparticle Dynamics, Stara Lesna, Slovakia, Sep 1995, hep-ph/9512272 ;
W.L. van Neerven, in G. Ingelman, A. De Roeck, R. Klanner (eds.), Proc. of the workshop "Future Physics at HERA", 1996, vol. 1, p. 56.
- [243] P. Haberl, F. Schrempp, H.- U. Martyn, B. Schrempp, in W. Buchmüller, G. Ingelman (eds.), Proc. of the workshop "Physics at HERA", Hamburg, Oct. 1991, vol. 2, p. 980.
- [244] H.- U. Martyn, in G. Ingelman, A. De Roeck, R. Klanner (eds.), Proc. of the workshop "Future Physics at HERA", 1996, vol. 1, p. 327.
- [245] H.- U. Martyn et al., in W. Buchmüller, G. Ingelman (eds.), Proc. of the workshop "Physics at HERA", Hamburg, Oct. 1991, vol. 2, p. 987.
- [246] P. Chiappeta, J.M. Virey, Phys. Lett. **B389** (1996) 89.
- [247] H1 Collab., C. Adloff et al., Z. Phys. **C74** (1997) 191;
ZEUS Collab., J. Breitweg et al., Z. Phys. **C74** (1997) 207.
- [248] S. Godfrey, Mod. Phys. Lett. **A12** (1997) 1859.
- [249] U. Baur et al., Phys. Rev. **D35** (1987) 95;
M. Kuroda et al., Nucl. Phys. **B261** (1985) 432.
- [250] C.S. Wood et al., Science **275** (1997) 1759.
- [251] P.A. Vetter et al., Phys. Rev. Lett. **74** (1995) 2658.
- [252] K.T. Mahanthappa, P.K. Mohapatra, Phys. Rev. **D43** (1991) 3093.
- [253] P. Langacker, Phys. Lett. **B256** (1991) 277.
- [254] W.J. Marciano, A. Sirlin, Phys. Rev. **D27** (1983) 552;
W.J. Marciano, J.L. Rosner, Phys. Rev. Lett. **65** (1990) 2963.
- [255] N.G. Deshpande, B. Dutta, X.-G. He, Phys. Lett. **B408** (1997) 288.
- [256] V. Barger, K. Cheung, D.P. Roy, D. Zeppenfeld, Phys. Rev. **D57** (1998) 3833, hep-ph/9710353.
- [257] P. Berge et al., Z. Phys. **C56** (1992) 175;
C.G. Arroyo et al., Phys. Rev. Lett. **72** (1994) 3452;
W.G. Seligman et al., Phys. Rev. Lett. **79** (1997) 1213.
- [258] P. Vilain et al., Phys. Lett. **B332** (1994) 465.

- [259] J.M. Conrad, M.H. Shaevitz, T. Bolton, hep-ex/9707015, to appear in Rev. Mod. Phys.
- [260] D.Yu. Bardin, O.M. Fedorenko, Sov. J. Nucl. Phys. **30** (1979) 418;
W.J. Marciano, A. Sirlin, Phys. Rev. **D22** (1980) 2695.
- [261] O.G. Miranda, V. Semikoz, J.W.F. Valle, hep-ph/9712215, to appear in Phys. Rev. **D**.
- [262] D.N. Schramm, M.S. Turner, astro-ph/9706069, Submitted to Rev. Mod. Phys.
- [263] C.J. Copi, D.N. Schramm, M.S. Turner, Phys. Rev. **D55** (1997) 3389.
- [264] J. Ellis, K. Enqvist, D.V. Nanopoulos, S. Sarkow, Phys. Lett. **B167** (1986) 457;
M.C. Gonzalez-Garcia, J.W.F. Valle, Phys. Lett. **B240** (1990) 163.
- [265] J.A. Grifols, E. Masso, T.G. Rizzo, Phys. Rev. **D42** (1990) 3293.
- [266] T.G. Rizzo, Phys. Rev. **D44** (1991) 202.
- [267] R. Barbieri, R.N. Mohapatra, Phys. Rev. **D39** (1989) 1229;
J.A. Grifols, E. Masso, Nucl. Phys. **B331** (1990) 244.
- [268] G.G. Raffelt, *Stars as Laboratories for Fundamental Physics*, The University of Chicago Press, Chicago, London, 1996.
- [269] P. Chiappetta, C. Verzegnassi (conv.), Proc. of the LEP 2 workshop, CERN yellow report CERN 96-01, vol. 1, p. 577.
- [270] D. Bardin et al., Phys. Lett. **B255** (1991) 290.
- [271] The code ZFITTER is used by all four LEP collaborations.
- [272] D. Lehner, Ph.D. thesis, Humboldt-Universität zu Berlin, Germany (1995), Internal Report DESY-IfH 95-07, hep-ph/9512301;
D. Bardin, D. Lehner and T. Riemann, Nucl. Phys. **B477** (1996) 27;
D. Bardin, A. Leike and T. Riemann, Phys. Lett. **B353** (1995) 513;
see reference [198].
- [273] OPAL Collab., Phys. Lett. **B389** (1996) 416;
DELPHI Collab., Phys. Lett. **B397** (1997) 158;
L3 Collab., Phys. Lett. **B398** (1997) 223;
ALEPH Collab., Phys. Lett. **B401** (1997) 347. CERN-PPE/97-025, to appear in Phys. Lett. **B**.
- [274] T. Sjöstrand, Comp. Phys. Commun. **82** (1994) 74;
T. Sjöstrand, Lund Univ. report LU TP 95-20 (1995);
on-line documentations of the different versions of Pythia may be also found at the same web-page as the source code.
- [275] See the Pythia web-page for the main references.
- [276] Pythia is used by many collaborations at e^+e^- , ep and hadron colliders.

Appendix A

Notation

For the convenience of the reader, we collect the main notation in the following tables. The notation appearing in chapter one has mainly to do with the definition of the Z' parameters. It follows the notation of kinematic parameters and observables introduced in chapter two. We conclude with the notation relevant in the remaining chapters.

| Symbol | Meaning | Chapter 1 |
|--|---|-----------|
| Z' | Vector particle associated with the extra $U'(1)$ group in (1.1). | |
| $\chi, \psi, \eta, LR, SSM$ | Particular Z' models, see sections 1.2 and 1.1.3. | |
| θ_M | Mixing angle between the symmetry eigenstates Z and Z' . | |
| Z_1, Z_2 | Mass eigenstates resulting from the mixing of the Z and Z' . | |
| $\Gamma_n^f, \Gamma_n^W, \Gamma_n^{ffV}$ | Partial decay widths of the Z_n as defined in section 1.1.4. | |
| $M_{Z'}, \Gamma_{Z'}$ | Mass and width of the Z' . | |
| M_n, Γ_n | Masses and total widths of the Z_n , $n = 0, 1, 2$, $Z_0 = \gamma$. | |
| m_n^2 | Complex mass, $m_n^2 = M_n^2 - i\Gamma_n M_n$. | |
| Br_n^f | Branching ratio of the Z_n decay to $f\bar{f}$, $Br_n^f = \Gamma_n^f/\Gamma_n$. | |
| e, g_1, g_2 | Coupling strengths of the γ, Z and Z' to fermions, see equation (1.20), $e \approx 0.31$, $g_1 = g = e/(2c_W s_W) \approx 0.37$. | |
| $v_f, a_f (v'_f, a'_f)$ | Vector and axial vector couplings of the $Z(Z')$ to the fermion f . | |
| $L_f, R_f (L'_f, R'_f)$ | Left and right handed couplings of the $Z(Z')$ to the fermion f . | |
| $v_f(n), a_f(n)$ | Vector and axial vector couplings of the Z_n to the fermion f . | |
| $L_f(n), R_f(n)$ | Left and right handed couplings of the Z_n to the fermion f . | |
| $\epsilon_A, P_V^e, P_L^q, P_R^u, P_R^d$ | Sign-dependent coupling combinations, see equation (1.36). | |
| $\epsilon_A, \gamma_L^l, \gamma_L^q, \tilde{U}, \tilde{D}$ | Sign-independent coupling combinations, see equation (1.37). | |

Table A.1 Main conventions and notation.

| Symbol | Meaning | Chapter 2 |
|---|--|-----------|
| $s(s')$ | Centre-of-mass energy squared of the considered (sub)process. | |
| L | Integrated luminosity | |
| $\lambda_1, \lambda_2, \lambda_3$ | Helicity combinations (2.9), (2.97) of the initial particles. | |
| $c = \cos \theta$ | θ is the angle between the initial electron and the final fermion f (or final W^-). | |
| $\chi_n(s)$ | Propagator as defined in equation (2.7). | |
| $\hat{\chi}_n(s)$ | Propagator in $e^+e^- \rightarrow e^+e^-$ as defined in equation (2.114). | |
| v_f^N, a_f^N | Normalized couplings of the Z' , as defined in equation (2.3). | |
| v_f^M, a_f^M | Mixing dependent couplings (2.4) of the Z' . | |
| δ_γ, δ_Z | Shifts (2.111) in the couplings $g_{WW\gamma}$ and g_{WWZ} due to a Z' . | |
| $O, \Delta O, O_{SM}$ | Some observable (total or differential cross section or asymmetry), its experimental error and its SM prediction. | |
| r | Ratio of the systematic and statistical errors, see (1.66) | |
| Δo | g_2 -depending error, of an observable, see equation (2.46). | |
| $\Delta^{Z'} O$ | Shift of the observable O from its SM prediction due to a Z' . | |
| σ_T^f | Total cross section of fermion pair production in different processes, see equations (2.6) and (3.1). | |
| $A_{FB}^f, A_{LR}^f, A_{pol}^f$ | Forward-backward, left-right and polarization asymmetries for fermion pair production in different processes, see equations (2.15), (3.7) and (4.4). | |
| $A_{LR,FB}^f, A_{pol,FB}^f, A_{LR,pol}^f$ | Combined asymmetries, see equations (2.16) and (3.7). | |
| $R^{had}, A_{LR}^{had}, R_b, R_c$ | Ratios and asymmetries as defined in equation (2.19). | |
| $M_{Z'}^{lim}$ | Largest M_2 , which can be detected. | |
| f_m | Ratio of M_2 and $M_{Z'}^{lim}$, see equation (2.62). | |
| θ_M^{lim} | Smallest mixing angle, which can be detected. | |
| g_2^{lim} | Smallest coupling strength, which can be detected. | |
| $\delta_\gamma^{lim}, \delta_Z^{lim}$ | Smallest shifts δ_γ and δ_Z , which can be detected, see (2.131). | |
| $H_A^e(v)$ | Flux function (2.21) describing QED initial state corrections. | |
| Δ | Cut on the photon energy in units of the beam energy. | |
| Δ^+, Δ^- | Boundaries of the considered range of the photon energy. | |
| $\Delta E_\gamma/E_\gamma$ | Photon energy resolution of the experiment. | |

Table A.2 Continuation of conventions and notation.

| Symbol | Meaning | Chapter 2 |
|--|---|------------------|
| $F_A(q^2)$ | Form factor taking into account the vacuum polarization of the photon, see equation (2.30). | |
| x_f, y_f | Form factors of the ZZ' mixing, see equation (1.29). | |
| $\kappa_f, \kappa_{ef}, \rho_{ef}$ | Form factors taking into account the weak corrections, see section 2.1.2.2. | |
| $\kappa_f^m, \kappa_{ef}^m, \rho_{ef}^m$ | Form factors (1.62) taking into account the ZZ' mixing. | |
| $\kappa_f^M, \kappa_{ef}^M, \rho_{ef}^M$ | Form factors (2.31) taking into account the weak corrections, and the ZZ' mixing. | |
| | | Chapters 3 and 4 |
| $r_{y1}, A_{FB}y1$ | Rapidity ratios as defined in equation (3.8). | |
| $r_{llZ}, r_{\nu\nu Z}, r_{l\nu W}$ | Ratios from rare Z' decays, see equation (3.9). | |
| $R_{Z'V}, V = Z, W, \gamma$ | Ratios from associated Z' production, see equation (3.10). | |
| $q_f(x, Q^2)$ | Structure function defining the distribution of partons q_f in the $p(\bar{p})$. | |
| $c_{Z'}$ | Model dependent constant defined in equation (3.16). | |
| $N_{Z'}$ | Number of expected Z' events, compare equation (3.16). | |
| $f^q(r_z, Q^2)$ | Integrated product of two structure functions, see equation (3.13). | |
| $f^u(r_z)$ | Approximation (3.15) of $f^q(r_z, Q^2)$ for large Q^2 and $q = u$. | |
| C_{ud} | Is defined below equation (3.14), $C_{ud} = f^u(r_Z)/f^d(r_z)$. | |
| x, y, Q^2 | Kinematic variables (4.3) in ep scattering. | |
| A_{XY}^{mn} | Asymmetries in (4.4) ep scattering. | |
| Q_W | Weak charge (4.6) measured in atomic parity violation. | |

Table A.3 Continuation of conventions and notation.

Appendix B

Available FORTRAN programs for Z' fits

Several computer programs are available allowing either theoretical investigations or direct fits to data. All officially released programs for Z' analyses known to the author are collected in table B.1. In the first column, the name of the program is listed. The second column contains references related to the program. If there exists a program description, its reference is printed in **bold**. References to original papers describing the underlying physics of the program are printed in roman. Examples of references, where the program was used in theoretical or experimental Z' studies, are printed in *italics*. In the last column the location of the program is given. It follows a short description of every program listed in the table.

ZCAMEL The program describes the pair production of massless fermions in e^+e^- collisions including the full $O(\alpha)$ QED corrections and the exponentiation of soft photons radiated from the initial state. It is a fast stand-alone program designed for theoretical studies. Use **ZEFIT** for fits to data.

ZEFIT The program must be used together with **ZFITTER**. It describes the fermion pair production in e^+e^- collisions. **ZEFIT** contains all additional Z' contributions needed for fits to data. Special attention is paid to the simultaneous treatment of electroweak corrections and ZZ' mixing needed for direct fits to data distributed around the Z peak. It is designed for fits to data above the Z peak too.

ZFITTER describes fermion pair production in e^+e^- collisions. It contains all known SM corrections needed for fits to data. It is designed for SM studies. It is required by **ZEFIT** and distributed together with this code. The description of **ZFITTER** is needed to work with **ZEFIT**. This is the reason why we list this code in table B.1.

GENTLE/4fan The stand-alone program describes the production of four fermions in e^+e^- collisions. It contains all known SM corrections needed for fits to data. It is originally designed for SM studies. It allows a study of Z' effects in W pair production using the branch of anomalous couplings, see appendix C of the program description. An on-line description can found at <http://www.ifh.de/theory/publist.html> .

PYTHIA is a general-purpose event generator for a multitude of processes in e^+e^- , ep and pp physics. The emphasis is on the detailed modeling of hadronic final states, i.e. QCD parton showers, string fragmentation and secondary decays. The electroweak description

is normally restricted to improved Born-level formulae. It contains physics beyond the SM as supersymmetry, extra neutral gauge bosons or leptoquarks. Pythia was used to obtain the present Z' limits at hadron colliders.

| Program | Main References | Location |
|--------------|-------------------------------|---|
| ZCAMEL | [78, 79], [130] | ftp://gluon.hep.physik.uni-muenchen.de/zcamel.f |
| ZEFIT | [30], [62, 100, 101, 126] | http://www.ifh.de/~riemanns/uu/zefit5_0.uu |
| ZFITTER | [58], [76, 85, 270], [271] | distributed together with ZEFIT |
| GENTLE/4fan | [199], [175, 182, 272], [273] | http://www.ifh.de/~biebel/gentle2.f |
| PYTHIA v.6.1 | [274], [275], [276] | http://www.thep.lu.se/tf2/staff/torbjorn |

Table B.1 Officially released FORTRAN programs designed for a Z' search.